SCIENTIFIC OPPORTUNITIES USING SATELLITE WIND STRESS MEASUREMENTS OVER THE OCEAN

Report of the Satellite Surface Stress Working Group

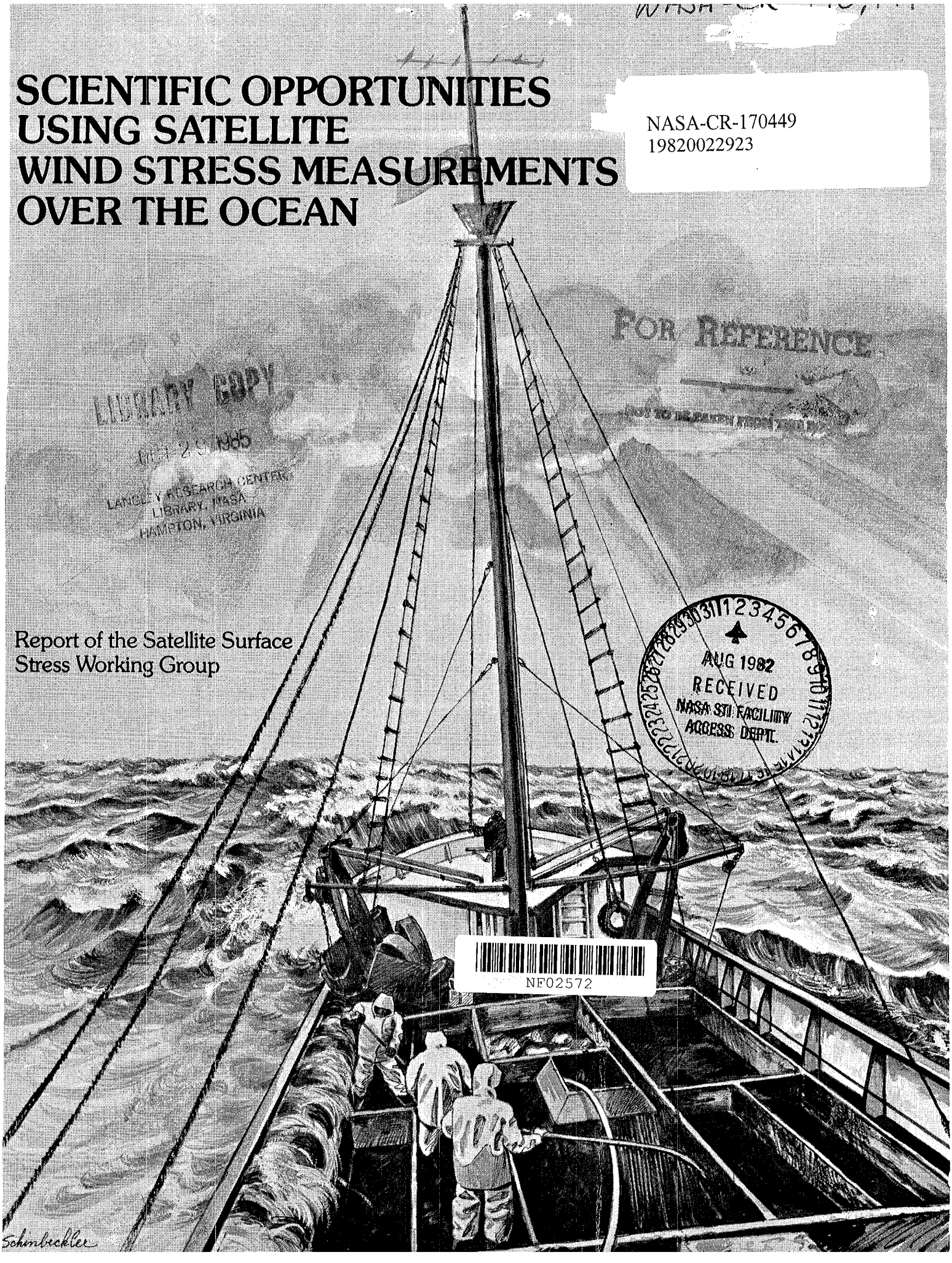

Schinbeckler

SCIENTIFIC OPPORTUNITIES USING SATELLITE SURFACE WIND STRESS MEASUREMENTS OVER THE OCEAN

Report of the Satellite Surface Stress Working Group

Prepared for:

National Aeronautics and Space Administration
June 1982

COVER: Artist Joanne Schinbeckler's rendering of a photograph by Nubar Alexanian.

FRONTISPIECE: SEASAT Scatterometer winds superimposed on an infrared picture in the JASIN area.

This document was produced under NASA Contract Number NAS5-26714.

Published by the Nova University/N.Y.I.T. Press, Fort Lauderdale, Florida, June 1982.

SEASAT-A VIRR: INFRARED TIME SPAN: 234/78 0-21- 1 TO 0-27- 9
TOP LEFT CORNER IS AT LATITUDE 67N LONGITUDE 338E
LATITUDE SCALE=100 PIXELS/DEGREE LONGITUDE SCALE= 50 PIXELS/DEGREE
TEXTAD

IPL PIC ID 81/04/25/061750 GMY/VIRRX
JPL IMAGE PROCESSING LABORATORY

FOREWORD

Based on SEASAT SASS measurements, it is possible to determine wind speed to much better than ±2 meters per second and wind direction to much better than ±20 degrees over the ocean. With some instrument improvements, based on scatterometer design studies, post-observation data processing can be dramatically reduced and nearly real time data gridding, reduction and dissemination to users appears feasible.

The Satellite Surface Stress (S^3) Working Group was formed by the Oceanic Processes Branch of NASA in September 1981 to identify scientific problem areas in which significant scientific advances might be expected if a new scatterometer were to be flown. A secondary consideration was to identify operational and commercial user communities. The S^3 group is composed of academic and government oceanographers and meteorologists as well as industrial managers.

Ocean waves and upper ocean currents are forced by the atmospheric wind stress on the sea surface. Many of these ocean motions have climatic, oceanographic or practical operational importance, which can be assessed only if accurate global scale forcing data are available for use in numerical models. These data are not now available from conventional observation and analysis systems. A satellite that can repeatedly observe the surface stress on an ocean-wide scale week after week could provide a uniquely valuable forcing data set to the ocean science and user communities.

In this report the S^3 Working Group highlights some of the new scientific opportunities that would be possible if we were to have the ability to collect wind data from space. We also attempt to assess the minimum requirements for the space platform and ground data reduction system in order to achieve major scientific discoveries. Besides a review of scientific opportunities, we review briefly the operational uses that may develop in government and commercial applications of these data. The entire investment in the late 1980's (say $150 M) can be offset by savings resulting from improved environmental knowledge for tactical Naval Fleet Operations or by commercial applications of oceanic forecasts of winds and waves. The

expected scientific benefits thus appear available at no net cost.

In this report we highlight a particularly exciting opportunity to predict the large-scale ocean anomaly called El Niño. By observing the wind stress field in the western Tropical Pacific, there is a good possibility for us to anticipate the formation of large sea-surface temperature anomalies in the eastern half of the Tropical Pacific Ocean. These warm anomalies appear to be precursors to severe cold winters over the eastern United States. This application of the winds is highlighted because the theory is well developed for the oceanic response.

We appreciate the excellent staff assistance of Ms. Jan Witte, Mrs. Ruth Pryor, and several NASA engineers in our study. Pat Teaf did a superb job of typing the draft versions of this report. The S^3 Working Group was supported through NASA contract NAS5-26714 at Nova University, Dania, Florida.

James J. O'Brien
Chairman

SATELLITE SURFACE STRESS WORKING GROUP

James J. O'Brien (Chairman)	The Florida State University
Robert Kirk (NASA Liaison)	Goddard Space Flight Center
Lawrence McGoldrick	NASA Headquarters
Janet Witte (Executive Assistant)	Nova University
Robert Atlas	Goddard Space Flight Center
Emedio Bracalente	NASA/Langley Research Center
Otis Brown	University of Miami
Robert Haney	U.S. Naval Postgraduate School
D. Edmunds Harrison	Massachusetts Institute of Technology
David Honhart, Cdr.	U.S. Navy, Chief of Naval Operations Staff
Harley Hurlburt	NORDA
Richard Johnson	Ocean Routes, Inc.
Linwood Jones	General Electric Company
Kristina Katsaros	University of Washington
Roger Lambertson	Control Data Corporation
Steven Peteherych	Atmospheric Environment Service, Canada
Willard Pierson	The City College of the City University of New York
James Price	Woods Hole Oceanographic Institution
Duncan Ross	NOAA-AOML
Robert Stewart	Jet Propulsion Laboratory and Scripps Institution of Oceanography
Peter Woiceshyn	Jet Propulsion Laboratory

EXECUTIVE SUMMARY

The Satellite Surface Stress Working Group was commissioned to suggest oceanic science that would be done if it were possible to determine the vector wind field at the sea surface. SEASAT demonstrated that it is possible to determine the wind speed and direction over the ocean to within very useful accuracies. The scientific community is generally very excited over the prospect of obtaining good wind fields over the ocean. While we believe that we know the relevant equations of motion for the ocean, we have never been capable of measuring the principal forcing function, the vector wind field, to calculate the ocean currents.

We have the ability to estimate wind fields over the oceans in the northern hemisphere on monthly time scales using ship data. The southern ocean does not have sufficient data for constructing maps and meteorological forecasts are not accurate enough for producing adequate wind fields.

- The one unequivocal conclusion is that conventional wind data do not suffice to meet the research and application needs of the oceanographic community.

- The vector stress or wind field from space will be a new and unique measurement for the study of upper ocean circulation.

The required measurement is the vector horizontal tangential stress, which is the lower boundary condition for the atmosphere and the upper boundary condition for any wind-driven wave or ocean current model. Since limited direct observations of vector stress have been obtained over the ocean, the SEASAT scientists have empirically estimated wind speed and direction at 19.5 m.

- Considerable basic research will be necessary to interpret space measurements as vector surface wind stress.

The vector wind stress fields collected over the ocean will be used to drive a wide variety of ocean models. It will be possible to obtain quantitative estimates of upper ocean currents from these models. In this report we highlight a particular experiment known as the El Niño phenomena, because knowledge of the ocean variability may lead to the ability to forecast severe winters over the eastern United states up to a year in advance. The international name for this scientific experiment is TOGA (Tropical Ocean - Global Atmosphere). Present ocean models indicate that previous El Niño events are excited by anomalous winds in the western Pacific. These winds excite an internal Kelvin wave, which takes 2-3 months to reach the coast of Peru and disturb the local heat budget.

- If our present ideas are correct, we should be able to make some predictions of El Niño if we measure the winds along the Pacific equator. For instance, the appearance of strong westerly winds would allow the forecast of an impending El Niño. If TOPEX were also in space we might be able to monitor the passage of the Kelvin wave as it moves eastward toward Ecuador. Using infrared sea surface temperature measurements, we would be able to verify from space whether the wind change were producing the characteristic El Niño warm anomaly along the coast. Verification of the existence of warm water would justify the initiation of plans for a severe winter over the eastern U.S. a few months later.

The vector wind stress fields are very important for many oceanographic problems. We recommend that NASA proceed with a formal study of a system to meet the following minimum data requirements:

- An accuracy of 2 m/s or 10% (whichever is greater) in wind speed and ±20 degrees in wind direction as met by SASS and designed for NOSS must be maintained.

Wind Speed	Requirements
≤ 3 m/s	None (light and variable)
> 3 ≤ 6 m/s	± 2 m/s, ±20°, 100 km resolution
> 6 < 100 m/s	Larger of ±2 m/s, or 10% of wind speed, ±20°, ≤ 50 km resolution

- We require that the wind vector at 90% of the points at the equator and also at 35 degrees North be observed to within 50 km at least every two days.

- The antenna and polarization design must be sufficient to allow determination of a wind stress direction with no more than 2 aliases which are nearly 180° out of phase at least 90% of the time.

- Absolute position location of data within 50 km is satisfactory. Relative position location between vectors of ±10 km is the minimum requirement.

- The ability to detect atmospheric liquid water is an essential component of any scatterometer program. The minimum requirement is a flag for amounts of liquid water which hinder scatterometer accuracy. This should be done with a resolution equal to or higher than the scatterometer cell resolution.

- Data available in satellite orbit configuration are awkward to use as a global data set. Meteorologists and oceanographers are very familiar with weather data which have been mapped onto a latitude-longitude grid for a fixed time. This is called earth-gridded data. If the

data are stored in a 3-dimensional matrix where the location in the matrix designates latitude, longitude and time, then the data are easily used for all purposes.

- Availability of data as earth-gridded stress vectors in a timely manner for scientific projects is essential.

- Maximum time delay between observation and availability of gridded surface winds is 6 hours for operational use.

- The user community will be responsible for data validation, and NASA would supply the resources for this activity.

Scatterometer data are extremely valuable for applications other than oceanographic research, such as meteorological modeling, special naval ocean products and industrial use. These applications are discussed in detail in Section IV. The impact of surface winds over the ocean on naval or industrial applications is sufficient to justify the investment in the scatterometer.

TABLE OF CONTENTS

I. WIND STRESS MEASUREMENTS OVER THE OCEAN

A. INTRODUCTION

Every person who has been to sea on a ship is aware of the influence of the wind on ocean waves and currents. Almost immediately, as a breeze appears, small waves and the upper ocean currents develop and influence the progress of a ship. As the winds strengthen, the waves and currents increase in amplitude. Clearly knowledge of the wind field over the ocean is useful for calculating the motion of the upper ocean and the properties of the wave field.

The mathematical approach is to assert that there is a set of physical laws that govern the motion of the sea. These laws may be expressed as a set of equations, say

$$L(\underset{\sim}{q}) = F$$

where L is a non-linear partial differential equation operator, $\underset{\sim}{q}$ is a vector of the state variables such as the velocity field, etc., and F represents a functional of the external forces. Given appropriate boundary conditions and initial conditions, we can solve this system of equations. For most practical problems various approximations are required and a computer is used to seek solutions. The external forces are the wind stress and heat flux as a function of time and space at the sea surface. The vector wind stress field determines the strength, distribution and character of ocean motions. Ocean motions occur on a range of space scales from basin-wide to very small wavelengths. Using wind climatological data on large scales, it has been possible to understand the occurrence and existence of the major semi-permanent currents in the ocean. However, in the past decade it has become evident that time-varying currents in the ocean are frequently more energetic than the "classical" semi-permanent currents. In essence there is significant "weather" in the ocean as in the

atmosphere. Understanding the time-varying currents is one of the primary problems of contemporary oceanography.

It is the belief of the S^3 working group that the routine availability of accurate global satellite wind stress data over the ocean surface will revolutionize our knowledge of upper ocean currents, because we envision that using the stress (wind) data will enable us to calculate approximate realizations of ocean motions. Thus, *knowledge of the wind forcing will enable us to understand more thoroughly the physics of the upper ocean*. Good surface wind stress patterns will allow us to construct pictures of ocean currents, and thus to see the ocean weather, in a way that will be as unique and as exciting as the first pictures of the earth taken by astronauts.

In section IB, we review what wind stress is and how it is measured directly, how it is generally inferred from wind vectors, and what is known about wind stress from historical and conventional data sources. Section IC reviews the history of scatterometer observation of surface wind stress.

B. CONVENTIONAL WIND STRESS OBSERVATIONS

Measurement Technique

The wind stress at the sea surface is the average turbulent transfer of horizontal momentum from the atmosphere to the ocean by vertical air movements. This transfer is difficult to measure even with a stable observing platform and very sensitive anemometers. The air-sea interface is a hostile environment for sensors. Turbulence time scales are short (as little as a few seconds); turbulent velocities are large (up to several meters per second), and the quantity of interest is the correlation between the vertical and horizontal motions. Very few direct stress measurements have been made. (See Davidson *et al.*, 1981, and Large and Pond, 1981.)

Various direct measurements have been used to construct empirical relationships ("bulk formulae") that permit values of wind speed and direction at a fixed height (usually 10 m) and gravitational stability of the atmosphere at the surface to be converted to a surface stress

value. The usual equation is

$$\vec{\tau} = \rho_A C_D |\vec{v}| \vec{v}$$

where ρ_A is the density of air and C_D is a drag coefficient whose value depends on wind speed and air-sea temperature difference. The preferred form of C_D is the subject of much study.

Recent papers on the subject are those of Businger *et al.* (1971), Garratt (1977), Smith (1980), Amorocho and DeVries (1980, 1981), Smith (1981), Large and Pond (1981), Davidson *et al.* (1981) and Liu and Large (1982). The paper by Large and Pond (1981) reports considerable success in relating different approaches to each other and in providing realistic results based on micrometeorological measurements. The agreement among three different methods (i.e., the Reynolds Flux, the Kolmozorov eddy dissipation method, and the bulk formula) is excellent.

Unfortunately, the bulk formula approach is not entirely satisfactory. Different formulae can lead to stress differences of up to a factor of two. Further, it is not clear that there should be a unique relationship between the stress and the wind at some height and atmospheric stability. However, many of the recent studies arrive at rather similar relationships and bulk formulae will continue to be widely used in the foreseeable future.

History

In spite of these difficulties, stress is estimated from wind observations for most oceanographic purposes; therefore, the history of conventional stress observations is the history of observations of the winds near the ocean surface. The bulk of wind information over the ocean, which contains either anemometer values or Beaufort estimates (based upon the characteristics of the ocean surface ripples, chop, barely white-capping, etc.), comes from ship observations. Ship data have been recorded for more than a century. In all, several tens of millions of records are available, beginning

around 1850. The highest quality ocean wind data have been collected by less than a dozen "Ocean Weather Ships" (OWS) which were set up to provide information for weather forecasting beginning in the 1950's. A limited amount of data has been collected from moored platforms, principally research buoys and offshore oil exploration or production platforms. These time series are generally of no more than a few months duration in a few locations. For mid-latitudes, ocean surface winds also have been inferred from analyzed surface pressure maps produced by the national weather facilities, and from small island observations (anemometer or Beaufort estimates). Table I-1 summarizes the data sources and gives some additional information about each source. The technique described above does not work for the relatively flat pressure gradients of the tropics, which encompass half of the earth's surface.

Table I-1. Conventional Ocean Surface Wind Stress

Type	Time Period	Spatial Coverage	Temporal Sampling	Notes
Ship reports	1850 to present	Global, but sporadic	Highly variable with location and time	Typically of poor accuracy
Ocean Weather Ships	1950 to late 1970's	Fewer than a dozen ships, mid-latitudes	Several times a day at fixed stations	Discontinued
Moored platforms	1960 to present	Predominantly near coasts	Several times a day at fixed stations	
Inferred from surface pressure maps	1960 to present	Extra-tropical	Typically 2-4 per day	Requires assumed model relating pressure to wind
Islands	1950's to present	Generally poor	Several times per day	May be affected by micro-meteorological factors

Surface Wind Field Characteristics

The OWS's, moored recorders and island stations provide good data on the frequency spectrum of the wind. Together, they establish that energetic variability exists on time scales of seconds to decades in all parts of the world ocean and that frequency spectra often vary significantly with location and season (Fig. I-1). This information enables wind sampling requirements to be determined for particular areas in order that aliasing of low frequencies by sampling too infrequently can be avoided.

The climatological monthly mean wind field is reasonably well known over much of the global ocean from ship reports (e.g., Hastenrath and Lamb, 1979; Wyrtki and Meyers, 1976; Evanson and Veronis, 1975) and exhibits widely different space scales in different areas. Some areas show only gradual changes over thousands of km while others change dramatically over the smallest scales resolved by the analysis procedure (say 100 km). The spatial structure on shorter time scales is more difficult to study from ship reports, because they so often provide poor spatial coverage even when data over a month are averaged together.

The only available wavenumber spectra of stress which resolve periods greater than 2 months (Fig. I-2) are based on analyses of synoptic sea surface or near-surface pressure charts. The synoptic scale winds from these charts show energetic variability on scales from tens to thousands of km. The ship data are inadequate for the study of the 50 km to several hundred km scales, which are not well resolved in the pressure analyses. The mesoscale variability can be as energetic as the larger scale variability and at times may be of considerable importance.

The northern hemisphere midlatitudes are best known; the tropics and southern latitudes are much more poorly sampled. In the tropics, where surface pressure cannot easily be related to surface winds, we know relatively little about spatial scales for periods shorter than years (but see Goldenberg and O'Brien, 1981). At higher latitudes, it is known that winds derived from pressure fields consistently and significantly underestimate the atmospheric

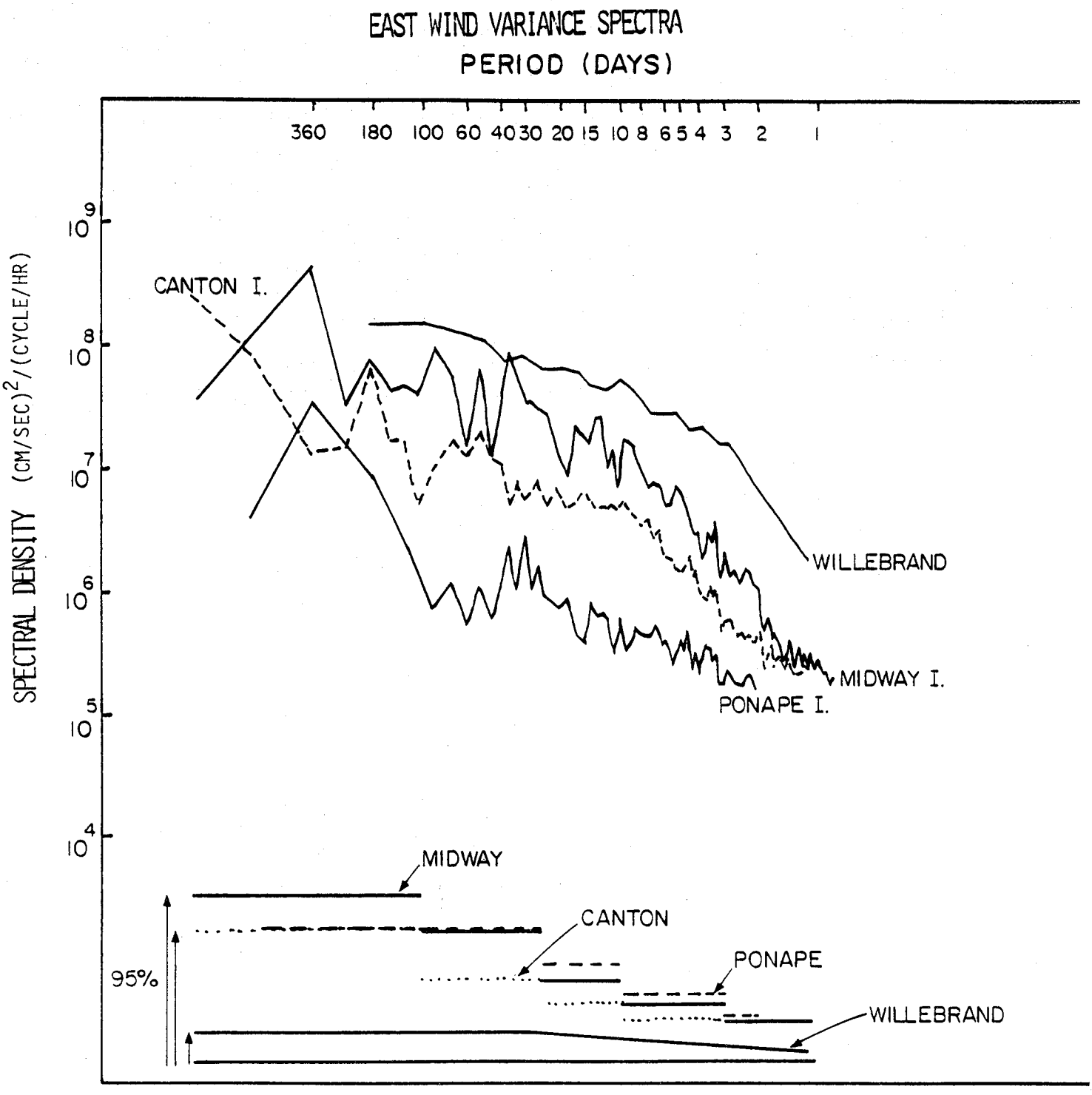

Figure I-1. Frequency spectra variation. (The Willebrand curve is from Willebrand, 1978.)

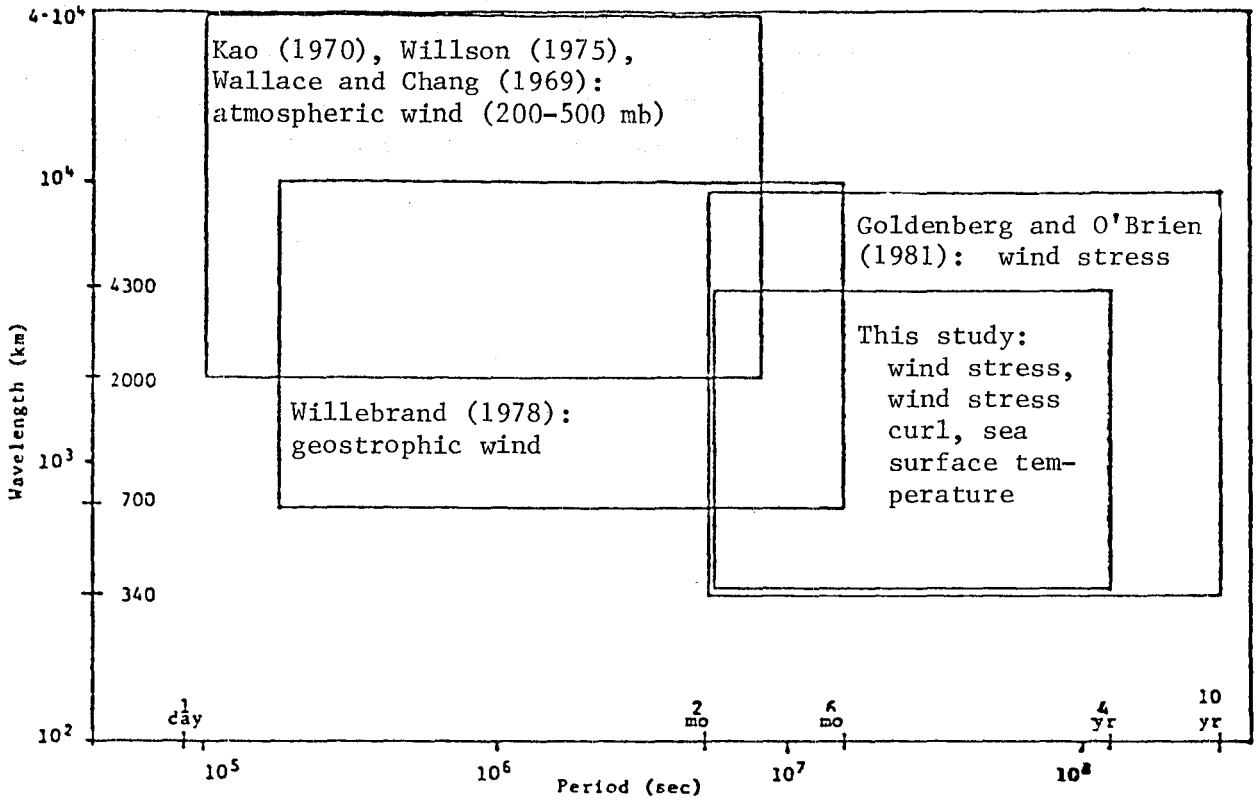

Figure I-2. Spectral windows sampled in recent studies of wind fields (from Gallegos-Garcia, et al., 1980). The high-frequency studies utilize synoptic charts; the two low-frequency studies utilize ship reports.

variance at spatial scales of a few hundred kilometers and less (Julian and Cline, 1974), where much of the eddy kinetic energy is found in the ocean. This problem has made it difficult to determine the extent to which these scales in the ocean are directly forced by the atmosphere.

As is the case with many other geophysical problems, the gaps in our knowledge about the scales of variability of wind stress make it difficult to establish observational requirements sufficient to ensure that the forcing data needed to answer the pressing questions of scientific interest will be available. *However, twice-daily observations on a spatial grid of 100 km appear likely to suffice except in near-coastal regions, where smaller spatial scales clearly exist.* Our estimates of the space and time scales needed for various ocean problems are given in the following sections. *The one unequivocal conclusion is that conventional data do not suffice to meet the research and application needs of the oceanographic community.*

C. MICROWAVE REMOTE SENSING OF WIND STRESS

Introduction

The microwave scatterometer (SASS) which flew on the SEASAT satellite demonstrated the practicality of sensing the ocean surface neutral-stability wind stress vector from space. The specifications for wind vector measurement from the SEASAT Users Working Group were met: viz., wind speed measurement range of 4 to 24 m/s with an accuracy of ±10% or ±2 m/s, whichever is greater; wind direction 0 to 360 degrees; 1000 km swath; 50 km resolution cell; cross-track and along-track spacing between resolution cells of 100 km.

The basic premise of the scatterometer as an anemometer is straightforward. A microwave radar transmits energy in wavelengths which are resonantly back scattered (Bragg scattered) from centimeter length ocean waves. The strength of the return signal is

related to the amplitude and density of these capillary waves and the slope of the shorter gravity waves (1-10 m), which are in turn related to the ocean surface stress and near-surface wind. The capillary wave spectrum is proportional to wind speed and its shape depends on wind direction, so that two radar "looks" from different azimuth angles give information about wind speed and direction.

However, quantifying these relationships involves detailed knowledge of the formation, evolution and interaction of these scale waves with their environment. The mechanism of the generation of waves by the wind is one of the fundamental unsolved problems of fluid dynamics, and the interaction of the short gravity and capillary waves with longer waves is complex. The existence of rain, white caps and breaking waves further complicates the problem. Moreover, the relationship between the wind at 10 m above the surface and the momentum flux into the ocean is dependent on the surface wave structure, the upper ocean stratification and the magnitude of the wind. These physical characteristics are poorly documented and experimental observations are sparse.

Given these limitations to obtaining an analytic relationship between the scatterometer signal and the surface stress, the practical approach is to establish an empirical relationship between the two parameters. The ability of microwave radar to measure stress depends on the existence of satisfactory parameterizations that are applicable under all environmental conditions that will be encountered. The number of variables entering between the microwave signal and the wind stress is large enough that no coherent relationship may exist under some conditions. When a good relationship exists only part of the time, then an understanding of the intervening processes may be used to suggest corrections or at least to "flag" data that should be rejected or subjected to special post-processing.

History

Active microwave remote sensing of the oceans had its beginnings during World War II when researchers were interested in

the effects of sea clutter (radar reflection from ocean waves) on the detection of low-flying aircraft, ships and other surface targets.

During the 1950's several radar ocean scattering experiments were conducted by Wiltse, *et al.* (1957), Grant and Yaplee (1957), and Boring, *et al.* (1957) from bridges and shore-based platforms. During the late 1950's and early 1960's, the Naval Research Laboratory conducted an extensive ocean measurement program using airborne multi-frequency radars to quantify sea clutter as a function of sea state and surface wind speed (Guinard, *et al.*, 1970; Daley, 1973).

NASA first considered the utility of microwave instruments for remote sensing of Earth's oceans in the mid-1960's, when a conference on the feasibility of conducting oceanographic explorations from aircraft and manned orbital and lunar laboratories was held at the Woods Hole Oceanographic Institution in August, 1964 (Ewing, 1965). At this conference, the rudiments of many of the remote sensing systems for measuring oceanographic parameters that eventually were orbited on Skylab, Geos-3 and SEASAT were described.

In 1966 the use of a satellite-borne scatterometer was proposed by Moore and Pierson (1966, 1971) for use on a polar orbiter to obtain oceanic wind and wave predictions, but there were two major problem areas to be resolved before this capability could be established. First, there was the debate on whether or not the normalized cross-section (NCRS), σ^o, successfully correlated with the wind speed. It was clear that 1-3 cm scale waves were related to some part of the momentum transfer from the atmosphere to the ocean, and that the wind stress is closely related to the surface wind speed. However, there were questions about the time constant for wave response, the constancy of the proportion of wind energy going into short versus long wavelengths, and the possibility of signal saturation above moderate wind speeds of 7-8 m/s. Secondly, it was unknown at that time whether the technology for radar hardware having good long-term stability could be developed, and whether the hardware could be calibrated to measure σ^o within the required accuracy of better than ± 2 dB absolute.

In the early 1970's, NASA sponsored the development of a special purpose radar sensor known as a scatterometer. Complementary airborne ocean experiments were conducted to develop the interpretation of these scatterometer measurements to infer geophysical oceanic surface parameters (Bradley, 1971; Krishen, 1971; Newton and Rouse, 1972). A few years later, a second conference sponsored by the National Academy of Sciences (NAS) at Woods Hole made a broader study of potential areas of activity for NASA, including the study of the oceans. The concepts of both high-precision radar altimetry and radar backscatter used to measure the winds received considerable attention (National Research Council, 1970). A third conference at Williamstown, Massachusetts (Kaula, 1970), also investigated the general subject. Ocean and atmospheric scientists postulated that satellite technology could provide the mechanism for monitoring the world oceans on a scale appropriate to the requirements of their research.

During the 1970's, scatterometer research and development were sponsored primarily by the NASA Office of Space and Terrestrial Applications. Under this program, improved aircraft (AAFE RADSCAT) and spacecraft (S-193 RADSCAT) scatterometers were developed which were stable. They demonstrated good absolute calibration and measurement precision. Comprehensive field experiments were conducted with these sensors. Strong empirical correlations were established between σ^0 and the surface oceanic vector wind (speed and direction) (Jones *et al.* 1977; Jones and Schroeder, 1978; Ross and Jones, 1978; Cardone *et al.*, 1976; Moore and Young, 1977). Data interpretation algorithms were developed using these empirical data.

In 1978 SEASAT, the first oceanographic remote sensing satellite, was launched with its complement of four microwave sensors, namely a radar altimeter, a multi-frequency radiometric imager, a synthetic aperture (imaging) radar and a radar scatterometer. Experiments were conducted to demonstrate the proof-of-concept for the measurement of sea surface winds, sea

surface temperatures, wave heights, internal waves, atmospheric water, sea-ice features, ocean topography and the marine geoid. On October 10, 1978, SEASAT failed in orbit because of a massive short circuit in the electrical power system. Fortunately, during the three months of orbital operations, the satellite returned a unique and voluminous set of data from Earth's oceans which allowed over 90% of the experiment objectives to be assessed. The SEASAT data demonstrated the feasibility of satellite-borne, active microwave remote sensing of ocean surface wind vectors (Jones *et al.*, 1982; Brown, 1982; Liu and Large, 1982).

Parameterizations

Given the fact that radar backscatter is produced by Bragg scattering from centimeter length ocean waves (Wright, 1966), then the friction velocity, $u_* = (\tau/\rho)^{1/2}$, possibly may be a better candidate for correlation to the normalized radar cross section, σ^0, than the wind measured at some constant height. However, while u_* is a practical parameter that finds frequent usage in oceanographic applications, it has not been routinely measured (see Section IB, Conventional Wind Stress Observations). It is the stress, ρu_*^2 (ρ is atmospheric density), which is used to drive ocean wave models or circulation models. Thus, the relative unavailability of stress measurements forced the remote sensing interpretation to be developed using neutral stability winds calculated from anemometer wind observations.

To account for the variation of surface wind profiles due to changes in atmospheric boundary layer stratification, empirical corrections have been obtained by means of the well established Monin-Obukov profiles:

$$U - U_S = \frac{u_*}{k} [\ln(z/z_0) - \psi(z/L)]$$

where U is the wind speed at height z; k is von Karman's constant, ≈ 0.4; z_0 is a roughness parameter; $\psi(z/L)$ is a function of

stratification; L is the Monin-Obukov length; and U_S is the current in the ocean, which is usually not zero. The Monin-Obukov length is related to the air-sea temperature difference. With an estimate of z_0 (or its variation with u_*), a value of u_* corrected for stratification effects can be derived from the measurements of U(z) and air-sea temperature differences. These measurements were obtained from aircraft and buoys (e.g., Jones and Schroeder, 1978), and were used to establish an empirical relation between σ^0 and the effective neutral wind at 19.5 m. This was one of many possible closure assumptions, which may not have been optimum, to relate u_* to σ^0. The correlation matrix (model function) depended on radar incidence angle, polarization and wind direction in the assumed form,

$$\sigma^0 = G(\theta,\chi,\varepsilon) + H(\theta,\chi,\varepsilon) \log U$$

where θ is incidence angle ($20° < \theta < 55°$), χ is the azimuth angle between radar beam and wind direction, and ε depends on beam polarization. A matrix of the empirical coefficients G and H comprises the SASS algorithm; σ^0 is assumed to vary harmonically with χ, with maximum parallel to the wind and minima normal to the wind, providing wind direction information. A discussion of the SEASAT wind parameterization algorithm can be found in Wentz (1978), Jones *et al.* (1978) and Schroeder *et al.* (1982a). A general discussion of the parameterization has been provided by Moore and Fung (1979).

The Monin-Obukov equation is often described as an empirical equation. Its form can be derived from the principles of turbulence theory by means of elegant theoretical considerations. However, the shape of the function, ψ, which depends on the non-dimensional variable, z/L, and either the quantity, $u_*/U_{10} = C_{10}$, or the function, $z_0 = z_0(u_*)$, cannot be derived theoretically at present. These relationships must be found from micrometeorological measurements of $-\overline{u'w'}$ and the variation of wind with height. These empirical relationships are used in the theoretical Monin-Obukov equation.

II. OCEAN SCIENCE OPPORTUNITIES

A. INTRODUCTION

The ocean is a forced system and the wind stress is the direct or indirect forcing for many of the most important ocean motions. Unfortunately, wind forcing data have never been available in sufficient number or with the accuracy necessary to address most of these problems. Instead, oceanographers have tried to explain observed ocean response in terms of ad hoc forcing patterns or have made ad hoc adjustments to known forcing data to bring forcing, an ocean model and ocean data into rough agreement. The prospect of having adequate wind forcing information opens many exciting research possibilities. In particular, good forcing data will make it possible for the first time to test the physical ocean models that have been developed, especially if ocean field programs can be carried out concurrently with the flight of the wind satellite. Appendix B contains a discussion of open ocean models.

In this chapter we highlight various research modeling activities in which scientific advances are likely to be made, if the needed wind stress distribution becomes available. We emphasize the tremendous potential of studies related to El Niño. An El Niño project is currently attracting the attention of the U.S. and international oceanographic and meteorological communities. Special National Academy of Sciences (NAS) committees are making research plans for increased emphasis in this area because of the impact of the ocean temperature signal on weather over the U.S. Good wind data during such a program are essential and could be provided only by a satellite sensor. Daily ocean forecasting also may be possible (see Section IID).

Finally, we review some of the verification and validation experiments which should be considered before launch and after launch of a satellite with a scatterometer onboard. Since the scatterometer does not measure wind stress directly, it will be

necessary to invest in additional field studies to refine the present parameterization between radar backscatter and wind stress. Basic physical studies of the air-sea interface will be required and scientific understanding of small-scale air-sea interaction processes will be gained. It is conceivable that an equation relating σ^0 to u_* can be obtained that will produce the wind stress from the backscatter more accurately. This has yet to be demonstrated.

B. RESEARCH MODELS

Until about 20 years ago, large-scale ocean currents were thought to be essentially steady in time, with only small variations about a "climatological" mean state. We now know that many important current systems display pronounced temporal and spatial variability. The variability in the currents, moreover, is often associated with variability in the ocean thermal structure, including the sea surface temperature distributions that have an important relation to climate variability. We also know that the observed variability of many current systems is directly related to variability in the surface wind field. In this section we describe two general classes of ocean currents that are importantly driven by the wind stress and have fine scales compatible with the lifetime of a wind satellite.

Large-Scale Ocean Currents

A large-scale current system whose behavior is almost completely ascribed to changes in the wind field is the Somali Current system in the Western Indian Ocean. Each year this current goes through a cycle that involves a complete reversal of flow, which is linked to the Indian Ocean monsoon wind changes. Evidence from both observational (Leetmaa, 1972, 1973) and theoretical modeling (Cox, 1981; Lin and Hurlburt, 1981) supports this relationship. Direct observations of the onset of the northward-flowing phase show that it occurs within a few days of the local onset of southerly winds. Model studies also suggest that the response of the current to the

wind is rapid with large changes occurring within a week. Unfortunately all model studies have been carried out with *ad hoc* forcing patterns. Better knowledge of the surface wind field and its spatial variations is critical to improved understanding of the variability of this important current system. The Arabian Basin is an important area for oil transport and military operations. Further, the influence of the upper ocean in this area on the monsoon is considered a key element in climatic variations affecting the agricultural productivity of India.

Other elements of the large-scale tropical and equatorial current systems also are known to respond predictably to changes in the wind field. The best specific example is the El Niño phenomenon, in which warm water abruptly appears at the eastern boundary of the southern equatorial Pacific. Observational evidence (Wyrtki, 1975; Barnett, 1977), analytical studies (McCreary, 1976; Moore and Philander, 1977) and numerical simulations (Hurlburt *et al.*, 1976; Kindle, 1979; Busalacchi and O'Brien, 1981) all associate El Niño with low-frequency variations in the wind. In this model of El Niño, a large-amplitude Kelvin wave in the ocean is excited by a relaxation of the zonal component of the surface winds somewhere along the equator, and it rapidly propagates eastward until impact with the boundary initiates the coastal warming. In the central equatorial Pacific the large-scale current and thermal structure variability are also closely related to the surface wind field, but here it is the local winds that are important (Philander, 1979; Leetmaa *et al.*, 1981). Such important phenomena as the north-south meandering of the subsurface, eastward-flowing Equatorial Undercurrent may result from wind-generated equatorially trapped waves. Many of the analytical and numerical studies that have been carried out are based on wind fields analyzed from very sparse data. Since the nature of the equatorial ocean's response depends critically on the spatial distribution of the surface wind field, it is essential to monitor

the detailed structure of the wind field in this region on at least seasonal, annual and interannual time scales.

Over large areas of the equatorial regions and the southern hemisphere, a global surface wind field perhaps will be the most important input toward determination of the surface current field. Recent developments in modeling the oceanic mixed layer have demonstrated the feasibility of simulating the wind-driven flow in the surface layers (Pollard, 1977; Davis *et al.*, 1981). If surface altimeter data were also available, say, from TOPEX in addition to the surface wind field, a good estimate of the surface geostrophic flow also could be made (Cheney *et al.*, 1981). The resulting surface currents would provide an excellent estimate of the geographical distribution and variability of large-scale current systems in the open ocean. The modeled currents might also be studied in relation to the observed motions of satellite-tracked drifting buoys. Some limited studies already have been made between the drifter motions and conventional wind observations (Kirwan *et al.*, 1979; McNally, 1981); however, more studies with far better surface wind data are needed.

Another large-scale ocean current system that results from wind forcing is the Gulf Stream System. As reviewed by Fofonoff (1981), our knowledge of the Gulf Stream System has been expanded during the last two decades through the development and application of remote sensing techniques, including instrumented buoys and moorings (Schmitz, 1978) and infrared radiation imaging to map the thermal patterns of the ocean surface from satellites (Legeckis, 1978). Despite these advances in our ability to measure, an understanding of the dynamic mechanisms by which the Gulf Stream forms, develops, decays, and finally merges into the large-scale circulation of the North Atlantic has not evolved satisfactorily. It has not been firmly established whether the path of the Gulf Stream, including its separation from the coast at Cape Hatteras, is controlled by bottom topography (Greenspan, 1963; Pedlosky, 1965; Veronis, 1973), by the

distribution of mean wind stress (Stommel, 1948; Munk, 1950; Veronis, 1981) or by a mechanism yet to be determined. Leetmaa and Bunker (1978) show that the mean curl of the wind stress reverses sign near Cape Hatteras and is zero over a path that is surprisingly like the mean Gulf Stream across the Western North Atlantic. Fofonoff (1981) suggests that the position of the line of zero wind stress curl may be a consequence, as well as a cause, of the observed Gulf Stream location. Harrison (1981) has argued that such a relation between the Gulf Stream and the zero curl may have important consequences for the circulation of the entire subtropical gyre. These and other important questions about the large-scale current systems and their relation to the wind can be addressed only when adequate observations of the surface winds over the oceans are available.

Mid-latitude Mid-ocean Currents

Inertial-internal and quasi-geostrophic waves are further examples of time-dependent oceanic motions that may be generated directly by meso- and synoptic-scale atmospheric systems. Inertial-internal waves generally have periods of slightly less than the local inertial frequency, 1 day/2Ω sin (lat), have horizontal wavelengths of tens to hundreds of kilometers, and can have short vertical scales. They may be quite energetic (Fig. II-1). Because of their large vertical shear they very likely contribute to vertical mixing in the ocean (Munk, 1981). Quasi-geostrophic waves have periods of from several tens to a few hundred days, and wavelengths from a hundred to several thousand kilometers. Quasi-geostrophic waves have large vertical scales and little vertical shear, but because of their long time scales they cause large horizontal particle displacements and contribute substantially to horizontal mixing in the ocean (Rhines, 1977).

Inertial-internal wave generation has been studied for individual forcing events, like the passage of an idealized storm

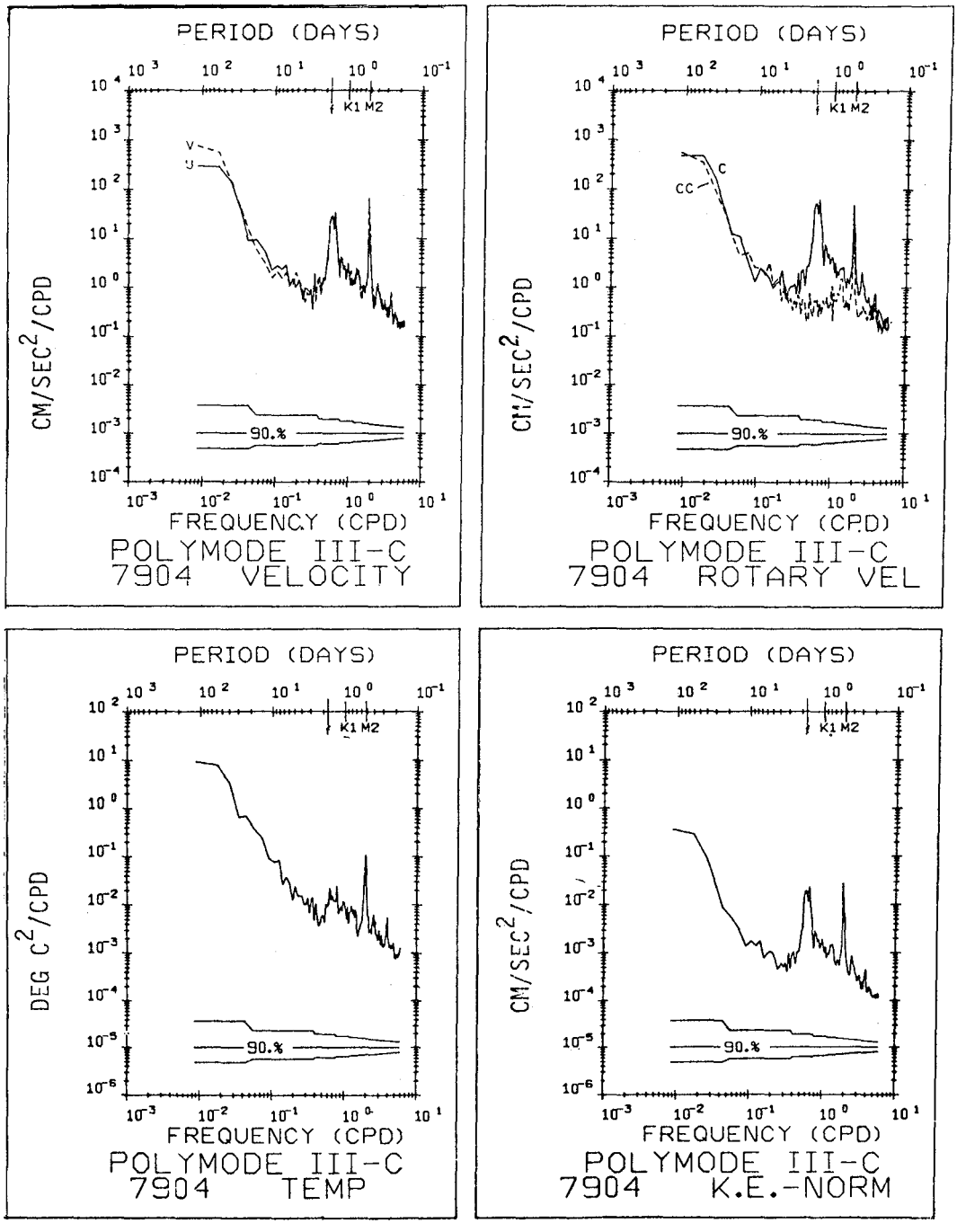

Figure II-1. Frequency spectra of velocity and temperature measured at 520 m depth in the subtropical central North Atlantic (from Koblinsky et al., 1979). The red low-frequency end of the spectra (period > 10 days) is the regime of quasi-geostrophic motion; the inertial-internal motions comprise the broad peak at periods of 2 days. (Corresponding wavenumber spectra are seldom available.)

(e.g., Price, 1982), and from a stochastic forcing perspective, in which a wind wavenumber-frequency spectrum is used to predict the statistical properties of the wave field (e.g., Käse and Olbers, 1980). Quasi-geostrophic motions are importantly forced by the curl of the windstress, rather than primarily by the stress itself. This requires even better wind stress information than does inertial-internal wave modeling. As above, both deterministic (e.g., White *et al.*, 1980; Willebrand *et al.*, 1980) and stochastic forcing (e.g., Müller and Frankignoul, 1981) studies have been carried out. In these types of studies details of the forcing pattern and spectrum can importantly affect the predicted response. The present discrepancies between model results and observations may result from inadequate models or inadequate forcing knowledge. At present we cannot say.

An important long-term goal of physical oceanography is to learn the overall energy balance for these kinds of oceanic motions. We need to identify and quantify their energy sources, and we need to understand how and where they ultimately give up their energy to mixing or to smaller (or larger) scale motions. Today we understand only some aspects of these problems. Satellite scatterometry holds the promise of providing the accurate and extensive wind stress measurements that are an essential element for learning the contributions of direct atmospheric forcing to the generation of half of the energy budget.

Models of Atmospheric Forcing

There are two complementary modeling approaches that are useful to understanding atmospheric forcing. In the first case, one can do an initial value problem, in which the model ocean is driven by a stress pattern prescribed in physical space. The product of this kind of calculation is a detailed simulation of some ocean variable (say thermocline height) also in physical space. This kind of modeling is essentially ocean forecasting (or, strictly speaking,

hindcasting) and is often the way that ocean models are tested for their physical dynamics or are used to interpret observations. Recent examples that include at least some treatment of both observations and modeling are those by Price (1982), who computed the inertial-internal wave response to a storm; by Busalacchi and O'Brien (1981), who computed the upper ocean response of the tropical ocean to large-scale interannual variations in winds; and by White *et al.* (1980), who computed the mid-latitude North Pacific thermocline response to purely local wind stress curl forcing.

In the second case, one can do the inherently statistical calculation of the inertial-internal and quasi-geostrophic wave "sea state." The atmospheric forcing is then taken to be the wave number and frequency spectrum of the wind stress, and the calculation gives back the wavenumber, frequency spectrum of the ocean's response. Recent examples include Käse and Olbers (1980), who computed some statistics of the inertial-internal wave sea state in the subtropical North Atlantic; and Müller and Frankignoul (1981) and Willebrand *et al.* (1980), who computed the quasi-geostrophic wave response for mid-latitudes. Consideration of this latter class of models best illustrates the shortcomings of currently available wind stress observations.

Sampling and Analysis Schemes

The projected sampling patterns and proposed analysis schemes for scatterometer data will provide nearly complete global synoptic scale coverage of stress at 6-hour intervals. This sampling scheme will be quite adequate for virtually the entire quasi-geostrophic spectrum of the wavelike fluctuations in ocean currents and should prove adequate for many initial value (i.e., deterministic) calculations as well. The high-frequency end of the spectrum required for the inertial-internal wave models is a subject that requires further research.

There are relatively simple ways to infer greater temporal resolution from scatterometer data. At least some of the

time-dependence of sea level winds can be thought of as frozen-field advection of quasi-stationary systems. For example, the wind shift accompanying the passage of frontal systems can be a very effective forcing mechanism for inertial motions. The rate of wind turning during a frontal passage is essentially given by the frontal propagation rate divided by the cross-frontal wind scale. Hence, high-resolution spatial sampling of wind stress patterns, which scatterometry can provide, together with standard operational meteorological procedures can be used in a space-to-time interpolation or prediction scheme.

There are phenomena for which this will still prove inadequate. For example, coastal sea breeze circulations have diurnal periods which cannot be viewed as frozen field advection. Fortunately, for most of the open ocean, where the dominant weather systems are synoptic scale, some approximations should be possible for the high frequency end of the spectral window.

C. EL NIÑO - A SPECIFIC EXPERIMENT

Background

El Niño is a large climatic fluctuation in the eastern equatorial Pacific. Every several years a large pool of anomalous warm water appears off Ecuador and Peru around Christmas time. During the year, it spreads westward across the equator inducing massive rains on tropical islands used to almost no rain. The fisheries of Ecuador and Peru lose an entire year class, because the young larvae cannot tolerate the abnormal ocean climate. The recent Los Niños were in 1976-77, 1972-73, 1968-69, 1965, and 1957-58. There is another interesting correlation with El Niño. These years also produced the most severe winters in the eastern half of the U.S. If we were able to forecast the occurrence of El Niño, we might be able to predict the likelihood of a severe winter in the northeastern United States. Such a forecast, if accurate, would

be of enormous value. At the present time, we do not understand how large, warm-temperature patches of ocean affect the weather thousands of kilometers away, although interesting atmospheric model studies have been carried out (Hoskins and Karoly, 1981; Webster, 1981). However, we do have some knowledge of the oceanic behavior which leads to El Niño.

We know that El Niño can occur when the winds cease to blow toward the west somewhere along the equator. We now believe that the region of weaker easterly winds occurs west of the dateline in October and November of the year preceding El Niño. The abnormal winds produce an internal Kelvin wave that propagates eastward toward Ecuador at speeds of 200-300 kilometers per day. When the wave front reaches the coast of South America it deepens the mixed layer and thermocline along the coast of Ecuador and Peru and north to Baja California. This deep surface layer isolates the cold water below so that the usual upwelling and entrainment of surface cold water is reduced, and a pool of warm water forms. Details of this complicated process are the subject of intense interest at present. If we could forecast the creation of the warm pool off South America, we might be able to predict very cold winters in the eastern U.S.

If our present ideas are correct, we should be able to make some prediction of El Niño if we measure the winds along the Pacific equator. The appearance of strong westerly winds would allow the forecast of an impending El Niño. If TOPEX were also in space we might be able to monitor the passage of the Kelvin wave as it moves eastward toward Ecuador. Using infrared sea surface temperature measurements, we would be able to verify from space if the wind change is producing the characteristic El Niño warm anomaly along the coast. Verification of the existence of warm water along the coast would justify the initiation of planning for a severe winter over the eastern U.S. a few months later.

The theoretical ideas for understanding the morphology (life-cycle) of El Niño have a sound basis. J. J. O'Brien and his students

have integrated a simple model of the Tropical Pacific forced with a ship wind analysis field for 18 years (1961-1978). They demonstrate that the model can reproduce the sea level variations and sea-surface temperature variations assuming that thermocline thickness anomalies relate inversely to sea surface temperature anomalies associated with each of the Los Niños in this 18-year period (Fig. II-2). Busalacchi and O'Brien (1981) discuss the calculation for 1961-1970. The remainder of the results are in press (Busalacchi, *et al.*, 1982). In Figures II-3 and II-4, we illustrate the observed and calculated anomalies for the 1972-73 event.

A research project of El Niño and its effect on the atmosphere is under study by the National Academy of Sciences (NAS). These climatic effects are described for the 1976-77 period in a draft of the NAS report.[1]

> The tradewinds in the tropical Pacific were unusually strong for a prolonged period during late 1974 and most of 1975. Further the southeast Trades move aggressively into the far western equatorial Pacific reaching nearly to Indonesia. Sea surface temperatures (SST) along the equator from South America to the dateline were relatively cold due to the upwelling of cold water induced by the stronger tradewinds. Accompanying these SST changes was a rise of sea level over a huge region of the western Pacific and a fall of sea level along the coast of South America. One extreme phase of the Southern Oscillation cycle had been reached.
>
> In late 1975 there were indications that important, unusual changes were taking place in the ocean and atmosphere in the tropical Pacific. Sea level pressure at many eastern and central South Pacific islands began to

[1] The following is from the prologue of "Southern Oscillation Program: A Scientific Prospectus," NAS, 1981.

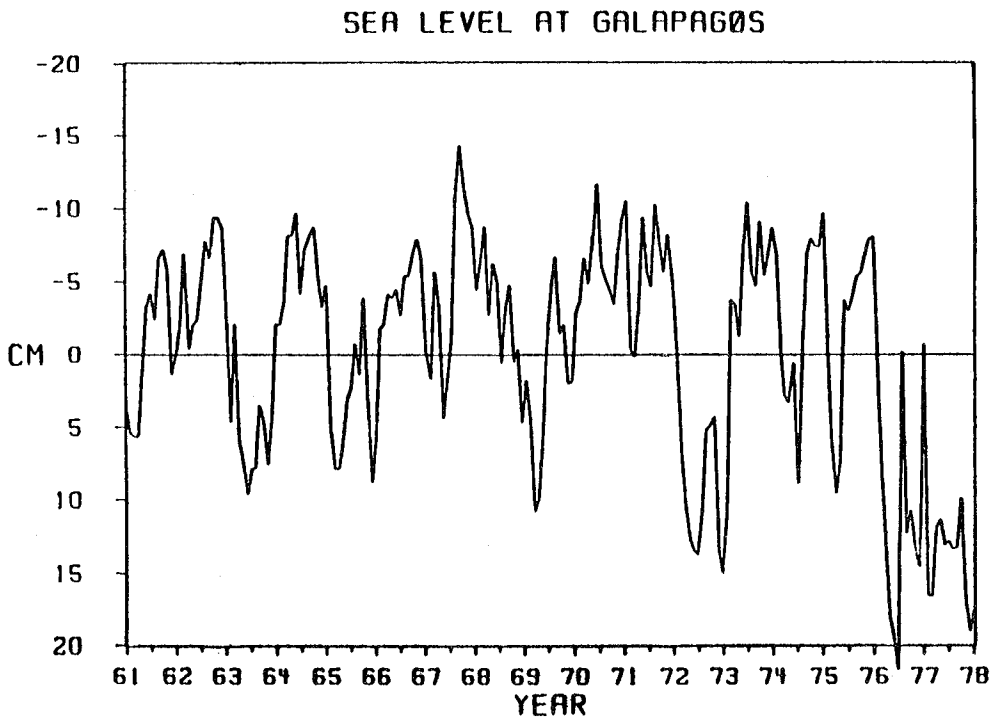

Figure II-2a. Sea level variations associated with Los Niños during 18-year period.

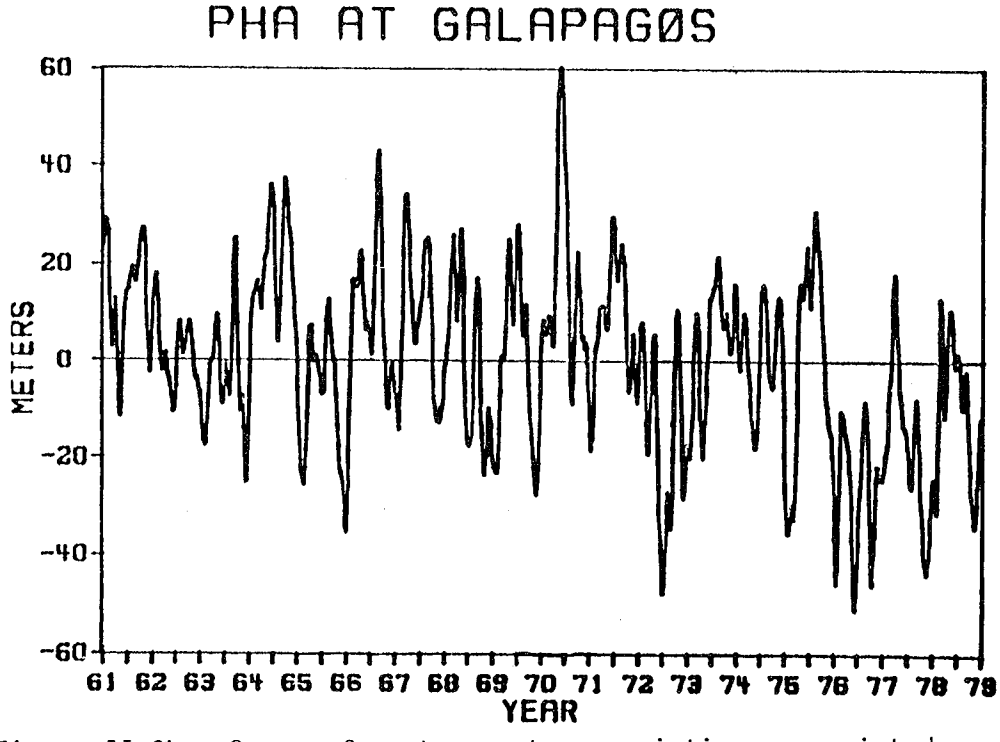

Figure II-2b. Sea surface temperature variations associated with Los Niños during 18-year period.

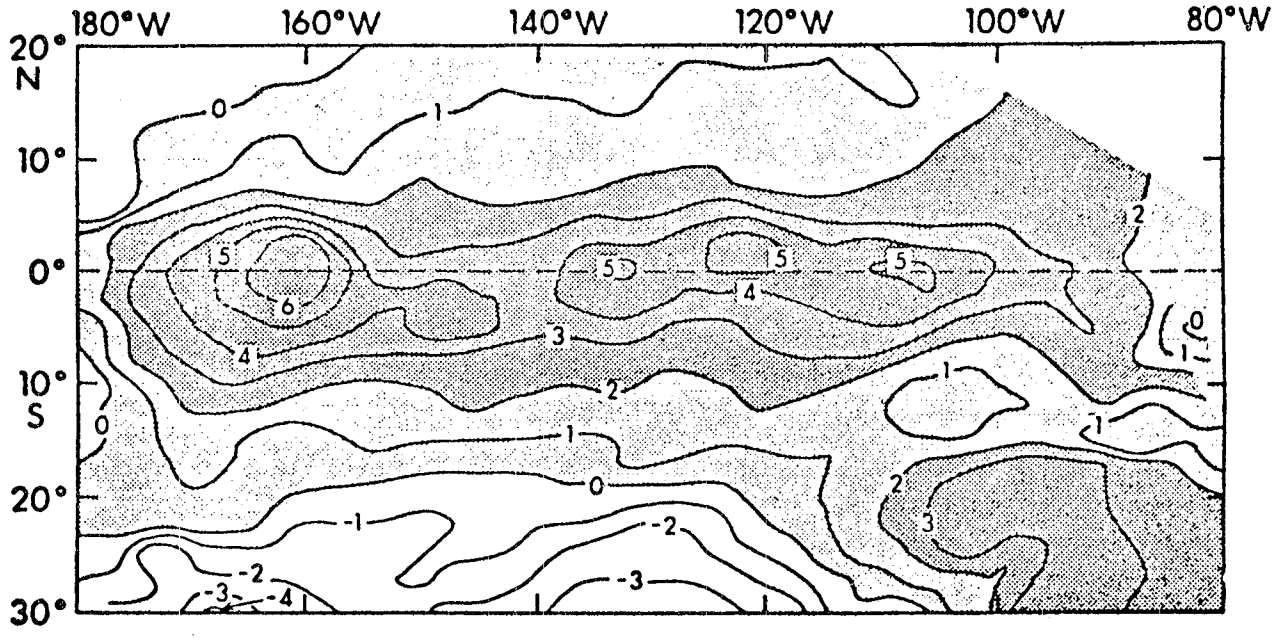

Figure II-3. The sea surface temperature difference between December 1972 El Niño and December 1973 anti-El Niño. Contours are in ^{o}C. For data bases, see Ramage *et al.* (1980). A positive number means 1972 December is warmer than 1973 December.

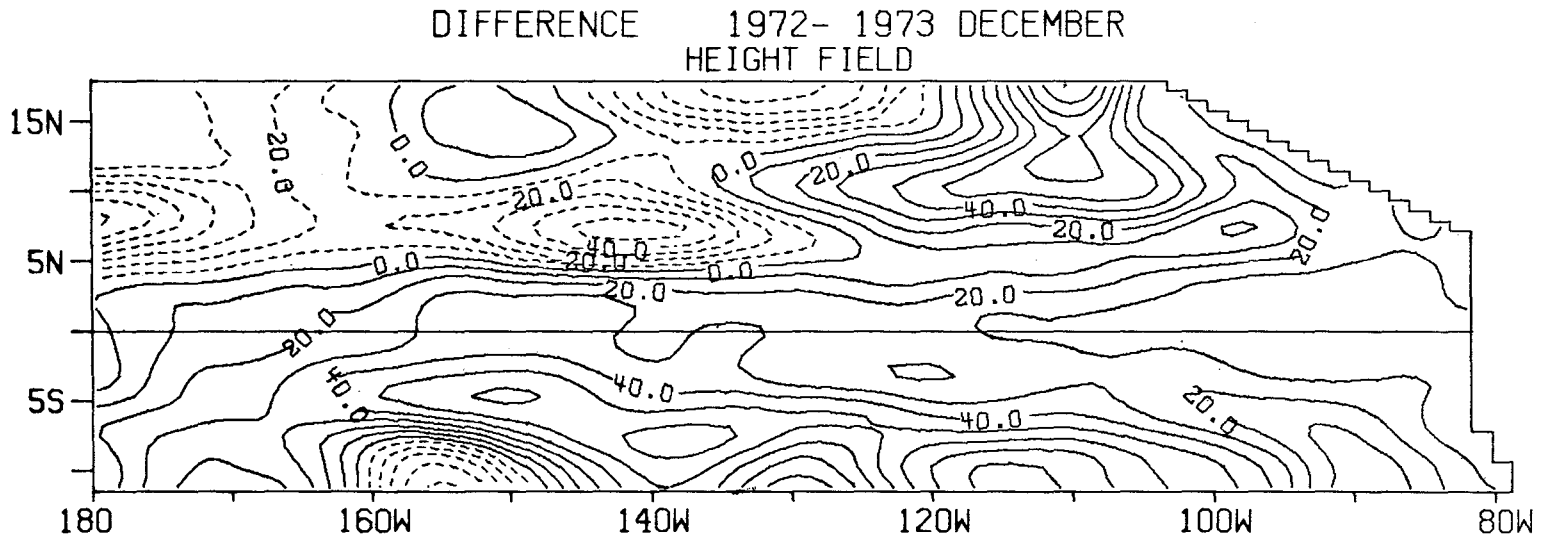

Figure II-4. Calculated thermocline depth anomalies for 1972-73 El Niño event. Contours in meters.

fall quite rapidly, signalling a weakening of the South Pacific high and the associated tradewind circulation. Nearly simultaneously the southeast Trades began a retreat from the western Pacific. By early 1976 sea surface temperatures began to rise rapidly along the coast of Ecuador and northern Peru and in a belt along the equator extending westward to the Galapagos Islands. Sea level in this region also rose rapidly. This rise was accompanied by a fall of sea level in the western Pacific. By August 1976 the sea-surface temperatures in the eastern Pacific had warmed to 4°C above normal. With the warm surface waters came a disruption of the local biological communities and flash flooding along the coast of Peru.

During the second half of the year the abnormally warm sea-surface temperatures spread westward across a broad belt of the equatorial Pacific [Fig. II-5] until they extended for nearly one quarter of the earth's circumference. Perhaps in response to this change in the SST pattern, the Intertropical Convergence Zone shifted southward from its climatological mean position near 7°N to near the equator bringing heavy rainfall to the Line Islands and a long zonal region about the equator that normally experienced only minor precipitation. Over a large region of the western equatorial Pacific, the zonal wind component had actually reversed its direction of flow affecting a clear separation between the northeast and southeast Trade winds. The Southern Oscillation had reached its other extreme.

By late 1976, SST along the South American coast had returned to near normal but the abnormal warmth across the central Pacific equatorial belt persisted and was associated with heavy rains at stations located in the vicinity of the dateline. The heavy rainfall in the equatorial central Pacific during the 1976-1977 Northern

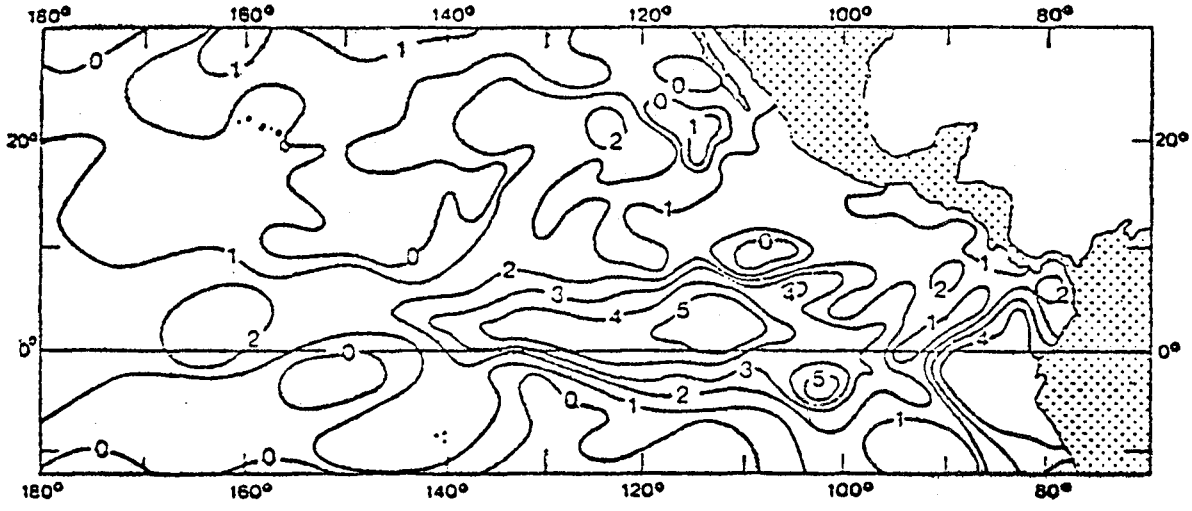

Figure II-5. Sea surface anomalies (^{o}C) during warm (El Niño) and cold epochs in the equatorial Pacific, July 1972. Data from the National Marine Fisheries Service, Fishing Information.

Hemisphere winter resulted in large releases of energy to the tropical atmosphere in unusual areas. For reasons that are not yet fully understood, the global wind systems, of which the mid-latitude jetstreams are a part, responded dramatically. The subtropical jetstream across the North Pacific strengthened. The Aleutian low deepened, and the Polar jet was deflected northward over western Canada and southward of its normal position over the eastern United States. Figure II-6 shows the resulting surface air temperature anomaly that occurred during the extreme 1976-77 winter, a winter that saw the nation's heating oil/energy reserves reduced to nil. It was also during this winter that the western parts of the United States experienced some of their worst droughts on record. Comparably large changes in the jetstream have, on similar occasions, brought serious droughts to the Hawaiian Islands, Northern Australia, Indonesia, and parts of the Philippines.

The Ocean and Interannual Climate Variability

The ocean plays many roles in the earth's climate system, almost all of which relate to its ability to store and transfer heat and to its exchange of heat with the overlying atmosphere. This coupling of the atmosphere and ocean is fundamental to the climate system but is poorly understood, because of the lack of adequate observations for the analysis of the highly non-linear processes involved. Moreover, changes in external forcing (e.g., insolation, anthropogenic effects, etc.) can disturb the balance of the climate system and require the establishment of a new equilibrium between the ocean and the atmosphere. It is only through the use of a variety of ocean models that the mechanics of ocean-atmosphere interaction can be discerned and an evaluation made of their role in the maintenance and change of climate on a variety of time scales.

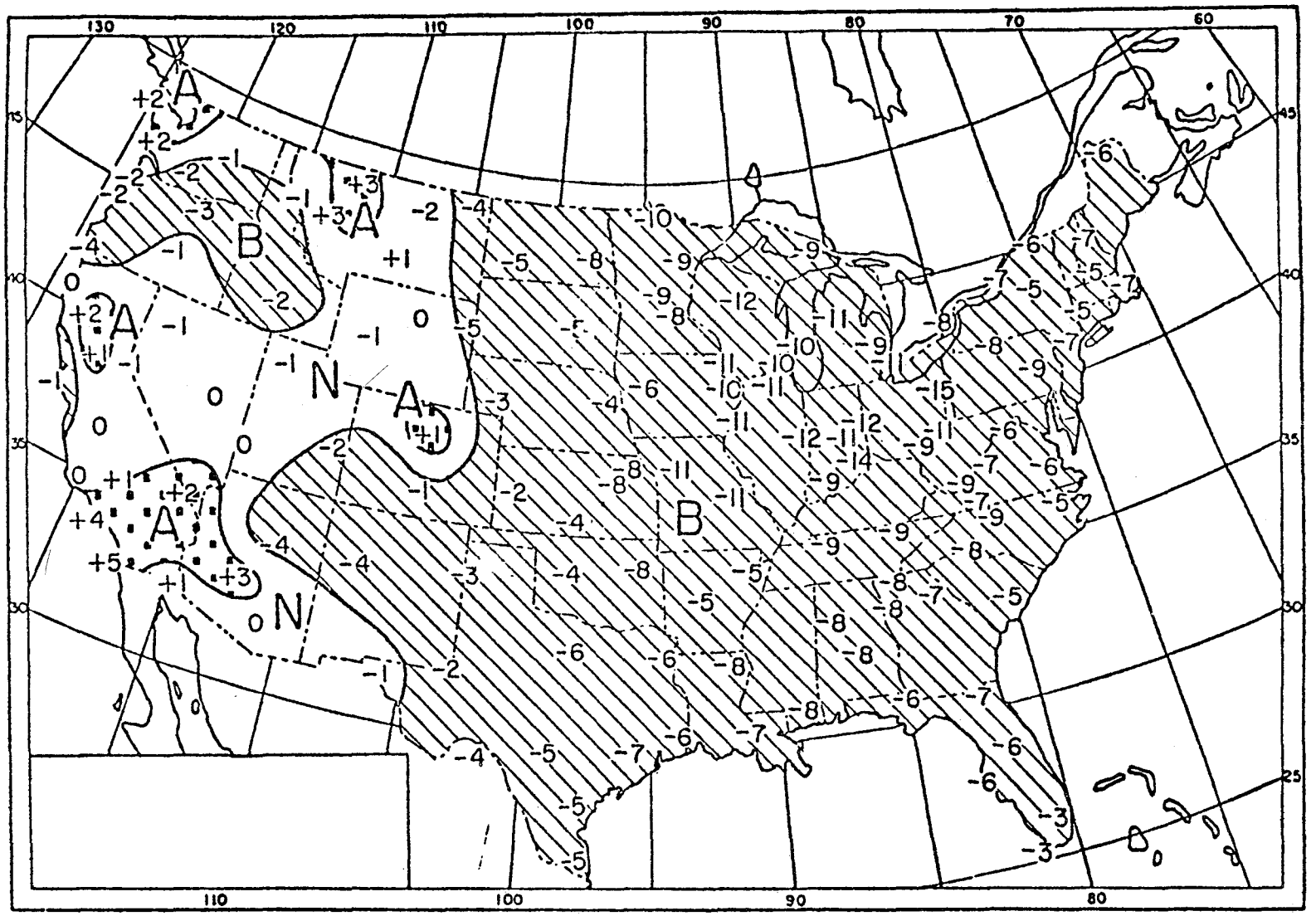

Figure II-6. Observed mean temperature anomalies, December 1, 1976, through January 31, 1977 (^{o}F). The letters A, N, B refer to temperatures above, normal, or below a 30-year mean. (Namias, 1978, Figure 1.)

On a monthly time scale, variations in the heat content of the oceanic surface mixed layer can lead to substantial sea-surface temperature (SST) anomalies, to which the atmosphere may in turn respond. On longer time scales of seasons to years, there are large-scale variations of ocean circulation which may transport heat from one part of the ocean to another and thereby lead to local climate anomalies (e.g., El Niño). In addition to their role in climate, such oceanic variations are important in the transport of essential nutrients for fisheries and in the transport and dispersion of man-made wastes in the ocean.

Our ability to study the coupled ocean-atmosphere system is limited today by a lack of knowledge of the physics of the boundary layers on either side of the air-sea interface, and by an inability to measure on a global basis the fluxes across this interface. We are also limited by the unavailability of computer resources required for a comprehensive modeling program. Such a program is needed to examine the ocean's sensitivity to atmospheric changes and to develop adequate models of the ocean's role in climate. The availability of scatterometer winds will allow us to study El Niño and other climatic effects.

Although considerable effort has been directed to the analysis of historical data sets and the collection of new oceanic surface data, our knowledge of surface wind stress, net surface heat flux, and the detailed thermal structure of the ocean on even the large scale is still quite limited. Greatly expanded data sets are needed to document the climate variability of the ocean and to support the development of improved models for climate research.

If a scatterometer could return the wind data in a timely manner, it is feasible to attempt predictions of severe winters over the U.S. up to a year in advance. This is an exciting prospect to consider.

D. SATELLITE DATA AND OCEAN FORECASTING

The U.S. Navy is developing a capability for operational forecasting of mesoscale and large-scale oceanographic features with oceanographic horizontal scales of 10 km or more and time scales of days to months. The following discussion is designed to show the need for satellite wind stress data in ocean forecasting and to show how these data could be utilized in the forecasts.

To understand the important role that satellite data must play in ocean forecasting, it is useful to compare the oceanic with the atmospheric forecasting problem, the latter of which has been investigated much more thoroughly. Meteorological forecast models are initialized from observations which have been analyzed and dynamically balanced in some way. The principal object is to forecast waves and eddies with scales of a few thousand kilometers that are marginally to adequately resolved by the observations. The initial state is the only data input upon which the forecast normally depends. Time variations in external forcing functions, such as sea surface temperature, are ignored.

With a few exceptions (Haney, 1980; Clancy and Martin, 1981), it is felt that the above approach is not feasible in oceanography today, because the subsurface observational network in space-time is much too coarse, considering that the spatial scales of important ocean currents and eddies are typically about 100 km. A dynamical ocean forecast initialized from such inadequate data would be useless - there would be aliasing of large-amplitude, small features to larger scales, and the forecast would not evolve in a dynamically realistic manner. Satellites provide the only real prospect for globally observed fields which are operationally useful as initial data or forcing functions for ocean forecasts. At present there appear to be good prospects for well observed fields of sea surface elevation, surface wind stress, and sea surface temperature that could be used in ocean forecasting.

The simplest dynamical ocean model with potential operational utility is a two-layer, reduced-gravity model with an active upper layer and a lower layer which is infinitely deep and at rest. Such models predict thermocline height and upper ocean current. They may be initialized by altimeter data alone, except near the equator where wind stress data also are required. Reduced gravity models have shown a remarkable ability to simulate certain ocean phenomena, e.g., the equatorial Pacific (Kindle, 1979; Busalacchi and O'Brien, 1980), the Indian Ocean (Cane, 1980), the Somali Current (Lin and Hurlburt, 1981), the Gulf of Mexico (Hurlburt and Thompson, 1980; 1982), ocean response to a hurricane (O'Brien and Reid, 1967; Chang and Anthes, 1978; Price, 1981), the Gulf of Guinea upwelling (Adamec and O'Brien, 1978), and the Alboran Sea (Preller and Hurlburt, 1982).

A second type of potentially useful ocean forecast model is an N x 1 - D mixed layer model (Clancy and Martin, 1981). At each grid point a one-dimensional mixed layer model is used to forecast subsurface (upper few hundred meters) fields with high vertical resolution. The all-important forcing functions at the surface currently are obtained from an atmospheric forecast model. The subsurface initial state is obtained from an operational analysis. Scatterometer wind stress data would be of great benefit here. For example, the data could increase the accuracy of the forcing functions from the atmospheric model by increasing the accuracy of the data input (Cane *et al.*, 1981). The scatterometer data also could directly provide one of the most important forcing functions for the N x 1 - D model when it was being used to update the subsurface initial state (provided the same field was used in initializing the atmospheric model giving the forecast forcing functions). That is, the model would be integrated forward in time using scatterometer-derived wind stress data as it became available.

The wind data would be required on a daily basis, but much longer repeat intervals (up to a month) probably could be tolerated for the altimeter data. The spatial resolution of the wind stress

data should be sufficient (100 km or better) to resolve the wind stress curl associated with atmospheric cyclones and anti-cyclones. Winds as close to coastlines as possible are highly desirable. In these regions horizontal resolution should be 20 km or better. The altimeter tracks must be designed so that the spatial resolution is sufficient (25 km or better) to resolve currents and eddies with substantial signatures in the sea surface elevation.

Thus, we envision a hierarchy of ocean modeling efforts which would be developed given good wind stress data. We have discussed improved research models for individual ocean basins. Regional or limited area models for process studies, such as the effect of individual storms on the upper ocean, also will be calculated. We have highlighted an intriguing ocean-climate problem, namely, the prediction of an El Niño. Finally, in this section we anticipate the day-to-day calculations of a world ocean model for practical use.

E. VERIFICATION/VALIDATION EXPERIMENTS

A great deal of scientific investigation remains to be done before and after launch of an S^3 sensor, in order to demonstrate the global validity of algorithms which compute either winds and their stress or stress directly from backscatter. The latter approach has not been accomplished successfully. Efforts can be grouped logically into two areas: (1) improvements in the knowledge of radar wave-sea surface interaction physics, and (2) better understanding of the governing relationships for capillary wave wind stress interaction in the deep, open ocean.

The theory of microwave backscatter from a realistic ocean surface needs to be developed.

The backscatter effects of the following processes must be understood: atmospheric stability, fetch and duration, swell, wave breaking and foam.

The physics of electromagnetic backscatter for an idealized wavy surface is simple and well understood, but backscatter from a realistic ocean surface with breaking waves, foam and spray is still unavailable. A well-founded theory of radar backscatter is needed to provide guidance in the choice of better models of backscatter versus wind speed (i.e., what parameters are important?).

Interpretation of σ^0 in terms of τ_0 requires an understanding of the relationship between atmospheric turbulent momentum transfer in terms of the $\overline{u'w'}$ cospectrum and the Bragg scattering waves, and the dependence of this relationship on such variables as atmospheric stratification, sea surface temperature, wave age, presence of swell and currents, breaking waves, foam, and precipitation. The downward flux of momentum cannot generate waves. Immediately above the wave surface, the fluctuations in momentum produce pressure fluctuations, which in turn generate the waves. Moreover, a stress in general produces motions with vorticity. Since wind-generated waves are dominantly irrotational, it remains to be proved that τ_0 or u_* will relate better to backscatter than the wind alone.

Observations of complete wave spectra for deep, open ocean surface waves that cover the longest waves present and extend continuously through capillary wavelength will provide extremely useful data.

We have not yet measured the capillary wave spectrum of the deep ocean. The rate of growth of surface waves was predicted by Miles (1960). In the Miles theory, $\beta_k = 2(\mu_k\omega_k - \nu_k)$, where μ_k is a coupling parameter between the atmosphere and the sea, ν is viscosity of the water, and ω_k and k are frequency and wave number of the wave. Plant and Wright (1977) found this predicted growth rate to be reasonable for capillary-gravity waves but not for gravity waves, as have other investigators. Viscosity in the water plays an important role in the theories for both types of waves. The variation of viscosity with temperature is from $\gamma = 0.01787\ cm^2s^{-1}$ at 0°, to $\gamma = 0.01004$ at 20°C, a substantial change. Several recent theoretical improvements on these theories have been or are about to be published

that need experimental investigation. Are the wave spectra at intermediate wave numbers important to scatterometer return, and are they different from the same u_* and fetch? Does this depend upon ocean temperature?

The σ^0 values from SEASAT's SASS were found to be proportional to mean wind speed long after the surface wave spectrum was saturated for a given wind speed at intermediate wave numbers. Many workers have found that the wave spectrum at the high frequency end continues to grow with the wind speed (e.g., Mitsuyasu and Honda, 1975; Katsaros and Richmond, 1981). Is this due to a real continued increase in the amplitude or to an increase in the fraction of the sea surface covered by the capillary waves? Do breaking waves produce blobs of water with strong backscatter properties?

We need to understand how stress is affected by variations in the gravity wave spectrum.

It has not been shown that the radar backscatter of the Bragg scattering waves is always the same for the same mean wind stress. We do not understand how σ^0 varies with the total surface stress - or some fraction of it - under all conditions. What are the influences of currents and current shears, and what are the influences of swell from distant storm centers? What is the influence of the "age" of the wind waves (fetch and duration dependent) on the Bragg scattering portion of the wave spectrum? It has been shown that backscatter is not a junction of fetch in a constant offshore wind.

Strategy for Verification of Experiments

Many of the topics described above could be attacked singly. Some could benefit from preliminary tests in a facility such as the IMST (Institute Mechanique de la Statistique de la Turbulence) wind wave tank in Marseilles (Coantic and Favre, 1973) or the wind wave tank at CCIW (The Canadian Center for Inland Waters). A comprehensive scatterometer verification experiment, in which the atmospheric, oceanic, and electromagnetic measurements were performed

simultaneously, preferably at two latitudes and/or in two seasons, would be most valuable. To answer any of these questions conclusively, a major, well-thought-out experimental field program is required.

The above recommendations reflect the desire of both meteorologists and oceanographers to obtain a deeper understanding of the physical phenomena involved in scatterometry. It is already clear that the winds obtained by the SEASAT SASS are more accurate than the winds reported by transient ships. In addition, the global wind fields and wind stress fields produced from the combination of conventional data and SASS data are far superior to any conventionally produced fields. These recommendations reflect a desire to do even better.

III. MINIMUM SCATTEROMETER REQUIREMENTS

A. INTRODUCTION

The previous chapters have reviewed our past knowledge and capability of obtaining wind data over the ocean and have outlined some new scientific opportunities for ocean research. Although S^3 was not asked to design a satellite system, the working group spent a considerable amount of time attempting to understand the limitations and compromises of a satellite observing system. From this background, we determined a set of minimum spacecraft and ground station requirements in order to accomplish the major scientific opportunities and operational uses for winds from space.

The research topics discussed in this report require a variety of accuracies and intervals between measurements of surface stress. There are also requirements for meteorological science and for operational and commercial usage. To propose a system which would satisfy all possible users is beyond the scope of this report.

The requirements listed below will satisfy many ocean science, meteorological and operational needs. In particular, they will provide adequate data for large-scale ocean circulation problems like El Niño and will dramatically improve our knowledge of the location of storm centers and other storm characteristics. We believe that the minimum requirements for a satellite wind stress system will receive the support of a significant portion of the science and operational communities. Appendix C discusses the feasibility of flying such a system and some of the trade-offs involved. While there are a number of possible system scenarios, *we recommend that NASA proceed with a formal study of a system to meet at least the minimum data requirements.*

B. PLATFORM SPECIFICATIONS

Measurement Accuracy

The SEASAT Program demonstrated (Brown, 1982; Jones *et al.*, 1982) that accuracies of ±2 m/s or 10% in wind speed and ±20 degrees in wind direction were achievable with a scatterometer. Since this program

also encompassed the requirements of all the potential research and operational users of the projected NOSS Program, it must be deemed a reasonable standard. We strongly recommend that every effort be made to remove any bias (offset) in the errors; randomness of errors becomes especially important as longer period information is sought.

An accuracy of 2 m/s or 10% (whichever is greater) in wind speed and ±20 degrees in wind direction as met by SASS and designed for NOSS must be maintained.

It is recognized that, at low wind speeds, accuracy will degrade at the outer edge of the swath. It seems reasonable to permit the resolution (see following subsection on Spatial Resolution) to degrade to 100 km for wind speeds below 6 m/s in order to achieve the desired wind speed accuracy. In addition, we recognize that the scatterometer has proven accurate for wind speeds to approximately 30 m/s. Assuming the backscatter signal continues to increase with increasing wind speed above 30 m/s, the instrument design should be capable of measuring the signal return for winds up to at least 100 m/s, as a goal.

Wind direction is important at wind speeds down to 3 m/s. However, at low wind speeds the errors in wind direction increase. It seems reasonable to allow horizontal resolution to degrade to 100 km below 6 m/s for determining wind direction to within ±20 degrees.

Spatial Resolution

The wind, and thus the wind stress and the curl of the wind stress, is variable at all spatial scales. Since we have never had adequate oceanic wind fields, we do not know the actual distribution of wind in wavenumber-frequency space. There is no simple minimum scale of resolution other than "the finer the better." Additionally, the finer the resolution, or cell size (see Appendix A), the closer one can come to the coast for special studies of upwelling and other near-shore ocean events and the less data are lost when atmospheric liquid water contaminated cells are discarded. For the purposes discussed above, the maximum resolution is 50 km; finer resolution to 10-20 km is highly desirable. At this resolution one can locate storm systems very well and resolve their stress curl marginally-to-well.

If a horizontal resolution of 50 km is utilized, there appear to be certain instrumental direction biases when the wind direction gradient is large, such as near atmospheric fronts. If a 10-25 km spot size is chosen, these directional biases may be minimized.

The wind field should be supplied on scales of 50 km.

From the instrumental perspective, resolution and accuracy are not independent. Accuracy is a function of the signal to noise ratio, which depends on the area being sampled, particularly at low wind speed when there is little sea surface structure to scatter the incidental microwave signal. For this reason it is useful to specify different requirements for different wind speeds.

Wind Speed	Requirements
$\leq$ 3 m/s	None (light and variable)
$>$ 3 $\leq$ 6 m/s	$\pm$ 2 m/s, $\pm 20°$, 100 km resolution
$>$ 6 $<$ 100 m/s	Larger of $\pm$2 m/s, or 10% of wind speed, $\pm 20°$, $\leq$ 50 km resolution

Observational Coverage

Coverage is here defined as the frequency at which a field of surface stress vectors is available for a given area. Satellites provide a high density of observations within their swaths. However, one must generally use data from more than one pass to construct a field of data over the area of interest. Thus coverage is a function of swath width and orbit configuration. Also of concern is the time it takes for some part of the satellite swath to revisit a particular spot, since this defines the minimum frequency that time series will resolve. To avoid aliasing the wind stress data, observations must be made on a time scale at least two or three times shorter than that of the wind events under study. Given a storm frequency of around 4-7 days at middle latitudes, a sampling frequency of at least every two days is desired and more rapid coverage is highly desirable.

We require that the wind vector at 90% of the points at the equator and also at 35 degrees North be observed to within 50 km at least every two days.

Directional Ambiguities

The SEASAT SASS system gave multiple solutions for winds, each being near the same magnitude, but with 2 to 4 possible directions for each observation. This was a result of the availability of only two directional looks at a given cell by the passing satellite. In many cases identification of the correct vector ("de-aliasing") is possible with detailed examination and further data sources. However, this process is time consuming and requires expert human intervention. It has been demonstrated by simulation techniques (see Appendix A) that the directional ambiguity problem can be largely overcome by adding a third antenna to each side of the scatterometer for another independent directional look, and by utilizing some combination of V and H polarization measurements. We consider it essential that this be done.

Preliminary studies seem to indicate that a 2-sided scatterometer instrument flown at an appropriate altitude and orbit is required in order to meet the revisit specifications. The orbit should be chosen to allow data recovery from 65°S to 65°N latitude as a minimum requirement. Some users would desire coverage at higher latitudes when the Arctic Ocean is ice-free.

> *The antenna and polarization design must be sufficient to allow determination of a wind stress direction with no more than 2 aliases which are nearly 180° out of phase at least 90% of the time.*

Navigational Accuracy

Location of a cell in earth coordinates, both for overlay with cells from other antennas (co-registration) and for gridding of the final data, may impose more stringent requirements than our spatial resolution on satellite pointing control, resolution, and data processing load (see Appendix A). Accurate co-registration of cells can minimize wind vector errors due to gradient conditions. To the extent that relaxing the absolute location requirements can simplify the satellite and data system, we feel that the final location of a stress vector on the earth within 50 km of its true position but

relatively accurate (typically ±10 km) in its relation to other vectors in the swath would be satisfactory.

Absolute position location of data within 50 km is satisfactory. Relative position location between vectors of ±10 km is the minimum requirement.

Atmospheric Liquid Water Determination

At scatterometer frequencies, backscatter power received at the antenna is primarily a function of surface roughness and liquid water droplets in the atmospheric path of the radar signal. For the purposes of measuring the ocean surface stress, the roughness is the signal and the atmospheric water is the noise. Moore *et al.* (1982) have shown that the contamination from precipitation and cloud liquid water droplets can significantly degrade the scatterometer-computed wind vector. Because the greatest stress input to the ocean is in the vicinity of storms where there are often areas of rain, it is vital to identify those cells which may be water contaminated. There is some promise (Moore *et al.* 1982; Wentz, 1981) of providing the capability to correct for this liquid water contamination by the use of a multi-frequency passive microwave radiometer that measures the atmospheric liquid water content in each cell. At minimum, it is essential that there be some way to identify cells with liquid water contamination so that the cell can be tagged. Note that if it is not possible to correct stress values for water contamination, and if a means of tagging rain contaminated cells is available, smaller cell size becomes desirable. Otherwise, a 10-km thunder shower would cause all data over a 50-km observation region to be discarded.

The ability to detect atmospheric liquid water is an essential component of any scatterometer program. The minimum requirement is a flag for amounts of liquid water which hinder scatterometer accuracy. This should be done with a resolution equal to or higher than the scatterometer cell resolution.

Length of Mission

Most oceanic time scales are long, compared with atmospheric scales. A mid-latitude atmospheric storm lasts a few days; a Gulf

Stream Ring may exist for a few weeks to a few years. Weather prediction models are run for a few days; atmospheric general circulation models might be integrated for several weeks. Almost all open ocean models are run for months to years.

In order to have wind data for all seasons and for at least one repeat of a season, the scatterometer mission should run a minimum of 18 months. It is desirable to have continuous wind data from space.

A minimum mission of 18 months is required for the wind stress scatterometer.

C. S^3 DATA DELIVERY

The details of data processing and delivery are complex and are discussed in more detail later in this section. Overall, it is sufficient to say here that we consider satisfactory data delivery to be one of the most vital concerns of the ocean science community. The history of other ocean-oriented satellite programs is not encouraging in this respect. Timeliness of data processing is most important in that if data processing time does not keep pace with the data flow, backlogs quickly develop and it can become literally years before the data are made available to the research community. (This implies that the software algorithms should be developed before the launch.) The vast majority of the data are then never really processed and are lost. When data are not quickly processed and archived and are not made available in a usable format, the scientific community will not use the satellite data and a multi-million dollar satellite is wasted.

Data available in satellite orbit configuration are awkward to use as a global data set. Meteorologists and oceanographers are very familiar with weather data that have been mapped onto a latitude-longitude grid for a fixed time. They are called earth-gridded data. If the data are stored in a 3-dimensional matrix where the location in the matrix designates latitude, longitude and time, then the data are easily used for all purposes.

Availability of data as earth-gridded stress vectors in a timely manner for scientific projects is essential.

Our experience with the SEASAT scatterometer data set shows that an efficient, highly capable data processing and delivery system must be in existence before the next scatterometer mission is flown. Without such a system, the stress measurements will have no operational value and reduced scientific value. A fully satisfactory system must be capable of processing all relevant data. It must be able to accomplish processing as fast as the data are obtained, with perhaps some time lag for the bulk of the data if it is not required for operational use. It was recognized that a real-time (6-hr) data processing facility for global data was required only for operational users. However, there are selected and important research studies which would need rapid (2-3 weeks) data availability for limited areas. To provide near real-time coverage only for research projects may be too costly. The system must have a means of delivering scientific outputs quickly while providing fast methods of sensor control, data indexing and validation. This scientific data delivery section is meant to give an overview of the proposed paths for ocean surface stress measurements from sensor to user. These descriptions are not meant to specify explicitly each component required, but rather to illustrate data pathways and to describe the requirements for data availability and processing methodology. As such, this is a series of recommendations which will require additional optimization before implementation. Perhaps the most important function is to indicate the magnitude of the data processing task presented by a satellite scatterometer.

General Assumptions

Raw Data:

S^3 satellite/sensor package generates 8-10 Kbit/s real-time data stream at 10-km resolution, or 0.8-1.0 Kbit/s at 50-km resolution.

A primary requirement of the wind processing algorithms is knowledge of spacecraft location, attitude, configuration and observation times. An interleaved data stream ensures that these ancillary data are available for direct broadcast and minimizes impact on space-earth links.

A special-purpose data buffer at the central spacecraft data nexus (e.g., FNOC/Monterey) separates S^3 and spacecraft clock/attitude data, reformats and forwards to S^3 processing activity via low-speed data links (9.6-19.2 kbits/s). This would be for an operational satellite.

This technique minimizes bandwidths needed to distribute data by reducing high rates (~ mbits/s) to low rates (~ kbits/s) at a central site. It further ensures inclusion of appropriate additional parameters needed for wind processing (e.g., clock correction, attitude offsets, spacecraft configuration, ephemeris).

Ground Processing Design

Processing activity will generate algorithm-time-location-quality tagged wind stress (or neutral wind) global matrices and will provide them to an archive facility.

This procedure probably means archiving raw data. Investigators whose requirements are not met by the standard output will thus have the option to reprocess data to meet special needs. Most investigators do not wish to undertake such tasks as data location and gridding, or they may not be able to do so. Embedding this additional information with the wind stress allows ready assimilation of the data by the general community.

Maximum time delay between observation and availability of gridded surface winds is 6 hours for operational use.

If it is intended that the resultant wind products will have operational utility, six hours is the weakest constraint which assures that utility. The use of global data for research would proceed at a more leisurely pace.

The intent of a User Interface Facility (UIF) is to provide data directories and regional products to investigators in a straightforward way.

A UIF will maintain catalogs of, for example, current data availability, location, and sensor health. Many of the present

systems concerned with providing user access to satellite data or data products do not in general keep all ancillary data on hand, which is a considerable hindrance.

A User Interface Facility will have interactive user accessible paths (≈30) for near-real-time data access.

Direct access via dial-up computer terminals seems to be an excellent method to accomplish these objectives. The number of ports is an estimate based on a projected number (1982); it is a minimum, and more may be needed.

The user community will be responsible for data validation; NASA will supply the resources for this activity.

A strong point in favor of the projected data delivery system is that it advocates compartmentalized responsibility and authority for various phases in a well structured way. The members of the S^3 committee believe that it is in the oceanographic community's interest to understand the basis of the satellite-derived surface stress product, that no currently constituted group has the requisite expertise to perform this function, and that consequently the community as a whole is best served by direct participation in the validation process. If the scatterometer were on a Navy platform, the Navy probably would be expected to assume principal responsibility for developing a validation plan for operational use.

The central ocean stress archive and user interface facilities need not be separate. For cost reasons one may wish to combine parts of them. They have been separated to illustrate the spectrum of functions required for scientific utilization of sea surface stress data.

An important issue is the question of instrument and algorithm calibration. It has been agreed that a period of one year after launch would be needed to calibrate the instrument. Calibration would be accomplished by performing carefully designed in-situ field experiments and continuous algorithm modification. These pre-launch and post-launch experiments would be planned by the Scientific Scatterometer Support team, which will succeed the present S^3 committee. The experiments would be supported by NASA.

IV. OTHER APPLICATIONS FOR SATELLITE WIND STRESS

A. METEOROLOGICAL APPLICATIONS FOR SATELLITE SURFACE WINDS

Introduction

The lack of adequate observational data has long been recognized as a major factor limiting both meteorological research studies and weather forecasting. Numerical weather prediction (NWP) models require the complete specification of initial state variables, yet only a fraction of the required initial data is available at any given time. The required data consist of the three-dimensional fields of temperature, humidity and horizontal velocity at locations comparable in number and spatial distribution with the number of grid points of the model used for NWP. Such data are provided at the synoptic times, 0000 and 1200 GMT, and numerical forecasts are performed every day at these times.

The conventional data available at synoptic times are not sufficient in number or coverage. Thus the use of space-based measurements offers an effective way to supplement the conventional synoptic network. Simulation studies and real data impact tests have demonstrated the potential of satellite sounding and cloud-track wind data to improve numerical weather prediction (Atlas *et al.*, 1982; Halem *et al.*, 1982), and such data are currently being used operationally. Similarly, quantitative surface wind data measured by satellites on a global basis could have great potential for improving our understanding of processes at the ocean-atmosphere interface as well as for providing initial state data for large-scale numerical models and local weather forecasting.

The limitations of conventional observations of surface winds over oceanic areas are well known. Ship-reported winds covering a small fraction of the ocean occur at irregular intervals in space and time and are not of consistent accuracy. This is true for a variety of reasons: (1) the height of wind measurement varies among

commercial vessels; (2) ship motion can affect anemometers; (3) the ship itself can disturb the airflow in its immediate vicinity; and (4) human errors occur in measurement, estimation, and transmission of the observations.

Due to these deficiencies, meteorological analyses of conventional data over oceanic areas often poorly represent synoptic- and subsynoptic-scale phenomena. Use of space-based surface wind measurements would provide improved surface analyses for weather prediction and forecast verification, as well as for the development of a more accurate surface climatology over the global oceans for the study of atmospheric phenomena. Examples of specific studies that would benefit from surface wind observations from space are (1) detailed investigations of the development, structure and evolution of tropical and extratropical cyclones; (2) interactions between synoptic- and subsynoptic-scale phenomena; (3) changes in the Intertropical Convergence Zone (ITCZ); and (4) the development and evolution of monsoon circulations.

Impact of Surface Wind Data on Weather Analysis and Prediction

One of the most important potential applications of remotely sensed surface wind observations is in the area of numerical weather prediction. A realistic quantitative assessment of the potential impact of global surface wind data has not yet been performed. However, simulation studies and limited forecast impact experiments have been carried out with data from the SEASAT satellite. SEASAT carried a scatterometer instrument designed to measure radar backscatter, which is sensitive to the presence of capillary waves and hence to surface wind stress. Such measurements provide information on the structure of the surface winds over global oceanic regions. The SEASAT scatterometer (SASS) winds differ from anemometer winds in three important respects. First, there is a directional ambiguity (or aliases) of the SASS winds. Second, the SASS winds are indirect; i.e., a model is required to infer wind

velocity. Third, the SASS measurements are averages over relatively large areas and are comparable to time averages of anemometer winds. Thus, the backscattered energy depends not only on the instantaneous wind but also on the recent time history of the wind. As a result of this averaging, the SASS winds are well suited for objective analysis and numerical prediction.

In order for satellite observations of surface wind to have a significant impact on numerical weather prediction, (1) substantial differences between the atmospheric state analyses produced with and without the data must occur, (2) the surface wind observations should not be inconsistent with the higher level analysis, and (3) the forecast model should be sensitive to the low level wind modifications. Assimilation of scatterometer data can work in two ways to modify the analysis: the satellite data can modify the wind field directly and the mass field indirectly through geostrophic adjustments. These changes can influence the forecast and thus the initialization at subsequent analysis times. In the data-sparse southern hemisphere, successive insertions of scatterometer data may be extremely important.

Results of Simulation Studies

Cane *et al.* (1981) performed a simulation study to assess the sensitivity of numerical models to satellite scatterometer wind data and the potential impact of such data on the quality of large scale numerical weather forecasts. They utilized a coarse mesh, second-order version of the Goddard Laboratory for Atmospheric Sciences (GLAS) general circulation model (GCM) to generate a nature run and the same model for assimilation and forecast experiments. The nature run was used to provide simulated conventional observations, satellite temperature profiles, and satellite scatterometer wind measurements. An analysis-forecast cycle was performed in which only conventional data were assimilated, and five 72-hour forecasts were made using the conventional analysis fields

as initial conditions. Additional analysis-forecast cycles for the same period, in which the simulated satellite surface wind or temperature sounding data were assimilated in addition to the conventional data, were then carried out. Special care was taken to simulate the spatial coverage and error characteristics of conventional surface and upper air reports. The satellite temperature sounding data were simulated without error along actual Nimbus orbits, while the scatterometer wind data were simulated with and without nominal SASS errors (±2 m sec^{-1} in magnitude, ±20° in direction) at model grid points which were intercepted by SEASAT scatterometer swaths. THE SASS wind data were specified at the lowest active level of the model (~ 945 mb).

These experiments were assessed by comparing the global forecasts made from initial states, which included simulated satellite data, with those which excluded these data. This comparison showed a substantial beneficial effect of the scatterometer wind data over and downstream of data-sparse ocean areas. The improvement due to perfect SASS wind data was only slightly diminished by the addition of nominal errors and was found to be comparable to the improvement resulting from the assimilation of perfect temperature sounding data. Several examples of improved predictions of the position, intensity, and structure of oceanic cyclones were observed.

These results indicate that NWP models are sensitive to low level wind observations. However, the magnitude of the potential improvement revealed by this study is questionable. The use of the same model for "nature" and for forecasting over-estimates the quality of the forecasts; the insertion of the simulated observations at the lowest forecast level does not account for errors made in estimating free atmospheric flow from surface data or in removing ambiguity.

Effect of SASS Data on Objective Analyses and Numerical Forecasts

Since the launch of SEASAT, several real data studies have been performed to assess the impact of SASS data on numerical weather

prediction. An investigation of the effects of SASS wind data on the National Meteorological Center (NMC) surface pressure analysis (Yu and McPherson, 1979) indicated large differences in surface pressure in regions with few ship reports. The pressure analysis in regions with dense ship data was not altered by SASS data. The authors suggested that the use of SASS data might be more beneficial in the modification of the lower troposphere winds rather than the pressure field. Another attempt to study the impact of SASS data on weather prediction was performed by Morford and Hubert (personal communication). They used the Navy 6-level model and a simple objective dealiasing scheme, choosing the vector closest to the forecast wind field in order to remove the wind ambiguity. This study also showed no significant improvement resulting from the use of SASS data.

More recently, Yu and McPherson (1981) performed a global data assimilation and forecast experiment for two days in July 1978 to determine the effect of directly assimilating SASS winds on NMC analyses and forecasts. In the northern (summer) hemisphere the effect of SASS data was small. However, in the southern (winter) hemisphere significant analysis and prognostic differences resulted from the assimilation of SASS wind data. Initial state differences extended from 1000-250 mb and were as large as 120 m in geopotential height and 20 m/sec^{-1} in wind. Figure IV-1 shows the 1000 mb and 250 mb vector wind differences in the southern hemisphere between analyses with and without SASS data assimilation, while Figure IV-2 shows the 72-hour forecast differences from these initial conditions. Significant initial state differences are amplified in the forecast and are as large as 30-35 m/sec^{-1}. Subjective comparison of the prognostic fields with cloud imagery indicates that the modifications resulting from the SASS data assimilation represent an improvement.

More sophisticated methods are needed to make full use of the SASS wind data for assimilation into the analysis/forecast cycle and to increase the impact, particularly in the northern hemisphere.

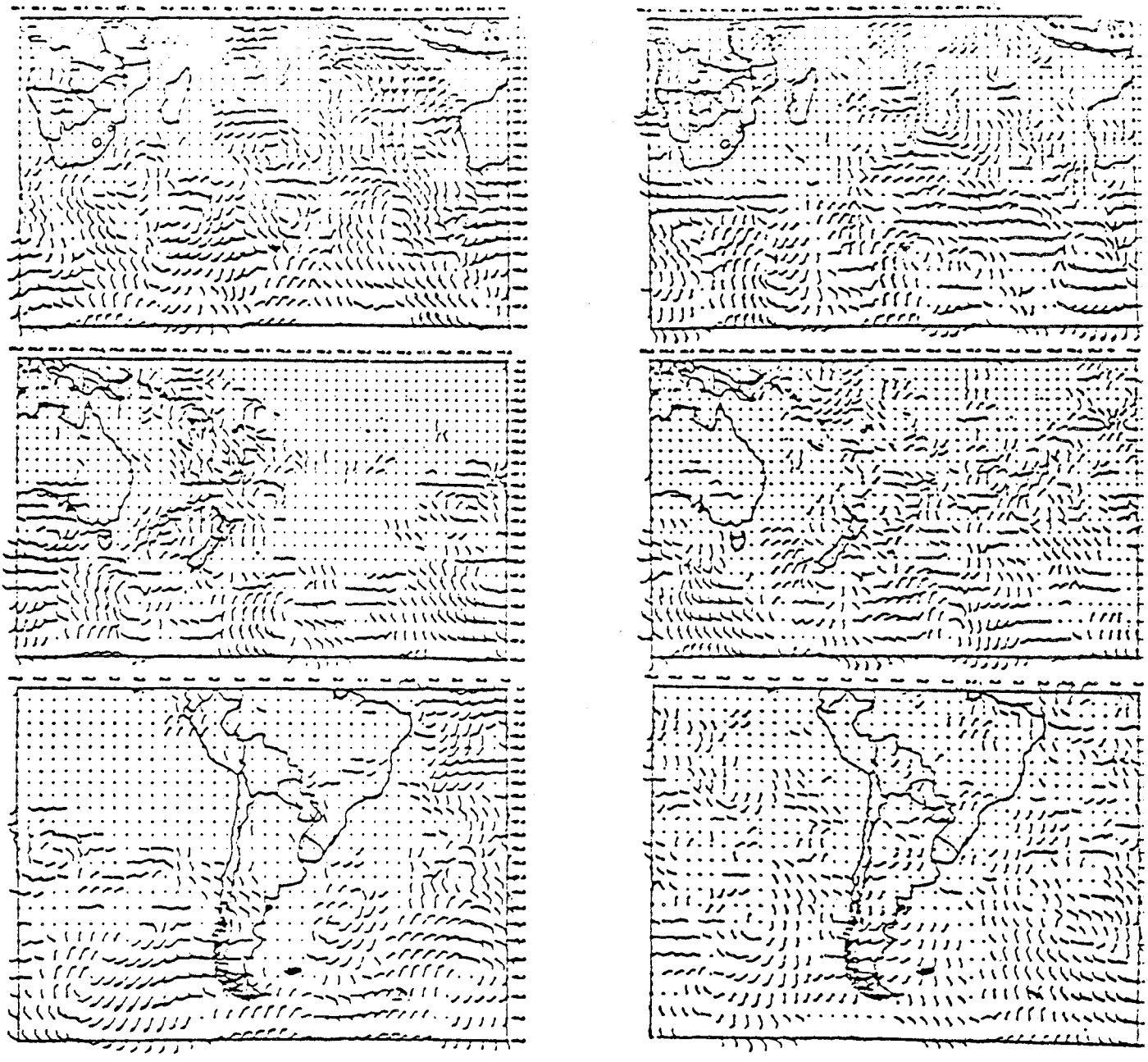

a.

b.

Figure IV-1. 1000 mb (a) and 250 mb (b) vector wind difference between analyses which included and excluded SASS data after 48 hours of assimilation. Full bar represents 10 m/s^{-1}; half bar represents 5 m/s^{-1}. (From Yu and McPherson, 1981.)

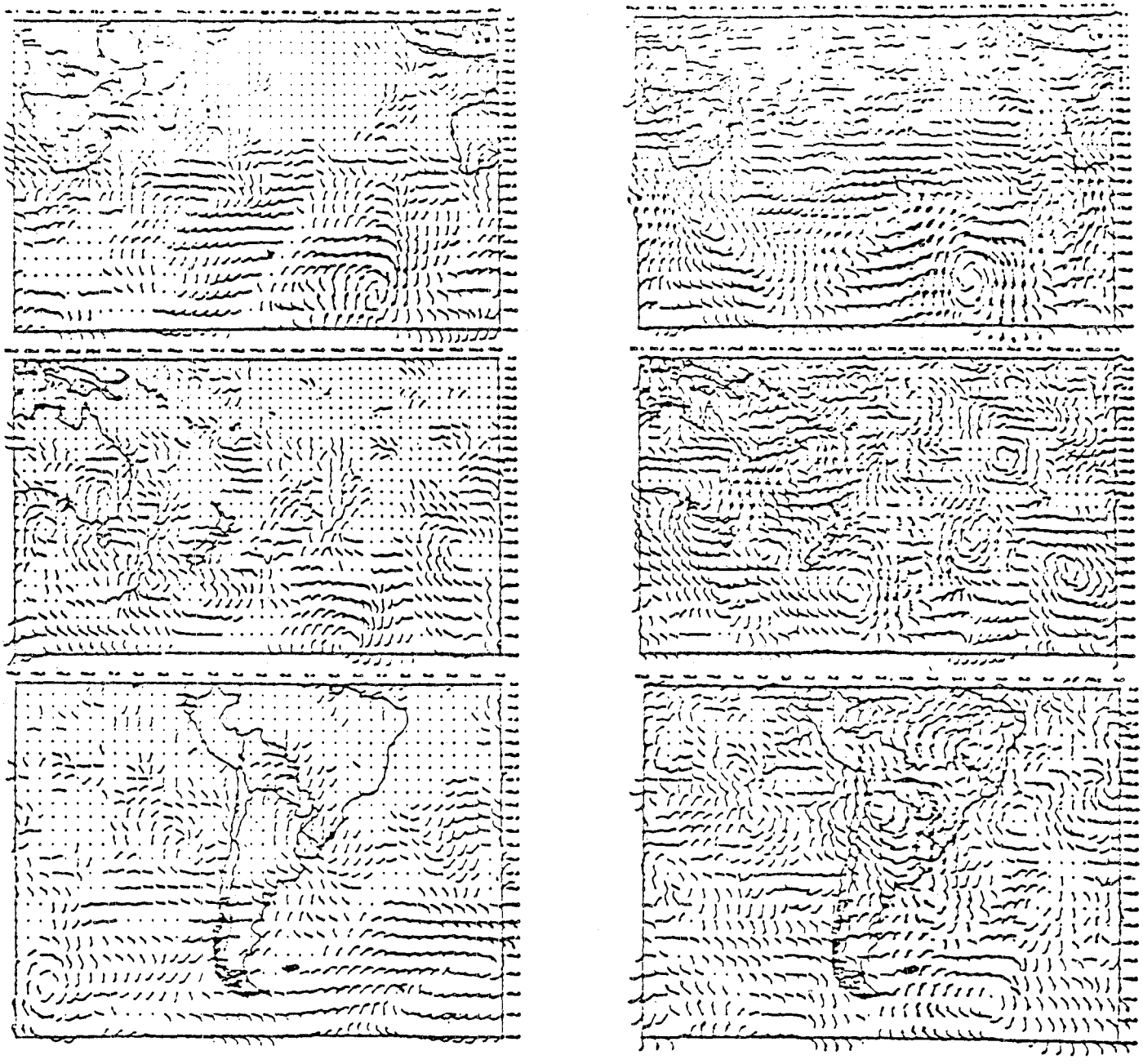

a. b.

Figure IV-2. 1000 mb (a) and 250 mb (b) 72-hour forecast difference in vector winds generated from analyses in Figure IV-1. (From Yu and McPherson, 1981.)

These methods include improved dealiasing procedures, asynoptic data assimilation, better planetary boundary layer (PBL) models for analysis and forecasting (discussed in Section IVA under "Inference of *In Situ* Wind") and larger statistical samples.

Recent results indicate that skilled meteorologists using auxiliary data, kinematic consistency, and pattern recognition techniques can effectively remove the ambiguity in the SASS wind data (Wurtele *et al.*, 1982). However, such an approach is extremely man-intensive and time-consuming. Combined iterative objective dealiasing with limited subjective enhancement may produce comparable results and is currently being utilized. In addition, objective variational wind dealiasing by direct minimization has recently demonstrated the potential for both removing the ambiguity and extracting the maximum information in the SASS wind aliases for gridded analysis (Hoffman, 1982). Figure IV-3 presents an example of the application of direct minimization dealiasing and analysis of SASS data. Figure IV-3a shows the NMC surface wind analysis for the intense storm which damaged the Queen Elizabeth II (QE II) on September 11, 1978, while Figure IV-3b shows the direct minimization analysis which included SASS data for the same time. Use of the SASS winds has (1) resulted in a repositioning of the cyclone center 3 degrees of latitude to the north, (2) greatly intensified the cyclonic circulation, and (3) improved the representation of frontal structure.

Effect of SASS Data on Subjective Analyses and Forecasting

In addition to the objective utilization of remotely sensed surface wind data in short- and extended-range global weather prediction, such data may be analyzed subjectively and utilized in short-range local weather prediction. A detailed study of the potential impact of SASS wind data on coastal marine forecasting has been performed by the Canadian Atmospheric Environment Service (Peteherych *et al.*, 1981). In their experiment, meteorologists at

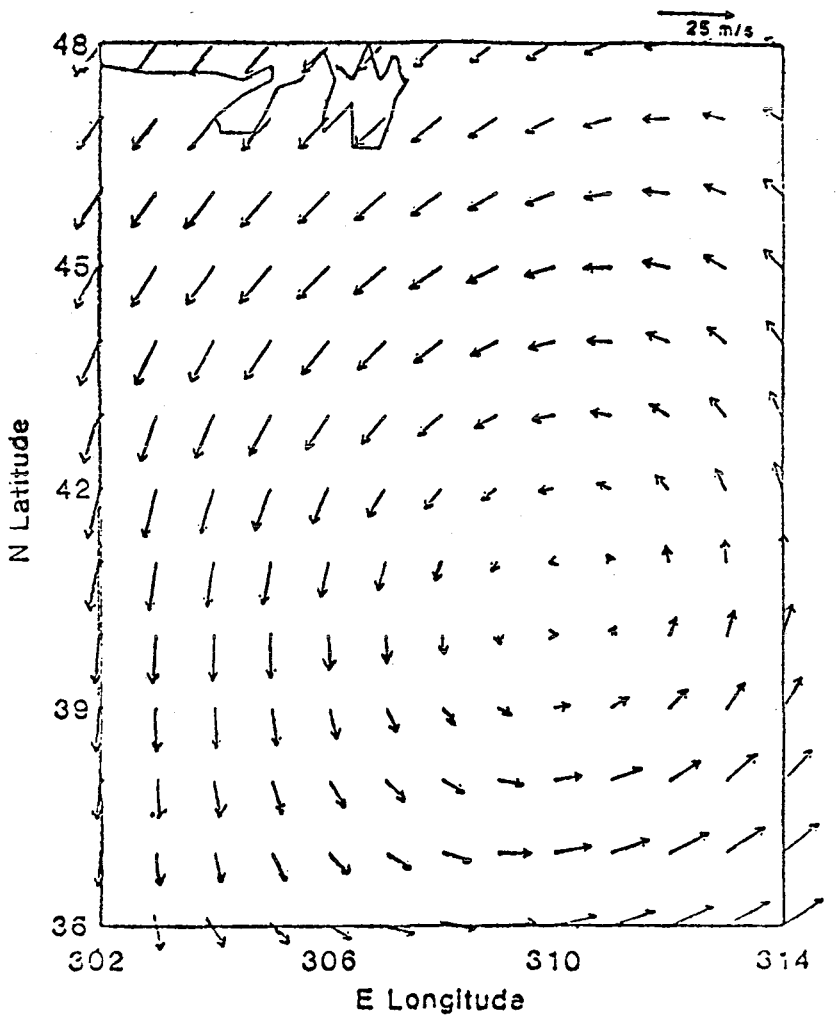

Figure IV-3a. NMC surface wind analysis for 0000 GMT 11 September 1970. (From Hoffman 1982.)

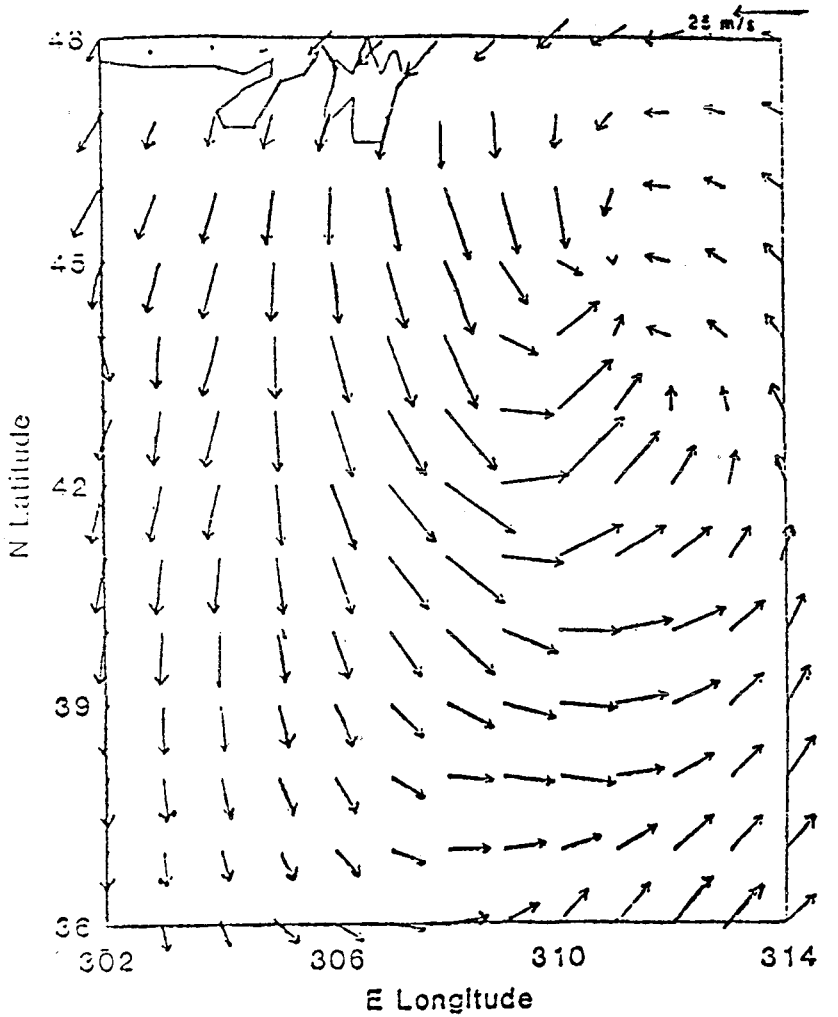

Figure IV-3b. Direct minimization analysis using SASS winds for 0000 GMT 11 September 1978. (From Hoffman, 1982.)

three regional weather centers in a simulated real-time mode utilized SEASAT wind data in addition to satellite cloud imagery and conventional observations to prepare regional analyses and forecasts. These new analyses and forecasts were then compared with those that had been prepared in real time, with particular emphasis on the representation of significant meteorological features and marine meteorological conditions. Figures IV-4a and IV-4b show an example of an improved analysis due to SASS data. The results of this study showed that:

1. SASS data permitted a more accurate placement of the lows, highs, troughs, ridges, and fronts and provided for the positive identification of synoptic features and small scale eddies and circulations that were not present in the conventional analysis.
2. SASS data permitted more accurate determination of pressure gradients, allowing for a finer resolution analysis. Normally pressure contours are drawn at 4 mb intervals. SASS permits contour intervals of 2 mb and on occasion 1 mb.
3. The combination of SASS data and Satellite Visible and IR imagery often illustrated very clearly the linkage between surface and upper air features.
4. Even where there is little change in the analysis by the input of SASS data, the degree of certainty in the final product is increased considerably. This should have its greatest impact on reducing the variability in subjective analyses. SASS data may also reduce the time required to do an analysis because uncertainties relating to placement and shape of meteorological features are minimized.
5. Fine resolution data over or near the area of responsibility would result in significant improvement of local forecasts.

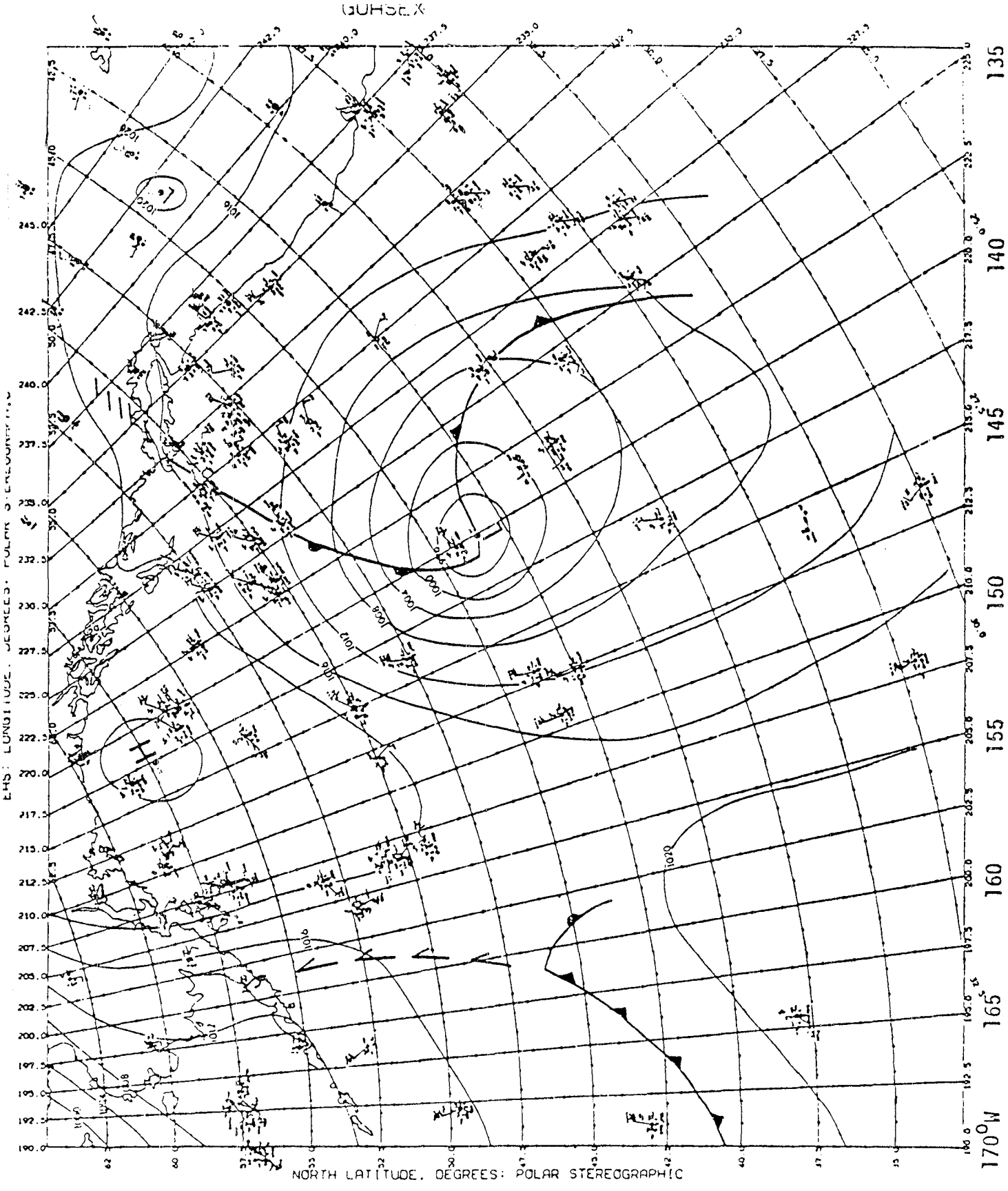

Figure IV-4a. Surface pressure analysis using conventional data. Sept. 25/78, 1800Z.

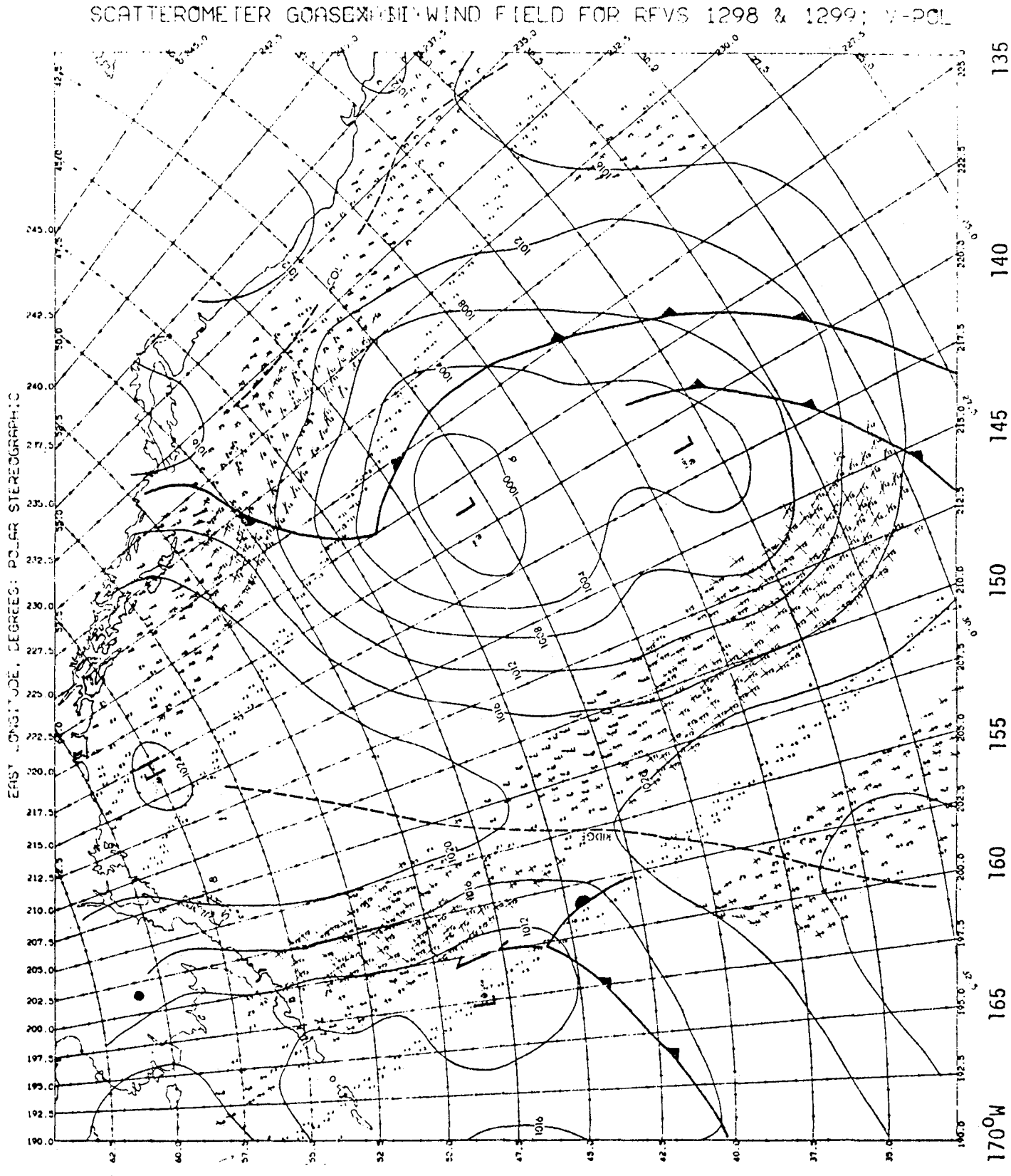

Figure AW-4b. Surface pressure analysis using conventional data and SEASAT wind data. Sept. 25/78, 1800Z.

Detection of Meteorological Features

An example of the use of SASS data in the detection of significant meteorological features is given in Figure IV-5. The subjective analysis of SEASAT data in this case clearly defines a tropical depression in the Gulf of Mexico which weather services in New Orleans and Texas had been unable to identify with conventional data and weather satellite imagery.

While forecasters were aware of a possible tropical depression on that date, neither GOES satellite imagery nor reconnaissance aircraft could locate it. The scatterometer data recorded on the morning of 9 September 1978 disclosed a marine circulation system with winds up to 28 knots over the Gulf. Availability of the SASS data in real time could have resulted in the forecast of the fairly intense tropical depression at least 13 hours before the subsequent verification about 125 miles off the coast of Brownsville, Texas.

The QE II Storm

One of the most striking examples of a synoptic feature that would have been better analyzed subjectively and predicted with the use of satellite wind measurements is the QE II storm (Cane and Cardone, 1981). On September 11, 1978, the oceanliner Queen Elizabeth II encountered 30 m/sec^{-1} winds and 39-ft seas. This storm caused about $50,000 in damage to the QE II. Bow rails were bent and hull plates torn; about 20 passengers were injured. In another incident, the fishing trawler Capt. Cosmo reported 15- to 20-ft. waves off Georges Bank late on September 8; the vessel disappeared on the 9th.

Gyakum (1980) has collected ship logs and other data that allow a better definition of the QE II storm than is possible from the information available to weather forecasters in real time. This storm is an example of what Sanders and Gyakum (1980) term a "bomb": an oceanic extratropical cyclone that deepens explosively. Bombs occur most frequently near the Gulf Stream and Kuroshio currents and

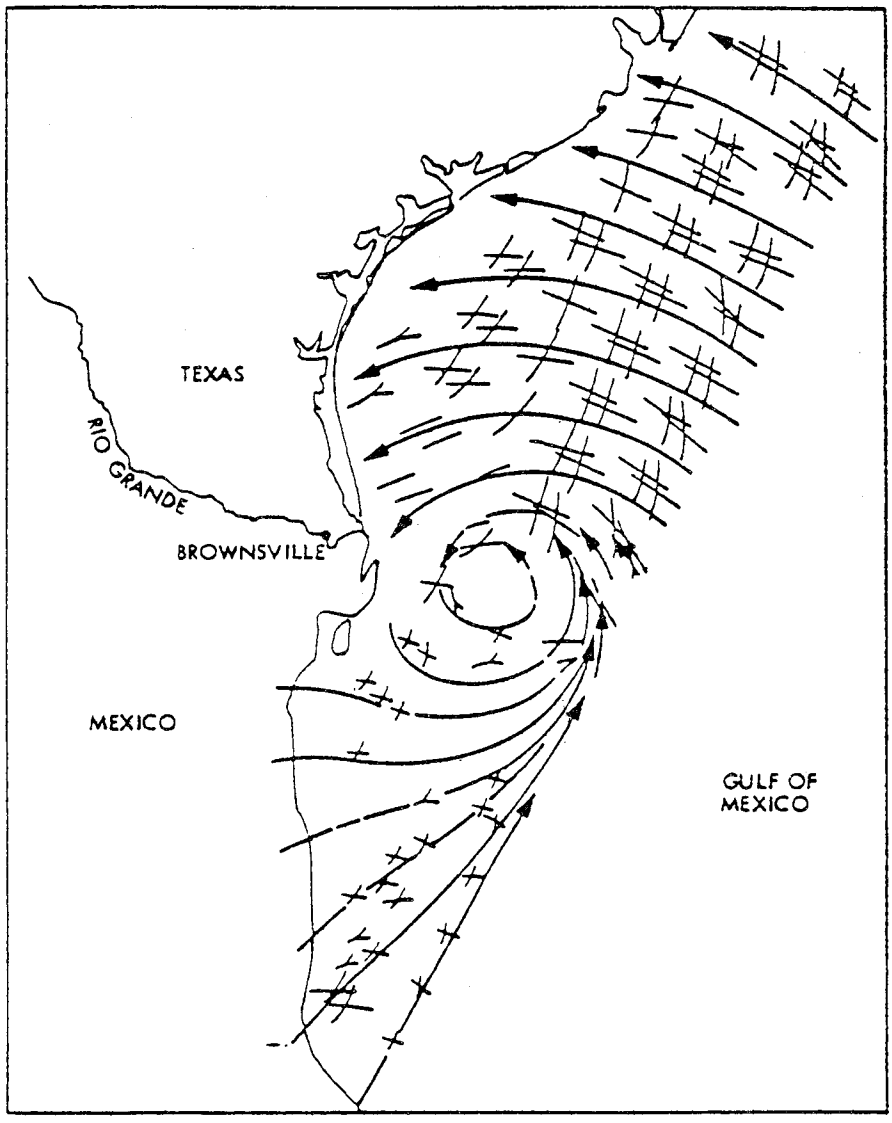

Figure IV-5. Analyzed raw scatterometer data showing streamlines (arrows) for Rev 1061 taken at 0500Z, 9 September 1978, in the Gulf of Mexico, indicating tropical depression near Brownsville, Texas.

in the east-central North Pacific Ocean; within each region several may occur in one cold season. Bombs are clearly a serious hazard to shipping and are largely responsible for weather-related loss of life and shipping on the high seas.

The physical mechanisms responsible for the explosive development of bombs can be studied more effectively with the addition of satellite wind measurements. Satellite data could provide early detection of bombs which would otherwise be missed or poorly diagnosed in the conventional marine data base, even in active shipping lanes. Early detection would contribute to improvements in forecasts in at least two ways. First, marine forecasters and ship-routers would be made aware of the severity of these systems much sooner, and short-range marine forecasts would thereby improve. Second, NWP models would be provided with a better initial state specification prior to and during the deepening stage.

The early stages of the QE II storm provide an example of explosive deepening. At 1200 GMT on September 9 (about the time the Capt. Cosmo was lost), Gyakum's (1980) analysis shows the storm developing southeast of Cape Cod. The National Meteorological Center analyst had only a single report indicating high winds. Lacking corroboration, he misplaced the low center and underestimated its intensity. (There was a SEASAT orbit passing over the storm center at this time.) At this stage the storm was probably of too small a scale and too early in its evolution for the NWP model to develop it correctly, but a better analysis would have been of value to marine forecasters. By 1200 GMT on the 10th, the storm was fully developed. As indicated by the barograph trace (see Gyakum, 1980) from a ship (the Euroliner) which passed near the center of the storm at 1200 GMT on September 10, there is solid evidence of the extreme intensity of the storm at a time when the operational analysis (Figure IV-6a) seriously mislocated and underestimated the storm. Figure IV-6b is a reanalysis, based on

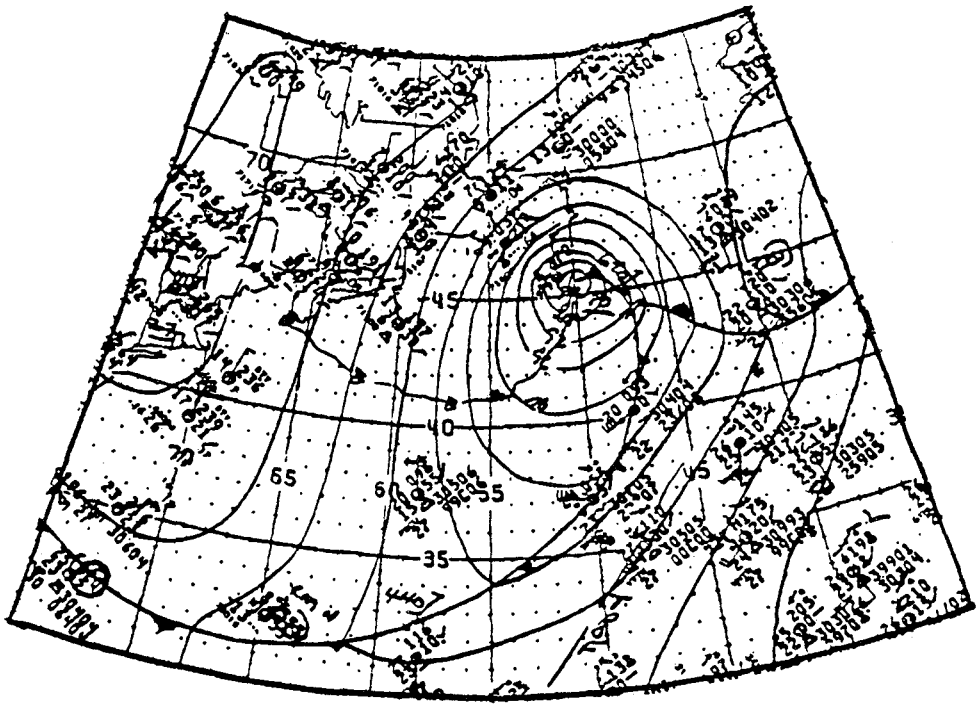

Figure IV-6a. NMC surface analysis for 1200 GMT 10 September 1978.

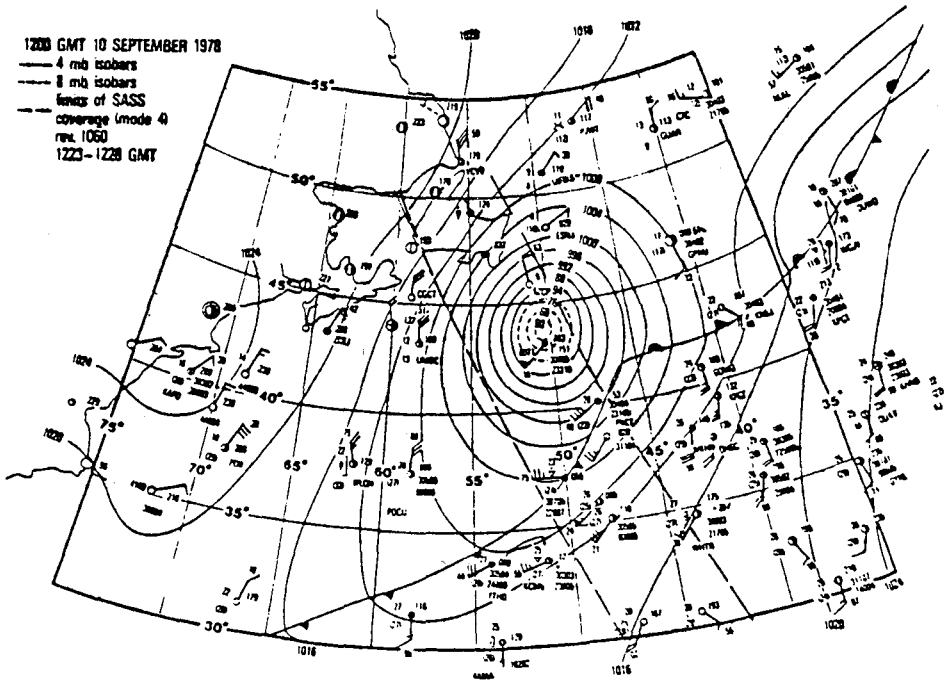

Figure IV-6b. Reanalyzed surface analysis which incorporated SASS data, for 1200 GMT 10 September 1978. SASS swath indicated by dotted line; storm track indicated by dashed line. (From Cane and Cardone, 1981.)

SASS data, which incorporates the Euroliner report. The central pressure is 20 mb lower (960 vs. 980), and since the scale of the system is the same, the new analysis implies surface winds higher by a factor of two.

The poor specification of initial conditions provided by the NMC analysis for September 10 contributed to a poor 24-hour forecast for September 11. The winds were forecast to be less than 15 m/sec^{-1} instead of the observed maximum of 25 to 30 m/sec^{-1}. It was at about this time that the QE II was battered by strong winds and heavy seas. Because the preceding NMC analyses had underestimated the surface winds by a factor of two, especially in the southern quadrant of the system, their wave analysis misforecast the significant wave heights: where the QE II reported 39-ft. waves, the forecast was for 10-ft. waves. The QE II turned south to avoid the storm at 0800 GMT on Septebmer 11. With better guidance such evasive action could have been taken earlier, avoiding damage and injury.

Relationship of Scatterometer Return to Actual Winds

Scatterometer return, σ^0, appears to be a direct measure of surface stress (i.e., it correlates well with surface stress), while for forecasting requirements.the need is for *in situ*, or geostrophic, wind.[1] We say "appears" because this correlation has not been demonstrated for all possible conditions (discussed more fully in section II-E), and at least the SEASAT σ^0 seems to correlate equally well with the neutral wind. The question then is - what is required to infer *in situ* wind from σ^0? One answer is simply to invert the familiar procedure for inferring stress from the actual wind and stability.

That stress and neutral wind speed both correlate well with σ^0 is not surprising, since they are themselves related approximately by

[1] An *in-situ* wind is an actual wind observation. A geostrophic wind is a wind measurement inferred from the pressure data.

the empirical Monin-Obukov profile,

$$U - U_S = \frac{u_*}{k}[\ln(z/z_0) - \psi(z/L)] , \qquad (1)$$

where U is the desired *in situ* wind speed at height z, and U_S is wind speed at height z_0, which is the so-called roughness length. (U_S is often set to zero, which can be a poor approximation at low wind speeds.) The stability function, ψ, is dependent on the atmospheric stability. For conditions of neutral stability, $\psi = 0$, and U is then called the neutral wind. Given an empirical form for $z_0(U)$ or $z_0(u_*)$, the log profile may then be easily solved for U. Equivalently, one could invert a bulk transfer formula which would then require specification of the neutral drag coefficient instead of z_0.

In the more common case of non-neutral stability, however, U may vary substantially with ψ for the same σ^0 (Figure IV-7). In that case the actual wind, U, is not so simply related to σ^0, and one must adapt either an atmospheric surface layer model (e.g., Eq. (1)), or a planetary boundary layer (PBL) model (e.g., Brown and Liu, 1982). In addition to σ^0, one must also *measure the atmospheric stratification in the surface PBL in order to evaluate ψ, the stability function.* The stability function usually is considered to be a function of the Obukhov length L,

$$L = \frac{-\overline{T}_v u_*^3}{g k \overline{w'T'_v}} \qquad (2)$$

where $\overline{T}_v$ is virtual temperature defined by $\overline{T}_v = T(1 + .61\,\overline{q})$, T is mean temperature, q is specific humidity, and $w'T'_v$ is a measure of the buoyancy flux. The buoyancy flux would ideally be measured directly, but unfortunately there is no known way to do this today by remote sensing. Alternatively, buoyancy flux may be estimated from bulk formulae, given estimates of sea surface temperature and wind

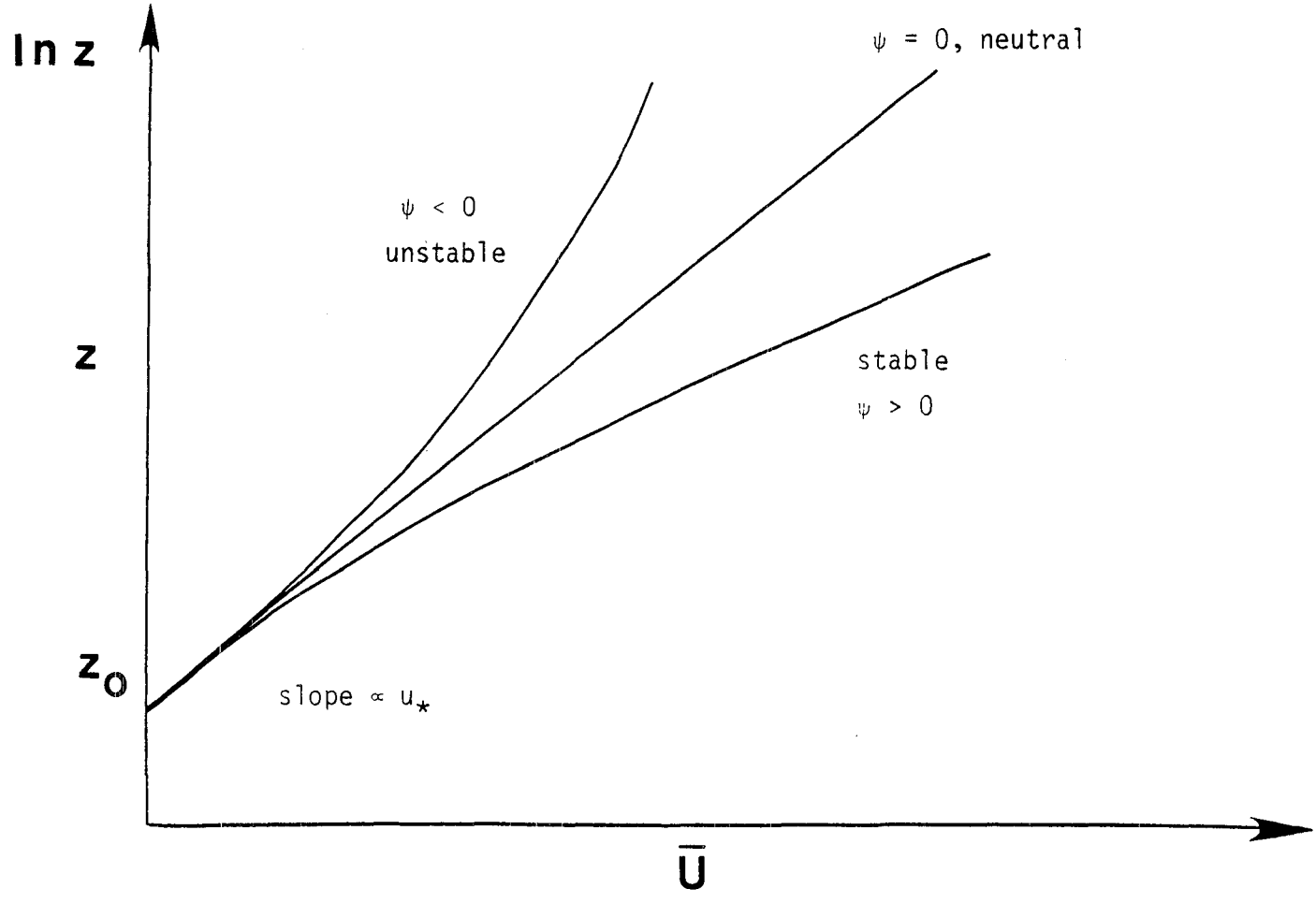

Figure IV-7. Schematic wind profiles near the sea surface for three values of stability. For the same wind stress and presumably σ (proportional to profile slope at z_o), one obtains very different $\bar{U}$ values at height z dependent on the sign of the stratification.

speed that may be observed, and also the PBL temperature and humidity, which at present cannot be observed remotely in sufficient detail. Perhaps future refinements of temperature sounding techniques will yield PBL temperature and humidity that will permit a complete specification of PBL stability and buoyancy flux. (The buoyancy flux is, of course, of great interest well beyond its role in the calculation of the Monin-Obukov length.) Scatterometer-inferred winds will be valuable to subjective analysts and forecasters, even in the complete absence of stability corrections, because of their coverage of data-poor ocean regions. But for incorporation into numerical forecasts, some at least rudimentary measure of L is certainly desirable.

Scatterometer Data Assimilation

The winds obtained by a scatterometer become available at different times as the spacecraft orbits the earth. For example, from Figure IV-8, each of the subsatellite tracks that start at the top at 60°N and move southwestward requires about 20 minutes for the spacecraft to travel from 60°N to 10°S. The four successive southbound orbits are about 100 minutes apart as they cross 60°N. Obtaining the full data set for the four southbound orbits requires about 420 minutes, or 7 hours. Since ship reports are transmitted every 6 hours, the scatterometer winds surely bracket one subset of the ship reports, and perhaps two subsets.

For synoptic meteorology, numerical weather prediction, and oceanographic applications we want to generate correct estimates of the surface wind fields and the wind stress over the world ocean at certain times, conventionally 0000, 0600, 1200 and 1800 Greenwich Mean Time (GMT). With scatterometer data, it should be possible to generate these same fields at additional in-between times, such as 0300, 0900, 1500, and 2100 GMT.

Scatterometer winds provide a much greater data density, compared with scattered ship reports. This should make it possible

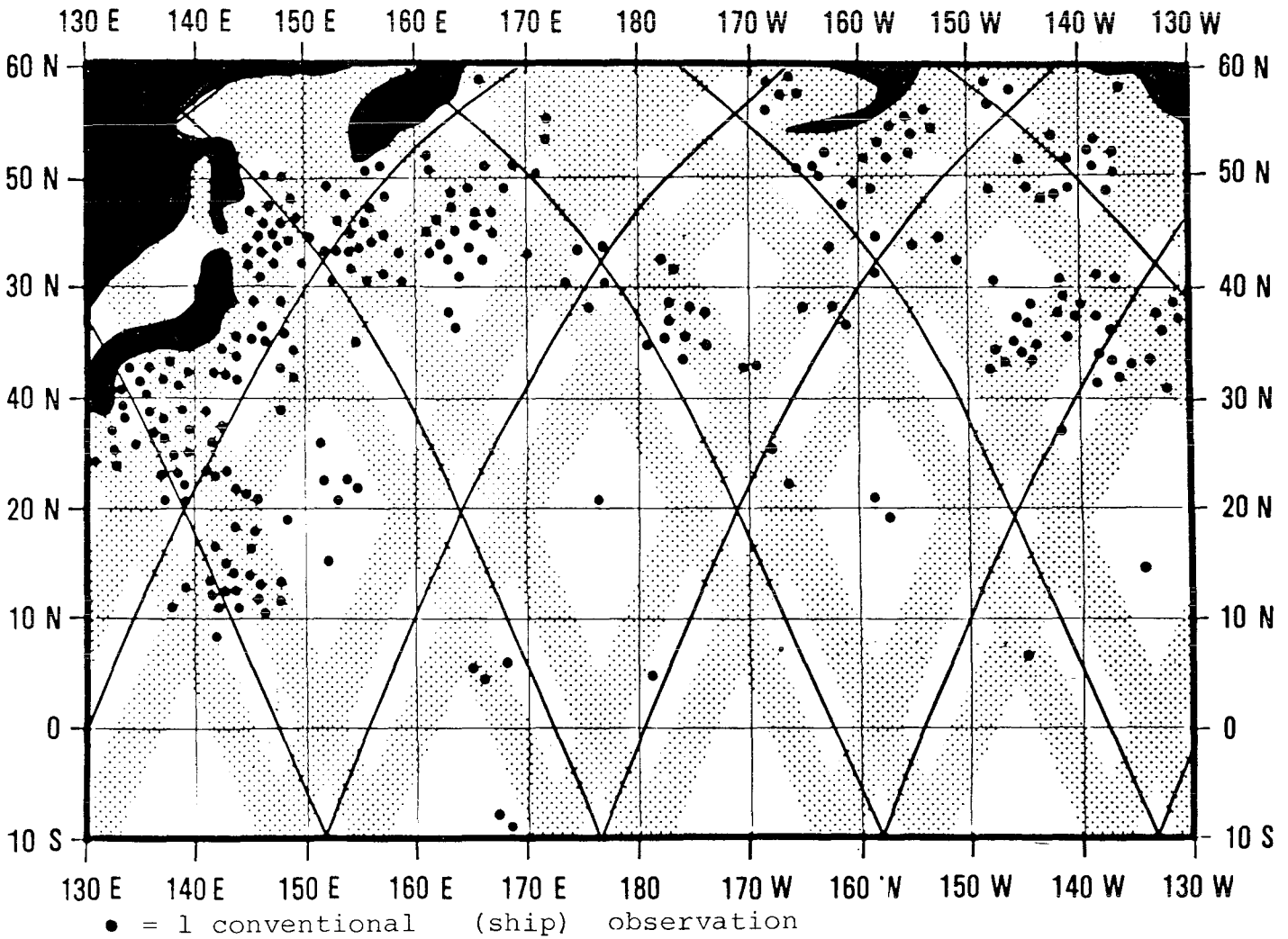

Figure IV-8. Surface projection of scatterometer data coverage during 24-hour period in North Pacific.

to obtain an improved analysis of the entire area under consideration, not just the area actually covered by the scatterometer swaths. That this is indeed the case is illustrated by Figures IV-1, IV-2, IV-3a and IV-3b, IV-4a and IV-4b, and IV-6a and IV-6b.

Figures IV-4a and IV-4b show analyses for the Gulf of Alaska, one without and one with the SEASAT SASS data. (For planned operational modes, there would have been a swath right through the 1000 mb low centered at 46°N and 221°E.) The analysis that used the SASS swath has been greatly altered, especially for the column near 45°N and 205°E.

Figures IV-6a and IV-6b show the analysis of a synoptic sea surface pressure field first without and then with SASS data. In the analysis based on ship reports alone, the low to the east of Nova Scotia has a fairly high central pressure. The SASS swath shown in Figure IV-6b occurred only 20 minutes after the synoptic time of 1200, so asynoptic effects can be neglected for the analysis. The low is in a different position, based on better wind data. The isobars are much more closely packed and the central pressure is much lower. Moreover, the information provided by SASS makes it possible to correct the entire isobaric analysis for the northeast quadrant of the cyclone for an additional distance of one and one-half times the original width of the SASS swath. Once the isobaric pattern is corrected outside of the original swath, it is then possible to compute the winds in these areas with much greater accuracy.

Figures IV-3a and IV-3b illustrate how drastic such corrections can be and at times how inadequately the present data base provides knowledge of the winds over the ocean for a particular storm. Figure IV-3b shows a wind field that is about four times stronger in speed at some locations. Consequently, the wind stress is at least 16 times stronger and perhaps 20 to 25 times stronger than that which would be computed from the conventional analysis.

Figure IV-1 shows that asynoptic SASS data can be assimilated over a 48-hour period in such a way that a synoptic scale wind field for all of the grid points of the model used can be generated for the entire southern hemisphere. For each of the two days there were data gaps such as those shown in Figure IV-8, but the gaps did not prohibit a full wind field and sea surface atmospheric pressure analysis at the synoptic scale of the entire earth.

Figure IV-8 can now be reinterpreted by just looking at the southbound passes defined previously. Currently available meteorological data assimilation procedures use only the ship reports and are capable of providing a synoptic scale analysis of the entire area (in fact the entire northern hemisphere) based on continuity and interpolation techniques. (These procedures may not be entirely correct, but they are the best available at present.) Using these same techniques, as shown by the three examples, the two SASS swaths on each side of the four southbound tracks usually will influence an additional area of analysis at least as wide as the swaths themselves to each side of each swath.

The white areas in Figure IV-8 almost completely disappear when only the four southbound passes are considered on the basis of this analysis. The four and one-half northbound passes, starting about 12 hours later, again influence the entire area to be analyzed. Whether or not a particular spot on the ocean surface is revisited within two, three, or four days is thus irrelevant at the most important scale of all, the synoptic scale.

Some features of the winds over the ocean will be missed by a single scatterometer on a spacecraft, no matter what the revisit time. A typhoon at 20°N 152°E would be reported only by ships and geostationary cloud imagery and probably would not have a great enough radius to influence the winds in the scatterometer swaths. If that area were revisited three days later, the typhoon would have moved on to some other location.

The asynoptic nature of the scatterometer data must be treated with care. Some preliminary investigations have treated all of the SASS winds obtained between, say, 0300 GMT and 0900 GMT as if they had been measured at 0600 GMT. The errors introduced in this way may greatly weaken the impact of the data on the ability to produce realistic fields and meteorological forecasts.

Other investigations use a model of the atmosphere that is stepped forward in small time steps. The winds from SASS are assimilated at each time step, as measured at that time, with care to have them influence as large a volume as possible around and above the region of available winds. By such a procedure the grid points of the model over water (and many of the grid points over land) are corrected many times by the SASS data and combined in an optimum way with conventional data. This procedure efficiently yields 6-hourly (or three-hourly) synoptic wind fields, sea surface pressure fields, and, in principal, vector wind stress fields, for the world ocean. For this to occur, the numerical model must be sufficiently sophisticated to produce valid data in the 12-hour interval between revisits by the spacecraft. Twelve-hour numerical weather predictions are quite good, so this is not a problem.

Data Requirements

For most meteorological applications the same accuracy and coverage provided by the SEASAT scatterometer would be sufficient. This is not true for many oceanographic applications. Horizontal resolution of the data should be no larger than 100 km, although higher resolution could be utilized in mesoscale studies, as well as in investigations of tropical storms and coastal processes. *The major improvement required for scatterometer data over the SEASAT capability is for unambiguous wind directions,* to be determined objectively in real time to meet operational forecast deadlines. For real-time operational forecasting, the data should be available within 1 to 1-1/2 hours of the observation time. In addition,

complementary measurements of upper-air temperature and moisture profiles could substantially increase the beneficial impact of scatterometer data.

Summary

Due to the deficiencies of conventional surface wind observations, a strong requirement for space-based surface wind measurements exists. A simulation study has shown that large-scale numerical weather prediction models are sensitive to low-level wind observations and that significant improvements to short- and extended-range global weather prediction could result from the assimilation of scatterometer winds.

Preliminary real-data impact tests show more accurate surface and upper air analyses and significant prognostic impacts over data-sparse areas. Regional studies demonstrate that synoptic and subsynoptic systems that are not detected or are poorly analyzed are accurately represented in scatterometer data, and short-range forecasts based on this data should be improved. The utilization of remotely sensed global surface wind data would provide a greatly improved surface climatology, which in turn would benefit investigations of dynamical and physical processes over the ocean.

B. NAVAL UTILIZATION OF SURFACE WIND DATA[1]

In the era of tall masts and wooden ships, a naval officer had to be a master in his application of the ocean environment. Winds, waves and currents were the elements of propulsion and tactical maneuvering in battle. With Robert Fulton's development of steam propulsion and the passing of sails, the perception passed that a capable mariner by necessity must be a master in the application of environmental elements. It is an interesting twist of irony that in

[1] Prepared by CDR David Crosby Honhart, Naval Oceanography Division, Chief of Naval Operations staff.

the 177 years since Admiral Nelson's stunning victory at Trafalgar, given the advances in ship design, propulsion systems, weapons and tactics, the technical complexities of war at sea once again dictate a keen working knowledge of the ocean environment. Admiral Gorshkov of the Soviet Union espouses the philosophy that the major navies of the world are technological equals. He states that the navy having the superior knowledge of the environment and how to take tactical advantage will be the victor.

The United States Navy is unique in its operational requirements for the forecasting of atmospheric and oceanographic conditions. To appreciate the magnitude of these requirements one must clearly understand the mission of the Navy to respond to a crisis in any sector of the globe. The required tactical environmental products include: *tactical weather forecasting, prediction of acoustic conditions for submarine and anti-submarine warfare, prediction of sea and surf conditions for amphibious warfare, mine warfare, underway replenishment, swimmer operations, and search and rescue operations.* In all of these applications it is necessary to define accurately the ocean surface wind field in order to calculate oceanic waves, currents and acoustic environmental fields.

There are five basic elements involved in the provision of timely and accurate atmospheric oceanographic tactical products to the fleet:

1. Scientifically accurate atmospheric and oceanographic forecast models
2. Fast large-capacity computers
3. Global atmospheric and oceanographic data base (real time)
4. Skilled personnel
5. Effective communications

Of the five elements listed, the one that stands alone as the Achilles heel is the global data base. The ship synoptic reports (which include observations of surface winds) are limited in numbers

of observations and are poorly distributed geographically. Figures IV-8 and IV-9 graphically depict the problem. An additional concern of the Navy is that for any given period of time 90 to 95 percent of the ship synoptic observations come from foreign sources.

When one assesses the Navy's global requirements for real-time atmospheric and oceanographic data in light of the present global sparsity of data, coupled with the possibility that in times of contingency operations there will be no guarantee that the foreign ship data sources will remain available, one quickly comes to the conclusion that we are walking on egg shells. The possibility for a U.S.-controlled, conventional (ship, aircraft, buoy), global ocean data collection system is unrealistic. In fact, the cost for an effective global ocean data collection system leaving no data-sparse areas based on conventional methods, regardless of participating nations, is potentially 4 times that of a single oceanographic satellite system over a 10-year period. Table IV-1 gives types of ocean observations for model requirements and their relative costs for collection by conventional means. Conventional data platforms in such systems (e.g., ships, islands, drifting buoys, fixed buoys) would provide only about three-fourths of the coverage available from one oceanographic satellite system. The 10-year systems cost for conventional platforms would total more than $2.4 billion. Of this figure, start-up costs are $295 million and the annual maintenance/replacement costs are $213 million. In comparison, the Navy Remote Ocean Sensing System (N-ROSS) 10-year projected cost for one satellite system totals $517 million. The latter figure consists of the following costs (in millions):

Research & Development	126.9
Equipment Procurement	51.4
Operations & Maintenance	18.7
Satellite Procurement	320.1

There are battle lines that exist among atmospheric scientists regarding the impact of a well-defined, global surface wind field on the accuracy of weather forecasts. Intuitively it seems that such a

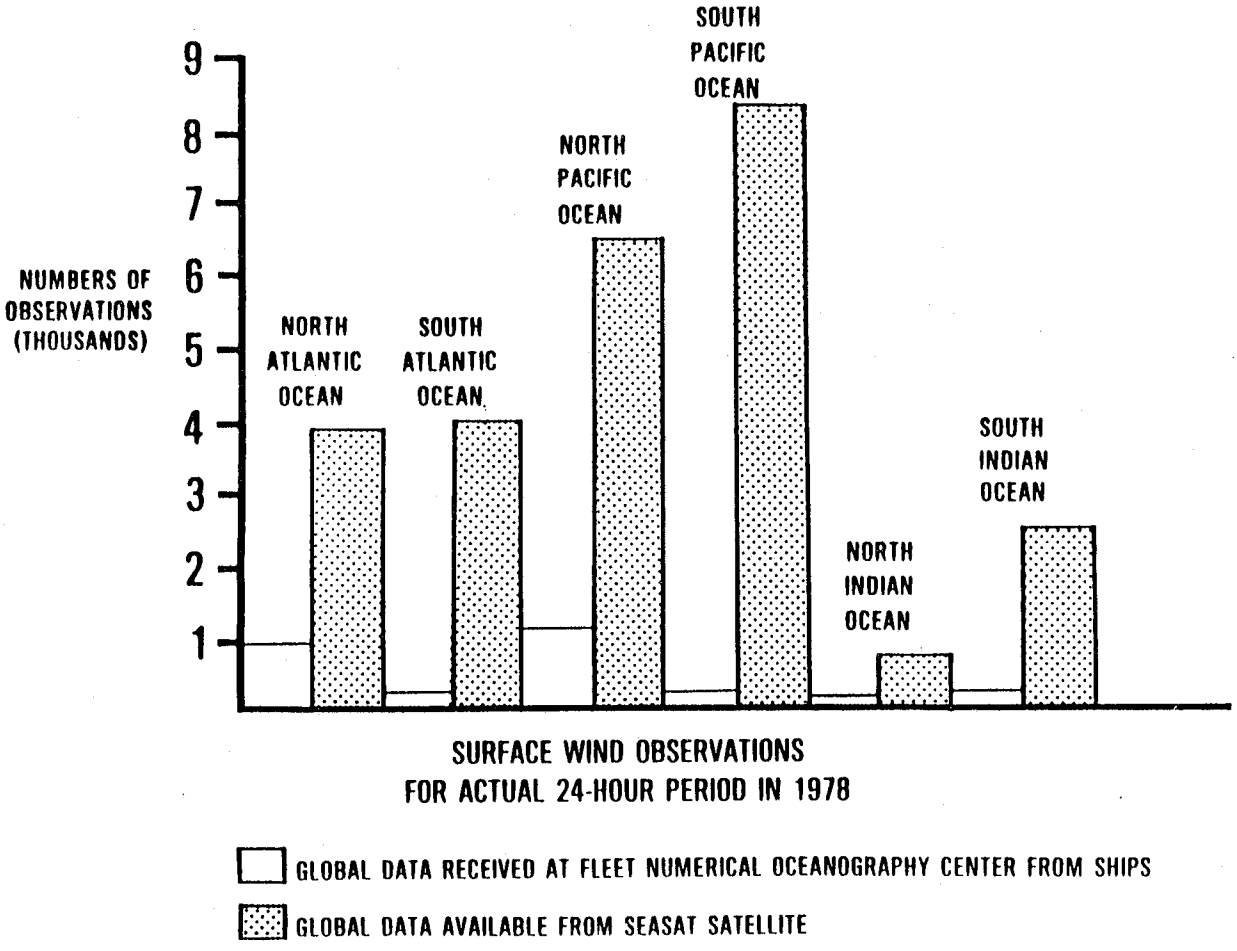

Figure IV-9. Environmental observations.

Table IV-1. Ocean Observations for Model Requirements [1]
(Ocean Data Systems, Inc., Monterey, CA; December, 1981)

Type of Observation	Number Needed	Cost Each	Annual Maintenance/ Replacement	Initial Cost x 10^6 $	Annual Cost x 10^6 $
Ship, Surface	4,000	10K	25%	40	10
Ship, Upper Air	500	200K	100%	100	100
Ship, Subsurface	500	20K	200%	10	20
Islands, Third World	200	250K	20%	50	10
Drifting Buoys	5,000	5K	30%	25	8
Reference Buoys, Platforms	300	100K	25%	30	8
TOTALS				255	156
Program Management				5	2
Data Collection, Validation, Communication				35	35
TOTALS				295	213

[1] The conventional type of platform-observed data listed are estimated to provide about 3/4 of the coverage available from SEASAT satellite system.

data base must improve the accuracy of our forecasts, and the qualitative analyses done to data seem to support this intuition. Unfortunately the analysis is model dependent and it is difficult to make a quantitative judgment.

Regarding naval applications other than tactical weather forecasting, there is no question that an accurately measured global surface wind field would improve the accuracy of tactical environmental support. Historically, for example, ships are routed around adverse weather systems. However, an improved system would route ships according to ship response frequencies, i.e., response to the spectral wave energy present. Simply stated, ships of various designs respond differently to the wave spectra present. In order to analyze accurately the spectral wave energy, one must be able to define accurately the global ocean surface winds.

In the arena of ocean acoustic forecasts, there is a need to improve the prediction of surface ambient noise and to develop an operational capability to forecast changes in the ocean thermal structure. Knowledge of an accurate thermal structure is important because it determines the sound speed profile that drives the tactical acoustic prediction models. An accurate measure of ambient noise is important because it is a determining factor of the range at which a submerged target may be detected, and therefore it plays a role in the selection of the most effective mode of sonar operation, ship spacing, sonobuoy spacing, etc. A real-time analysis of global ocean surface winds would provide a more accurate determination of ambient noise. Knowledge of surface winds also would allow a more accurate computation of vertical mixing and horizontal changes in thermal structure due to advection.

In the annals of naval history there are unfortunate accounts of ships capsizing in heavy seas when not ballasted down due to a need to refuel, landing craft broaching in heavy surf, and ships being driven up on rocks while anchored in a supposedly safe harbor. Today there can be no excuse for such occurrences because the scientific know-how exists to forewarn of impending catastrophic

environmental conditions. As stated before, however, the Achilles heel is the global atmospheric and oceanographic data base.

The above discussion focused on but a few examples regarding the importance of environmental products in the execution of naval operations. In all of the examples cited, ocean surface winds were a critical factor (directly or indirectly). The true value of accurate environmental data is often hard to assess in terms of cost effectiveness and force multiplier (i.e., how to use your operational forces more effectively). However, the ship that capsizes, broaches, or sustains structural damage, the submarine that goes undetected, or the missile or torpedo that fails to acquire its intended target is the true index of environmental data value.

The question is whether or not the Navy has a need for a scatterometer to be flown. Without equivocation, the answer is yes. The U.S. Navy will have environmental advantages for tactical operations if improved oceanographic and meteorological products are available from quality satellite surface wind stress measurements.

C. COMMERCIAL APPLICATIONS

The uncertain political situation in the world today indicates that the United States may be unable to obtain resources on which it depends through trade. This situation has been realized and industry and government agencies have started programs to obtain oil, gas, minerals and other important resources from the sea in coastal waters of the United States and in remote areas of the globe.

A recent paper on the commercial application of satellite oceanography (Montgomery, 1981) indicates that in the next decade, the ocean's commercial users will require an operational oceanographic satellite system over all ocean areas. It is stated that the sensor suite should contain, among other instruments, an instrument to measure surface stress. Potential dollar benefits that that ocean surface winds (stress) would provide are shown in Table IV-2.

Table IV-2. Potential Dollar Benefits Provided by Ocean Surface Winds

MEASUREMENT	PRIMARY BENEFICIARIES	APPLICATION	ESTIMATED ANNUAL BENEFITS ($M)
Ocean Surface Winds (stress)	National Environmental Centers	Short-range Prediction	500-1,000
	Shipping	Ship routing/ scheduling	20-30
	Deep Ocean Mining	Operations/ scheduling/design	2-5
	Offshore Oil	Operations/ scheduling/design	25-50
	Commercial Fishing	Tactics/ scheduling	4-10
	Total		551-1,095

This section addresses the commercial applications of satellite-derived surface stress to offshore oil and gas, the fishing industry, deep ocean mining and ship routing.

OffShore Oil and Gas

The production of offshore oil and gas is rapidly expanding; the proportion of offshore oil and gas within the world's total production is dramatically rising and may reach 50 percent in the next few decades. Recent technological advances have allowed both the search for and the recovery of petroleum to extend far out of sight of land and into much deeper waters than were previously accessible. It has been estimated that the largest reserves lie in much deeper water at greater distances from shore. Therefore, it is logical to assume that offshore drilling and production operations will increase at far greater depths than are considered feasible now.

As oil companies attempt to expand operations into more lucrative production areas, a major problem is the lack of

environmental data upon which to base design, development and operations decisions. Surface stress data measured by satellite would improve the data base that is required for making such decisions. In addition, if these wind data were used in a forecast model (such as Fleet Numerical Oceanography Center's (FNOC) wave forecast model) to predict wind and wave conditions at some time in the future, their value would be increased significantly.

A study performed by the Marine Weather Sciences Division of Ocean Routes, Inc. (Palo Alto, California) as part of the SEASAT experiment (ASVT Experiment 16) produced some interesting results for the offshore oil/gas industry planners. In oceanic areas where conventional observations are relatively dense, SEASAT wind and wave data aid more in the determination of the shapes of major map features rather than their locations. In data-sparse areas measurements provided by SEASAT are often the only means by which a reasonably accurate surface analysis can be prepared. In the Gulf of Alaska, where conventional data quality and quantity are often variable, SEASAT measurements permit more precise location and identification of pressure centers, frontal systems and wave height patterns.

The offshore hindcast comparisons illustrate great potential for SEASAT in the offshore drilling industry. At today's skyrocketing prices, the daily rate for an "average" mobile rig runs about $60,000. Supplementary costs, such as work-boats, drilling crews, supplies and transportation, average at least an additional $60,000 per day. In two of the hindcast comparisons alone, up to 9 hours of drilling time could have been saved (depending on the type of rig and current operations), along with 11 hours of supplementary operation time. Incorporating the costs outlined above, a per-rig dollar saving for the period October 5-9, 1978 (one of the case study periods), can be estimated to be 20 hrs./rig x $120,000/day x 1 day/24 hrs. = $100,000/rig. A conservative estimate of the average frequency at which a similar period would occur is once every 18 days during the months of September to May. During

1976-1977, five rigs were operating in the Gulf of Alaska. At the above prices, an average annual dollar saving for these rigs would have been $100,000/rig occurrence x 5 rigs x 270 days/yr. x 1 occurrence/18 days = $7,500,000/yr.

A recent study by the Getty Oil Company's Exploration and Production Research Center (EPRC Report 80-291), as part of the SEASAT Project Final Data Evaluation, concluded that data from SEASAT can be retrieved to determine site specific wind and wave conditions for operational planning and can be used with other data bases for design studies. Applications of this data base include:

1. Determination of weather windows for performing weather-sensitive offshore operations such as pipelaying, platform installation, and other offshore construction operations.
2. Drilling vessel site evaluations to determine expected operating limits of the drilling riser and mooring system and to estimate weather downtime.
3. Simulation studies for determining expected regularity of offshore loading and storage terminals, and floating production systems.

A minimum of one year of data is necessary, however, to use this data base effectively.

The study also concluded that the utility for offshore drilling and production operations of satellite data, such as that obtained from SEASAT, is maximized if the data can be incorporated into a wind and wave forecast model.

Fishing Industry

The world fishing industry is undergoing a process of transformation. Overkill technologies, lack of sound management principles and legal infra-structure, pollution and other uses and abuses of the ocean space (drilling and dredging, coastal development, and the destruction of many breeding and fishing areas) have led to severe problems in the industry. For example, some of

the major commercial fisheries have collapsed, the yearly rate of increase in world catches has been reduced, and the limits of the sustainable annual yield have been set at a much lower level than that of the more optimistic forecasts of a decade ago. In addition, rising fuel prices and legal restrictions resulting from the new law of the sea may accelerate the downward trend. The industry may move away from distant-water fisheries to coastal and inshore fisheries. Some of these problems are being addressed by internationally mandated organizations, but solutions will be a long time in coming. In the meantime, rampant inflation and foreign competition have caused some problems for fishermen in the United States.

Overkill is one of the factors causing economic problems for the industry. For instance, fishermen can no longer fish within twenty miles of land and rely on conventional observations. To obtain an adequate catch, fishermen must go farther offshore, into deeper water. They need better data so as not to be caught too far from a haven if a storm hits. The king crab industry has suffered from overfishing in the near-shore waters of the Gulf of Alaska. Fishermen are going farther into the Gulf for their catches. Storm-related damage to vessels has increased by a factor of three during the last decade.

An overnight remedy for the ailments afflicting the fishing industry is not apparent. Therefore, every potential source of assistance must be utilized if an economic recovery is to occur. The availability and use of improved environmental data would be helpful. Commercial fishermen cannot afford to take to the seas in conditions that are not advantageous to good fishing. Satellite-derived surface wind data would provide an improved decision-making capability for the fisherman. Safety as well as economy of operations can be improved. Fisherman may need to be educated on the capabilities available and the merits of using near real-time satellite surface stress data. Similar programs using real-time sea surface temperature observations have been successful in the past.

Deep Ocean Mining

Although still under debate, mining the oceans is increasingly seen as becoming a reality by as early as the next decade. Expansion of ocean mining could be triggered by land-environment considerations, the need to conserve dwindling continental reserves, the ready availability of bulk materials absent or depleted on adjacent lands, higher-quality ores easily reachable in coastal waters, improved techniques to reduce exploitation costs, the rarity of some minerals, and economic considerations such as equilibrating balance-of-payment budgets and conserving hard foreign currency.

The bedrock beneath the ocean basins also may contain large concentrations of the same suite of metals as do the ocean basins themselves, namely, manganese, iron, nickel, copper, and cobalt. Such metals as zinc, mercury, chromium, molybdenum, and the precious metals silver, gold, and platinum also may be present. The ... metals and some nickel, copper, and lead could be present in deposits resulting from the differentiation of the molten mantle material from which the basalt itself was derived, or from the melting of crustal plates that were thrust into the mantle. However, there is a smaller variety (but not a smaller quantity) of minerals on the great ocean basin floor than on the various segments of the continental margin (shelf, slope, rise) and in small ocean basins.

Ocean mining will be complex, difficult, and costly. A 1975 report of the National Research Council nevertheless concludes that marine mining offers enormous potential for U.S. independence from foreign countries for some important minerals, including those used as sources of energy.

Deep ocean mining will be strongly impacted by environmental conditions. The equipment required to carry on the complex operations needed to bring these materials to the surface will be unique. Design and operation of such equipment will require knowledge of the environment in which it will exist.

Satellite-sensed information will be the foundation of these data bases, and satellite surface stress measurements will be a major component. As with the data needed to support offshore oil and gas operations, a lengthy record of measurements (minimum of one year) is required. Site-specific wind data will be used for making decisions on operational techniques. Stress data will be used with other data in design and development work. The environmental problems associated with deep ocean mining are large.

Deep ocean mining on a production scale requires a staggering initial capital investment. In 1975 dollars, $240-$900 million would be needed to extract manganese, copper, and cobalt near Hawaii and to process 5,000 tons a day in California. Perhaps 20 years would be required to bring the project on stream. This seems to point toward a need for governmental incentives to encourage capital investment in ocean mining. But besides money, further refinement of the technology must be encouraged and manpower appropriately trained.

Ship Routing

Weather forecasts over the ocean are routinely used to produce optimum ship routing forecasts for commercial and naval ships. Unfortunately, weather forecasts at sea are relatively poor due to the lack of measurements needed to initialize the weather model. Direct measurement of wind stress over the sea and near real-time availability of these winds would permit the preparation of improved weather and seastate forecasts. These forecasts would, in turn, provide improved ship routing services.

Applications of SEASAT SASS data in optimizing commercial ship routing between the Far East and the United States over northerly routes indicate a potential reduction of 85,000 nm of travel per year. This translates to a potential savings of $2,700,000 per year for this route alone. Ships traveling between Australia and Africa through the southern Indian Ocean can expect mileage and monetary savings of 36,700 nm and $1,200,000 per year, respectively, when they incorporate SEASAT-enhanced commercial routing.

Before a vessel departs on a transoceanic voyage, the route analyst uses long-range forecast charts (beyond 48 hours) to map out a suitable route. Of primary concern to the route analyst are the locations of major patterns in the upper atmosphere, such as ridges and troughs, and accompanying surface features, such as high and low pressure centers. These pressure patterns, in turn, illustrate the orientation and characteristics of major wind and wave fields across the ocean. During the actual voyage, however, analyses and short-range forecasts are required to institute route diversions if there are unexpected changes in the movements of the wind and wave fields. Since only SEASAT SASS-aided analyses are available for the comparison, the route improvements consist of small diversions from original courses. Many ships sailing between North America and the Far East follow more northerly routes through the Gulf of Alaska, approximating the shorter, great circle routes. The positions of low pressure systems in the Gulf must be accurately determined so that vessels can avoid the systems and accompanying gales and rough seas. The farther north the lows occur, the farther north ships can sail, more closely approximating a great circle. Considering all vessels traveling over a northerly route (through the Gulf of Alaska) between the Far East and the United States, the SEASAT SASS-aided analyses result in a repositioning of the low pressure systems to the extent that a total mileage saving of over 85,000 nm per year is realized.

Restated in monetary terms, assuming an average direct operating cost for a vessel moving at 15 knots and consuming 40 tons of fuel per day, the total annual savings for these vessels is estimated to be $2,700,000.

Similarly, ships traveling through the southern Indian Ocean between the continents of Australia and Africa (Cape of Good Hope) might expect from SEASAT SASS-aided analyses a potential mileage savings of nearly 37,000 nm per year. In monetary terms, this is equivalent to $1,200,000/year.

In summary, the incorporation of SEASAT SASS-aided measurements into conventional surface analyses potentially could save the shipping industry nearly $4 million per annum in the North Pacific and southern Indian Oceans. These figures do not take into account the role of SEASAT SASS analyses in the avoidance of ship damage and excessive wear or the incorporation of SEASAT SASS measurements into numerical forecast models.

APPENDIX A

REVIEW OF MICROWAVE SCATTEROMETRY

SEASAT Scatterometer

The SEASAT Satellite Scatterometer (SASS) was one of several microwave remote sensors launched on the SEASAT oceanographic satellite in June 1978 (Grantham *et al.*, 1977). The purpose of the SASS was to provide global measurements of the synoptic scale ocean-surface vector wind stress and neutral stability wind vector at a 19.5 m reference height. The physical basis for this technique is the Bragg scattering of microwaves from centimeter-length capillary ocean waves. The strength of the radar backscatter, σ^0, is proportional to the capillary wave amplitude, which is in equilibrium with the wind stress at the sea surface. Moreover, the backscatter is anisotropic; therefore, wind direction can also be derived from radar measurements at different azimuths.

The method used by SASS to obtain two azimuth "looks" is illustrated in Figure A-1. Four dual-polarized, fan-beam antennas were aligned so that they pointed 45 degrees and 135 degrees relative to the subsatellite track to produce an "X"-shaped pattern of illumination on the earth. In this way, a given surface location was first viewed by the forward antenna and, approximately 1 to 3 minutes later (depending on whether the location was at the inner or outer portion of the swath, respectively), it was viewed orthogonally by the aft beam. Fifteen Doppler filters were used to subdivide the antenna footprint electronically into resolution cells (see hyperbolic constant Doppler frequency lines in Figure A-1). Because the SEASAT hardware used a single set of analog filters to process forward and aft antenna beams, and because of the earth's rotation, the actual Doppler contours were slightly rotated relative to the satellite velocity. This effect is illustrated in Figure A-2, where

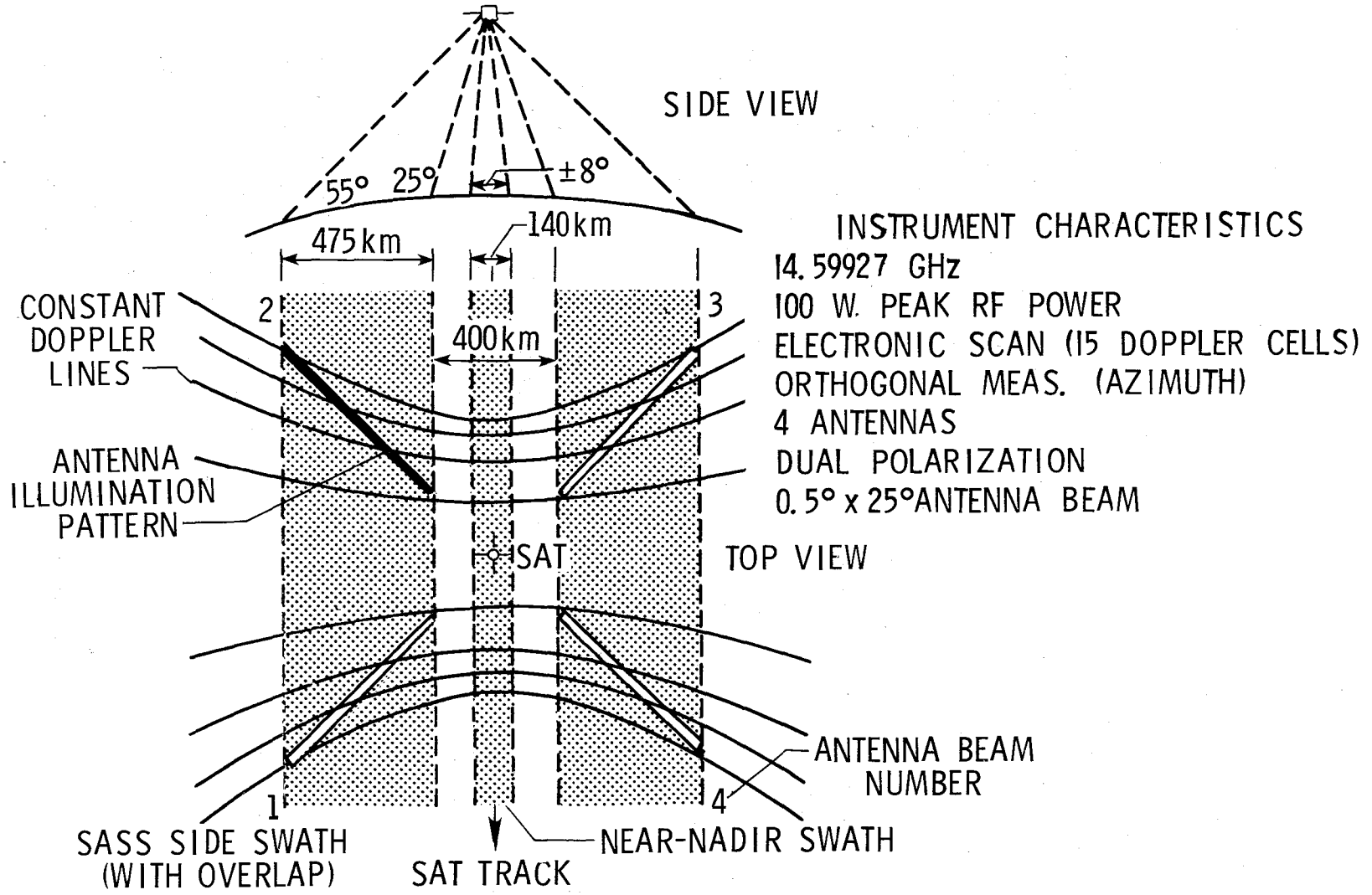

Figure A-1. SEASAT scatterometer illumination pattern and instrument characteristics.

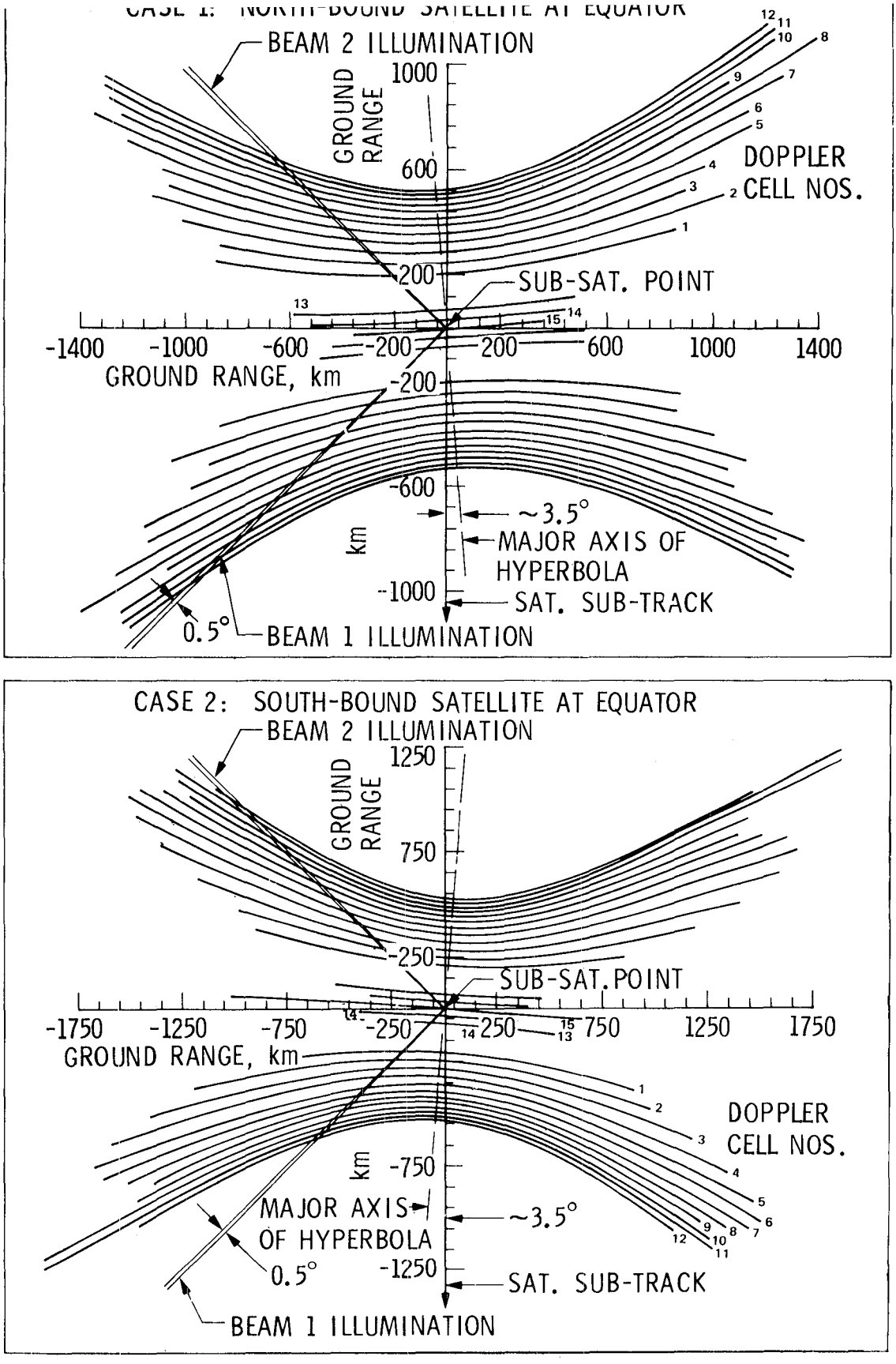

Figure A-2. Plot of constant Doppler lines.

the constant Doppler lines corresponding to the 15 scatterometer cell center frequencies are given for antenna beams 1 and 2. Both the northbound (ascending) and the southbound (descending) orbit cases at 0° latitude are shown. Note that the Doppler lines are not quite symmetrical about the spacecraft subtrack, but have a symmetry axis that is rotated by approximately 3.5°. This turning of the Doppler lines, caused by the earth's rotation, results in an asymmetrical overlap of the Doppler cell surface footprint patterns generated by the forward and aft beams. The Doppler line rotation decreases with increasing latitudes.

The intersection of the antenna beam pattern and Doppler lines determines the resolution cell size, orientation, and location on the earth. Figure A-3 is an enlarged view of one of the 15 Doppler cells which are synthesized along the beam. As illustrated, the Doppler cell area is determined by the Doppler filter noise bandwidth and the antenna 3-dB beam-width in the narrow-beam plane. The resolution (integrated) cell resulting after a 1.89-s measurement period, T_p, is diagrammed in the lower inset of Figure A-3. Typical cell dimensions are 15 km (across beam) by 70 km (along beam).

An example of the resulting SASS resolution cell locations for Hurricane Fico (SEASAT Rev. 331) is given in Figure A-4. Because of the Doppler frequency shift caused by the earth's rotation, one antenna beam is expanded and one is compressed so that approximately 7 cells of the expanded beam overlap 12 cells of the compressed beam (note that 3 cells of the 15 are located near the satellite subtrack). This distortion is at maximum at the equator and decreases at the maximum latitude of the orbit. Distortion for the opposite swath (antennas 3 and 4) is the mirror image of this figure. (See Appendix A, Advanced Scatterometer Design subsection, for further discussion as to why cells move in and out along the beam when constant Doppler filters are used.)

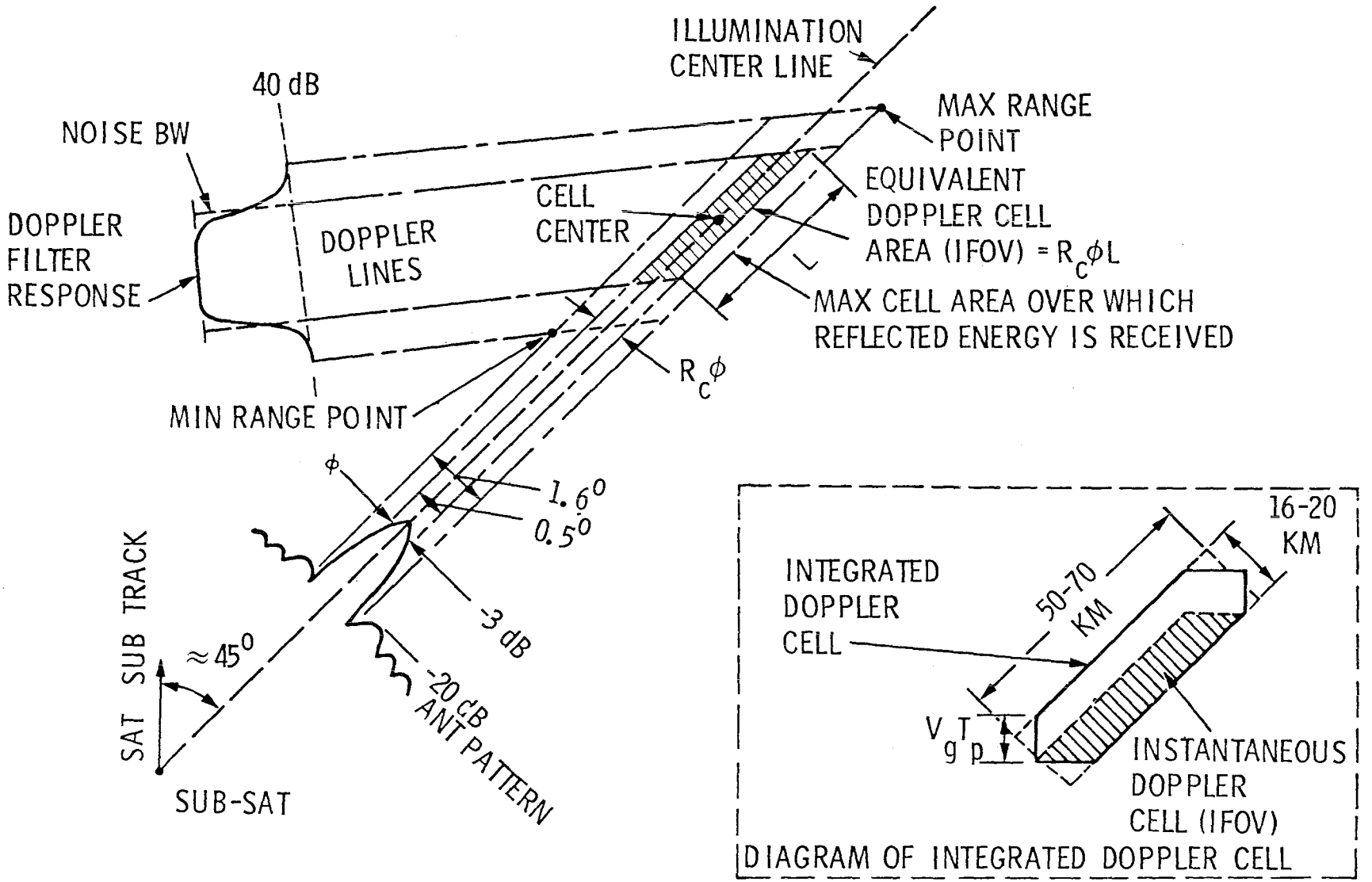

Figure A-3. Doppler cell area as determined by antenna pattern and filter response.

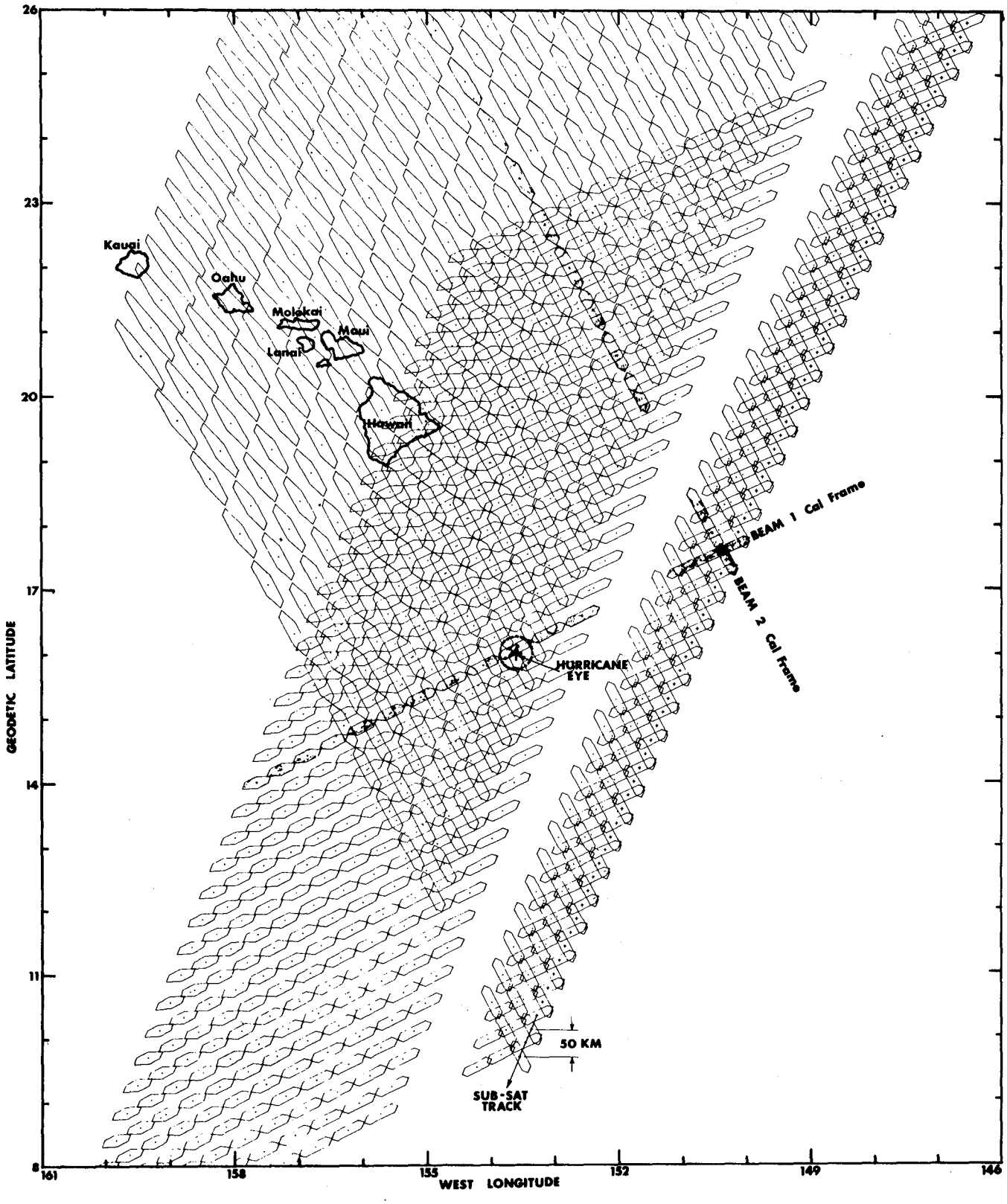

Figure A-4. Doppler cell locations for beams 1 and 2 over hurricane Fico. (SEASAT Rev. 331.)

Geophysical Algorithm

The SASS geophysical algorithm computes the sea-surface wind speed and direction from radar backscatter σ^0 measurements. The algorithm is of a modular design having three components: measurement grouping, least-squares estimator, and σ^0 model function table.

The measurement grouping routines can either pair the closest two orthogonal σ^0 measurements (generally less that 50-km spacing) or group the measurements into latitude-longitude bins ranging in size from 0.5 to 2 degrees. In areas of strong wind gradients, such as storms or fronts, pairing offers the desired high resolution. On the other hand, for light steady winds, data grouping provides improved measurement accuracy, as well as the capability to rank or evaluate the most likely alias.

The least-square estimator (Jones *et al.*, 1978) finds the wind speed, U, and direction, χ, that minimizes the following sum of squares (SOS):

$$SOS = \sum[\sigma^0 - F(U,\chi)]^2/(\Delta\sigma^0)^2$$

where the sum is over either a pair of σ^0 measurements or a group of measurements. The σ^0 model function, $F(U,\chi)$, is interpolated from the model function table. The measurement value and its standard deviation uncertainty are denoted by σ^0 and $\Delta\sigma^0$. The estimator finds two to four wind vectors (aliases) that minimize the SOS. The magnitude of these vectors is nearly equal, but the direction varies widely. These multiple local minima, called aliases, are attributable to the harmonic dependence of σ^0 on the wind direction. A graphical representation of the wind vector estimator is given in Figure A-5. Here loci of wind speed and direction for given σ^0 measurements are plotted for forward and aft antennas. The intersections of the two curves are the aliases described above. Depending upon the σ^0 values (vertical displacements of these

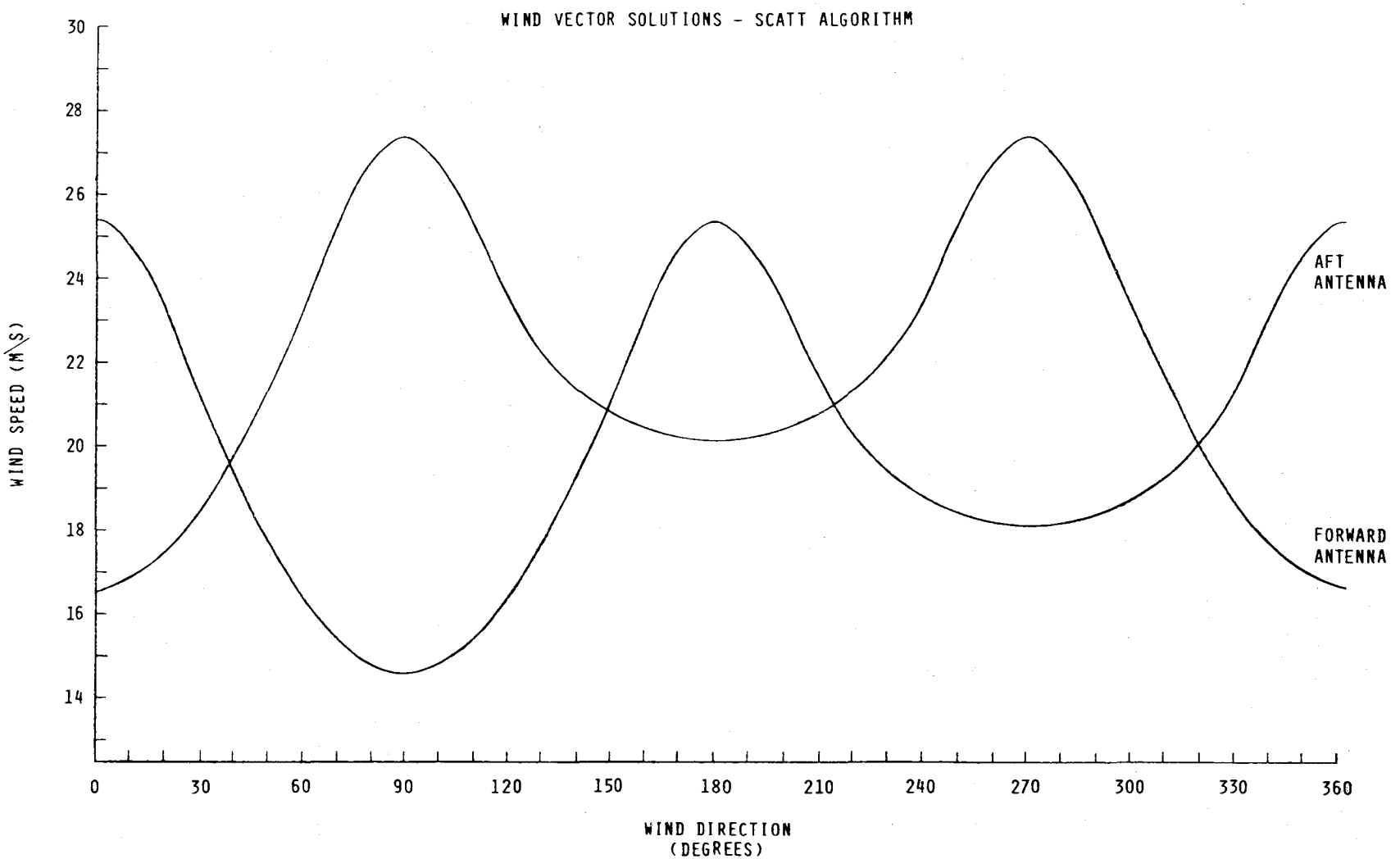

Figure A-5. Wind vector solutions of the scatterometer algorithm, for a given incidence angle and measured σ^0 value from the forward and aft antennas.

curves), the number of intersections varies from one to four. Typically two or four solutions result; the two-solution case occurs when one antenna views either upwind or downwind. Note that the selection of the proper wind solution requires further processing that was not available for SASS, except by manual data processing.

The model function is a correlation matrix which consists of 2736 G and H coefficients that relate wind speed and direction to the σ^0 measurement:

$$\sigma^0(U,\chi) = G(\theta_i,\chi,\varepsilon) + H(\theta_i,\chi,\varepsilon)\log U$$

where θ is incidence angle ($20° < \theta < 60°$), χ is the azimuth angle between radar beam and wind direction, and ε depends on beam polarization. A matrix of the empirical coefficients G and H comprises the SASS algorithm; σ^0 is assumed to vary harmonically with χ, with maxima parallel to the wind and minima normal to the wind, providing wind direction information. A discussion of the SEASAT wind parameterization algorithm can be found in Jones *et al.* (1978) and Schroeder *et al.* (1982a). A general discussion of the parameterization was done by Moore and Fung (1979).

The SASS wind vector algorithm has been evaluated by comparison of SEASAT data with *in-situ* measurements, field analyses, etc. Typical results for the Joint Air-Sea Interaction Experiment (JASIN) comparisons are given in Figures A-6 and A-7. In-depth analyses of the accuracy of SASS measurements are found in Wentz (1978), Jones *et al.* (1982), Brown (1982), and Liu and Large (1982).

SEASAT orbited Earth approximately 14 times a day. Figure A-8 is a black and white copy of a false color map (Schroeder, *et al.*, 1982b) of winds derived from actual SASS σ^0 measurements for a 48-hour period. The figure illustrates the diamond-shaped patterns which result where SASS measurements do not exist. Appendix C describes further the coverage patterns that result for various satellite altitudes and scatterometer configurations.

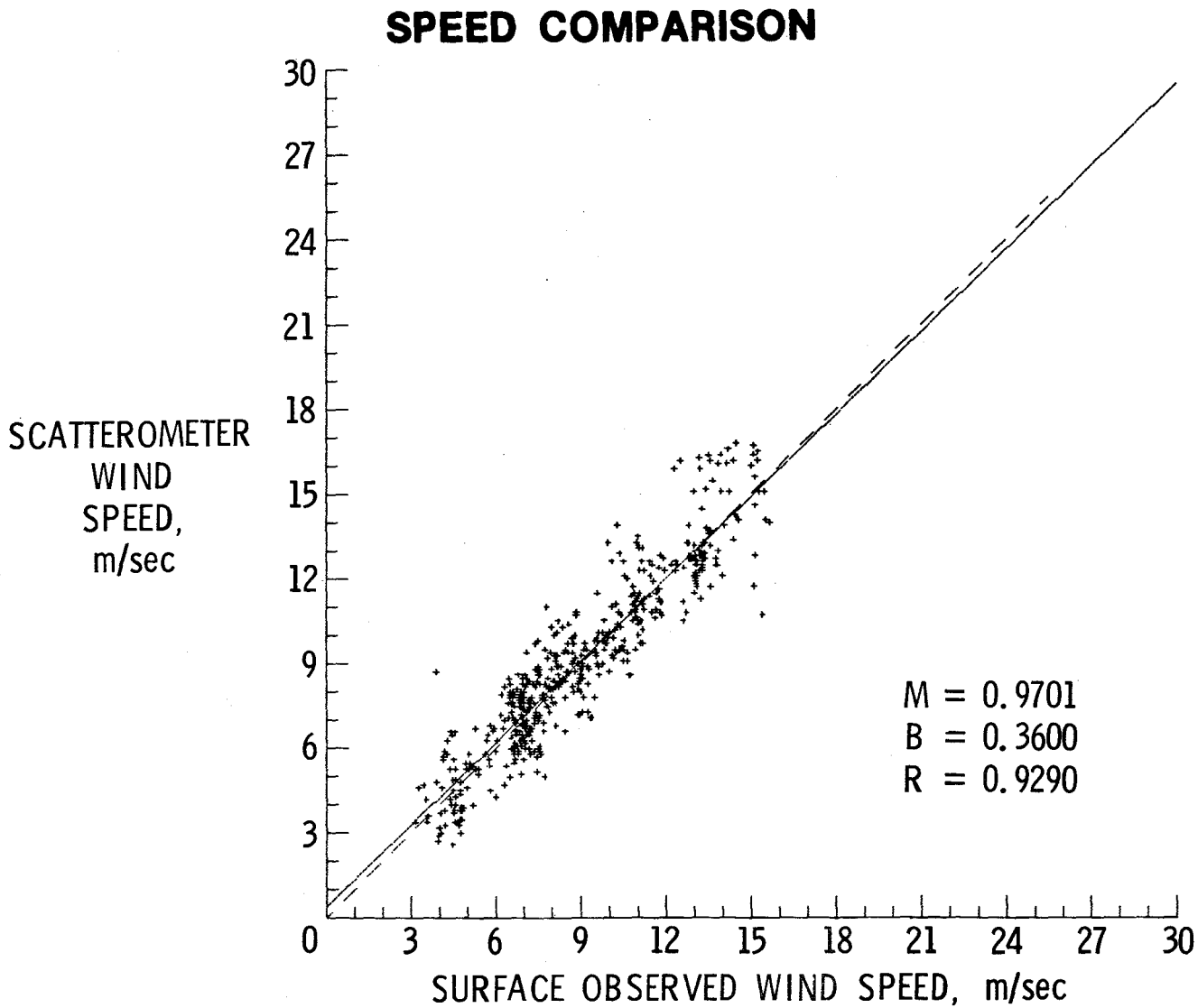

Figure A-6. Comparisons of SASS wind speed solutions with surface wind speed observations in the JASIN experiment.

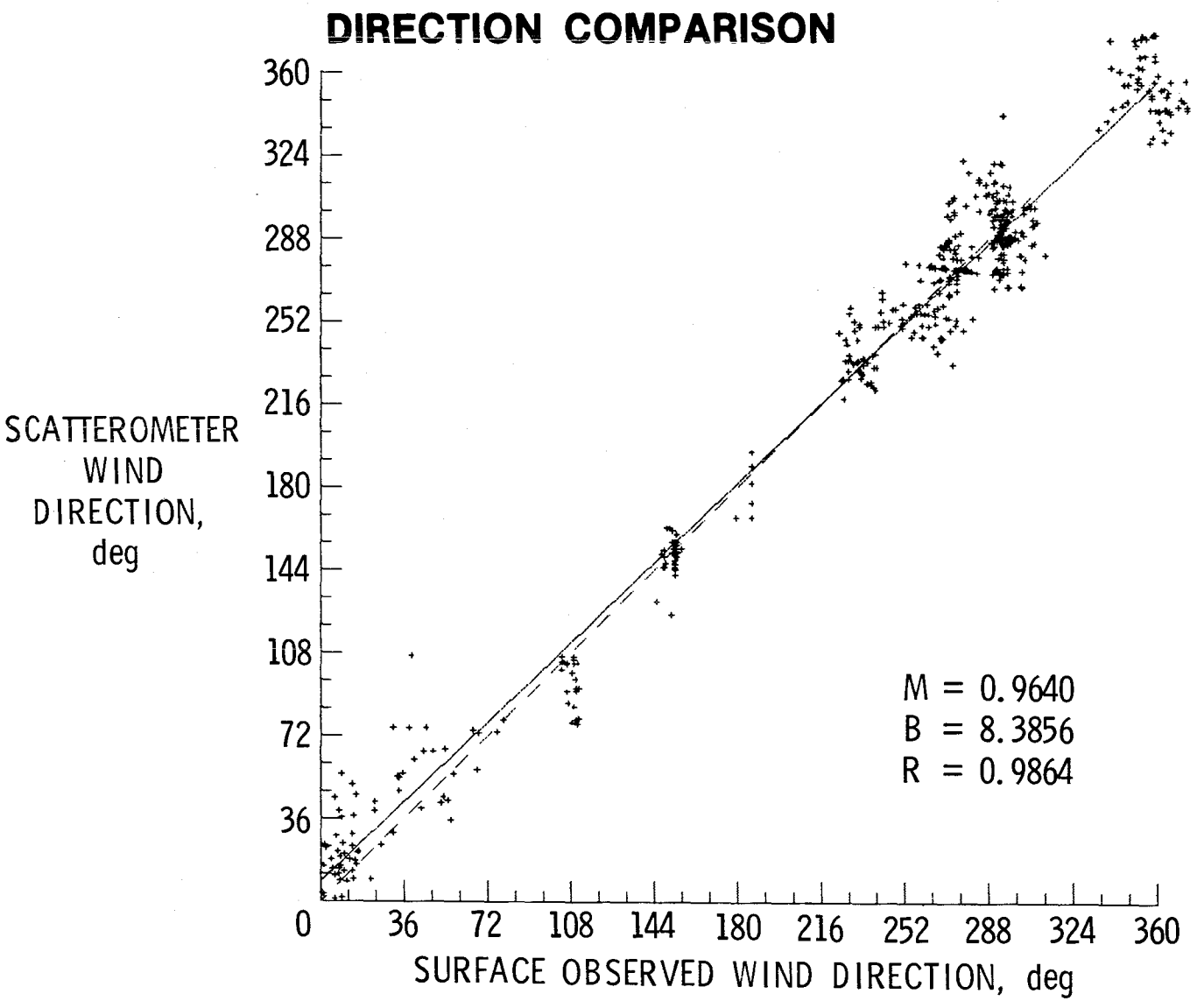

Figure A-7. Comparisons of SASS wind direction solutions with surface wind direction observations in the JASIN experiment.

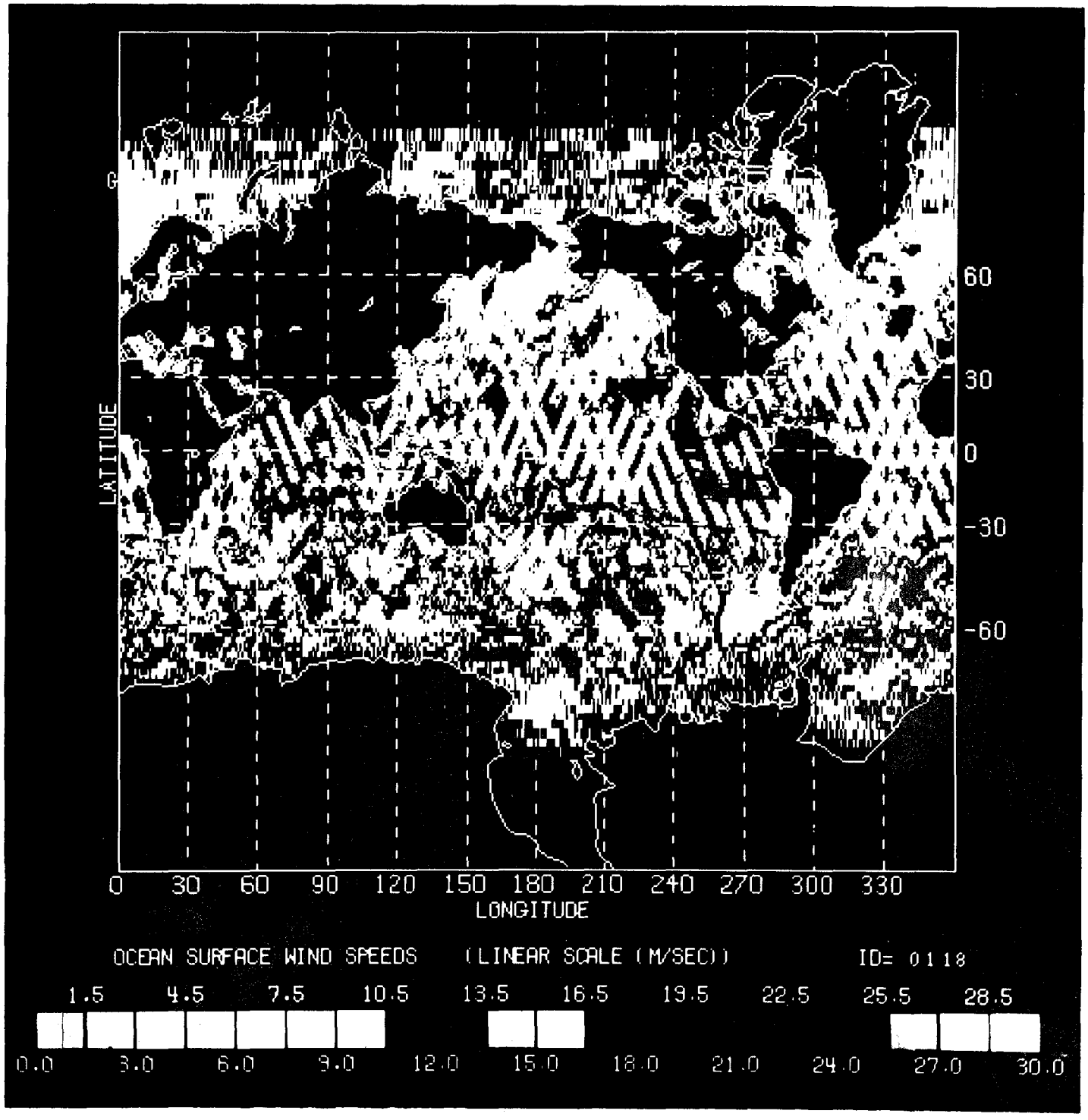

Figure A-8. Black and white print of SASS global wind speed false color map for July 16-17, 2-day period. (See Schroeder, *et al.*, 1982b.)

Advanced Scatterometer Design

Various improvements over the SEASAT scatterometer design are being considered for the design of a future scatterometer. These improvements include (1) the use of additional antennas to provide measurements at a third azimuth angle, along with V and H polarization, to improve instrument alias removal skill; (2) the use of digital Doppler filters and higher sampling resolution, to provide accurate co-registration of measurements from three antennas and thus minimize errors caused by wind gradients; and (3) the use of a sufficient number of antennas and polarizations to provide swath coverage on both sides of the spacecraft.

The use of digital Doppler filtering can significantly improve the design of a scatterometer. To better understand the difference between this technique and the analog (constant Doppler) filtering technique, and the significance of the techniques in the performance of a scatterometer, a brief description of each is presented below.

Doppler filter processing is used in the scatterometer to separate the backscattered signal from the surface into separate frequency bands or resolution cells. Due to the Doppler effect, caused by spacecraft velocity and the earth's rotation, the backscattered signal along the beam is spread over a band of frequencies that increases from zero hertz at nadir incidence angle to approximately 400 kilohertz at a 60° incidence angle. Each Doppler filter has a different center frequency, so that the output energy from each filter corresponds to the backscatter from a different ocean surface location along the beam. The bandwidth of the filter determines the energy spectrum along the beam included in each filter, and thus the cell resolution. Two basic techniques can be used to provide Doppler filter processing: (1) analog filtering, which incorporates a bank of fixed narrow-band crystal filters such as that used in the SEASAT scatterometer; and (2) digital signal processing, which incorporates a Fast Fourier Transform (FFT) technique for digital filtering.

Analog Filter Processing. An analog filter processor for a 50 km resolution system consists of 15 to 20 (15 on SEASAT) parallel channels. Each channel contains a crystal filter, square-law detector, and signal integrator. Each crystal filter is tuned to a different center frequency and a different bandwidth. The frequency is chosen to provide the desired cross-track coverage and range of incidence angles for the primary wind vector swath. Additional filters are usually provided for wind speed measurements near nadir. The bandwidth is chosen to provide the desired resolution. Since the fore and aft antennas cover approximately the same frequency band, the same crystal filters can be used for these beams. However, the middle antenna must use a different bank of filters, since the range of frequency on this antenna is much different from that of the fore or aft antenna. This means that an additional 15-20 crystal filters are required for use when the middle beam is sampled.

Since the earth's velocity vector rotates with respect to the satellite's velocity vector, the net Doppler frequency for any particular cross-track position changes as the spacecraft moves around the orbit. The Doppler frequency for each beam at a specific cross-track location also is different. Since the analog filters have fixed center frequencies, the cells' corresponding surface position will move in and out along the beam as the spacecraft travels around the orbit. The bandwidth required for each filter for a specified resolution is different for each position along the beam. Thus as the cells move in and out along the beam, the cell size changes. Misregistration of the cells from the forward, middle, and aft beams will occur as a result of the shifting of the cells' surface position. The dimensions of the cells from each beam for a grouped set of measurements can also be significantly different. These differences, plus the misregistration, can cause significant wind speed and direction errors in a gradient situation, since the cell from each beam will see a different surface condition. By providing center frequency adjustment capability in the Doppler filter

processor, and by sampling the surface at closer intervals using higher resolution cells, the measurements from each beam can be made to co-register accurately and view the same surface conditions, thus minimizing gradient errors.

Analog Doppler filtering systems are not well suited for adjustable frequency capability or high resolution. Increasing the resolution requires a significant increase in the number of processing channels and crystal filters. To provide adjustable frequency capability, a significant increase in the complexity of the receiver design is required. Such design changes would be costly and probably would significantly increase both the weight and the power requirement. A digital processing technique, however, can provide frequency adjustment capability and higher resolution at little or no cost or weight increase, along with a minor power increase over a twenty-channel analog system.

Digital Filter Processing. The digital filter processor uses a Discrete Fourier Transform (DFT) technique, which transforms the backscattered signal from the time domain to the frequency domain. The backscattered signal is sampled N times at a rate f_s, which is equal to the signal bandwidth, B, being processed. The DFT of these time samples, $x(t_i)$, is calculated as

$$X(f_k) = \frac{1}{N} \sum_{i=0}^{N-1} x(t_i) e^{-j2\pi iK/N} \qquad (1)$$

yielding components at a finite set of discrete frequencies that are harmonics of f_s/N, so that $f_k = kf_s/N$ for $k = 0, 1 \ldots N-1$. In order to process the full band of interest, the input signal is divided into its in-phase and quadrature components. With this process performed, the in-phase and quadrature (real and imaginary) parts of equation (1) can be calculated as follows:

$$X_R(f_k) = \frac{1}{N} \sum_{i=0}^{N-1} x(t_i) \cos \frac{2\pi ik}{N} \qquad (2)$$

$$X_I(f_k) = \frac{1}{N} \sum_{i=0}^{N-1} x(t_i) \sin \frac{2\pi ik}{N} \qquad (3)$$

The power spectral density, or average power, contained at each discrete frequency (frequency bin) is computed by summing the squares of equations (2) and (3), that is, $|X(f_k)|^2 = X_R^2 + X_I^2$. To evaluate equations (2) and (3) in an efficient manner with feasible hardware, an FFT computational algorithm is employed. This algorithm is based on factoring the DFT matrix, which is required to compute equations (2) and (3), into a series of simple matrix operations that can be implemented in hardware in a straightforward manner.

The resulting bin spacing, or resolution bandwidth, is $B_r = f_s/N = 1/N\Delta t = 1/T$, where $\Delta t = 1/f_s$ is the sampling time interval and T is the total data period. Once the power estimate, $|X(f_k)|^2$, of the backscattered signal is computed in each resolution bandwidth, then the total power in a desired Doppler bandwidth can be determined by summing up the power from a number of resolution bandwidths. Since the spacing of these resolution bandwidths corresponds directly with positional location along the beam, by properly choosing the right set of bins to form the Doppler filter, the backscatter from any cross-track location can be determined. In addition, the particular set of bins used to form a specific Doppler filter can be changed to vary the center frequency of the filter and thus determine the backscatter power from the same cross-track location. The Doppler frequency at a particular location varies as an approximate sine wave around the orbit. A simple program can be implemented to shift the bins being combined at fixed intervals of time from the ascending node. Figure A-9 shows a time frequency output of the FFT, illustrating how the Doppler filter channels are formed. (For a more detailed discussion of digital filtering and the FFT algorithm, see General Electric Co., 1980.)

After the failure of the SEASAT spacecraft, the development of a new oceanic spacecraft, called the National Oceanic Satellite System (NOSS), was initiated. The NOSS was to be a limited operational demonstration ocean-monitoring mission proposed jointly by NASA, the

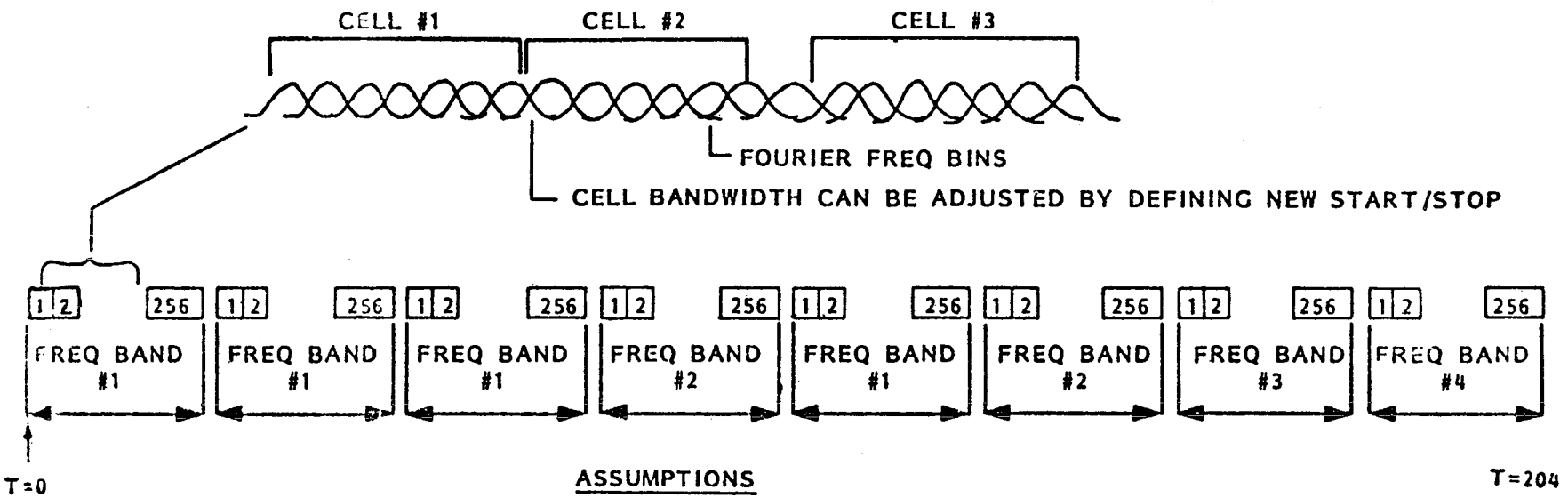

ASSUMPTIONS

4 FREQUENCY BANDS
256 POINT FFT'S
8 FFT'S → 2048 COMPLEX FREQ ESTIMATES
1024 INDEPENDENT FREQ ESTIMATES
60 FREQUENCY CELLS FOR10 KM RESOLUTION
CELL ARE COMPRISED OF ADJACENT (INTIME & FREQUENCY) FOURIER FREQ BINS
CELLS CAN BE ARRANGED IN SUCCESSIVE ORDER
6 ANTENNAS
CELLS ARE LIMITED TO ONE FFT.

Figure A-9. Time/frequency output of Fast Fourier Transform.

Department of Commerce/National Oceanic and Atmospheric Administration (DOC/NOAA), and the Department of Defense (DOD). Using the experience gained from earlier proof-of-concept satellite ocean-monitoring experiments on SEASAT and Nimbus 7, the NOSS mission was to provide data for developing and testing new techniques for incorporating routine global satellite observations of ocean parameters into civil and military operational weather and oceanographic forecast systems. The NOSS mission was designed to collect, process, and distribute satellite ocean data in an operational mode for 5 years, beginning in 1986 (this project was canceled in early 1981).

A summary of the technical characteristics of the NOSS scatterometer is given in Figure A-10. The design incorporated a programmed digital filter to compensate for the effects of the earth's rotation. Two complete instruments, each sampling 3 dual-polarized antennas on each side of the spacecraft, were to be used. An example of the improved cell co-registration is shown in Figure A-11.

The scatterometer operated with a 10-km resolution, providing σ^0 measurements every 10 km along the track and cross-track. Wind vector solutions could be provided at a global resolution of 50 x 50 km by binning 25 of the 10-km σ^0 measurements from each beam. A regional resolution of 25 x 25 km could be provided for high wind speed/gradient conditions. In special situations, such as hurricanes, wind vectors at the highest resolution also could be provided. Since 3 antennas with both polarizations were used for each wind vector solution, the preferred alias could be specified with relatively high skill.

Simulation studies were performed by Grantham *et al.* (1982) to evaluate the improvements in the NOSS scatterometer design. A program that simulates the flight of an in-orbit scatterometer over a realistic wind field was developed. The instrument operation is simulated, and noisy measurements of normalized radar cross sections (σ^0) are generated for each cell location on the windfield. Communication noise error, attitude errors, and model function errors are incorporated, using Monte Carlo techniques to simulate error

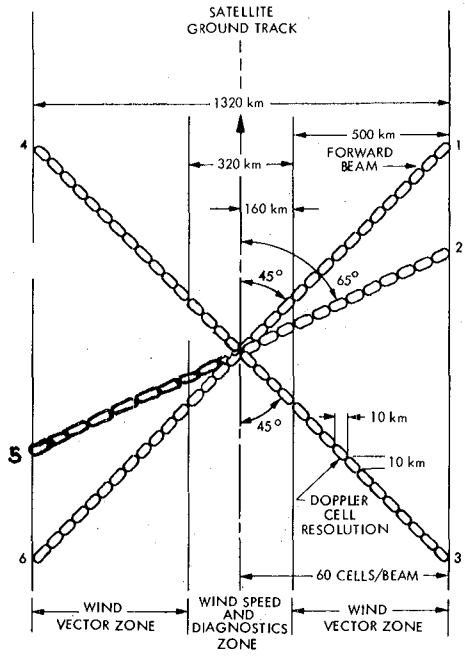

PERFORMANCE

- OCEAN SURFACE WIND SPEED 4 TO >24 m/s, ACCURATE TO WITHIN ±2 m/s OR 10%, WHICHEVER IS GREATER
- OCEAN SURFACE WIND DIRECTION 0-360°, ACCURATE TO WITHIN ±20° AND WITH DIRECTIONAL AMBIGUITY 66% CORRECT
- WIND VECTOR GRID SPACING - 50 km (GLOBAL), 25 km (REGIONAL)

TECHNICAL CHARACTERISTICS

• ORBITAL ATTITUDE	700 km
• SWATH WIDTH	1320 km
• GRID SPACING (σ^0)	10 km
• CELL RESOLUTION (σ^0)	10 km x 10 km (EQUIVALENT)
• CELL RESOLUTION (WIND VECTOR, LEVEL II)	
• GLOBAL AT FULL PRECISION	50 km x 50 km
• REGIONAL AT REDUCED PRECISION	25 km x 25 km
• FREQUENCY	13.99 GHz
• BANDWIDTH	±500 kHz
• ANTENNA POLARIZATION	HORIZ/VERTICAL
• ANTENNA PEAK GAIN	32.5 dB
• BEAMWIDTH (NOMINAL)	1/2° x 25°
• MEASUREMENT SAMPLING PERIOD FOR EACH ANTENNA	0.25 s
• MEASUREMNT CALIBRATION PEROID	4 min
• DIGITIZATION	12 bits
• DATA RATE	12 kb/s

• PULSE WIDTH	~ 5 ms
• PULSE REPETITION RATE	61 pulses/s
• AVERAGE TRANSMITTED POWER	21 W
• PEAK TRANSMITTED POWER	100 W
• RECEIVER NOISE	4.5 dB
• GAIN CONTROL	AUTOMATIC (3 STEPS)
• MAXIMUM BIAS ERROR	≤±2 dB
• SYSTEM PRECISION	±0.1 dB
• ELECTRONIC SYSTEMS (2) SIMULTANEOUS OPERATION	3 ANTENNAS EACH SYSTEM WITH DUAL POLARIZATION
• WEIGHT	240 kg
• POWER	260 W REGULATED 170 W UNREGULATED
• DIMENSIONS	
• ANTENNAS	310 x 10 x 15 cm (EACH)
• ELECTRONICS	115 x 55 x 31 cm (EACH)

Figure A-10. Technical characteristics of the NOSS scatterometer design.

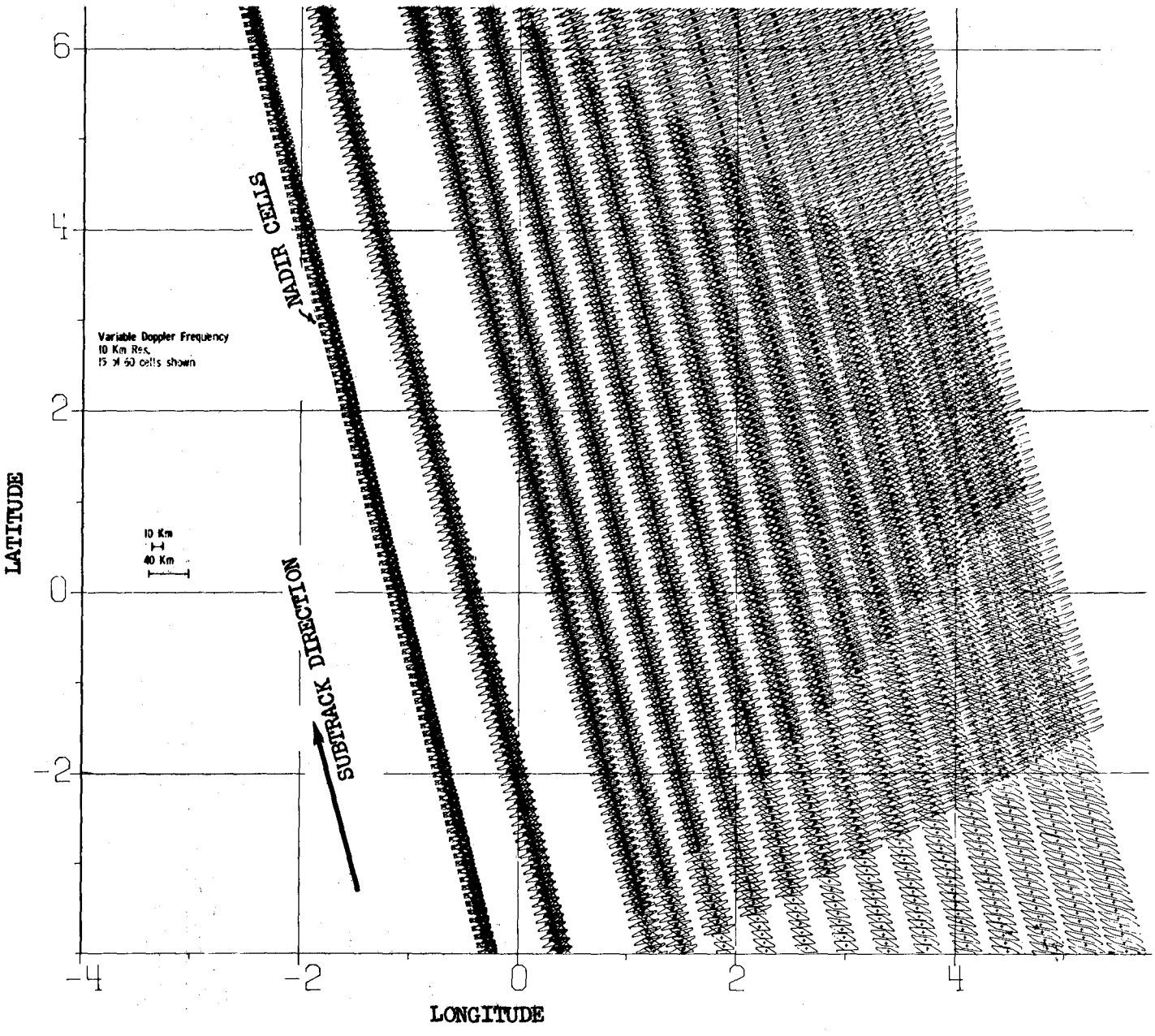

Figure A-11. Doppler cell location plots, beams 1, 2 and 3 for the NOSS 10-km design, using digital variable Doppler frequency processing. 15 of the 60 cells are shown.

on the σ^0 measurements. Wind vector solutions are generated from these noisy measurements. The solutions are then compared to the original wind field, error statistics are computed, and intercomparisons are made.

Six simulated overflights using different wind fields have been studied. These fields were taken from the inventory of actual surface truth data (developed by SEASAT) to make them as realistic as possible. The results of all cases are given in Table A-1. In each case, the RMS and bias errors are given for both wind speed and direction. Percentages are given for the times that each multiple solution value is correct. The column to the extreme right shows that the scatterometer specifications for the closest alias are met more than 95% of the time for any of the wind fields considered.

The results of this study show that an operational scatterometer can meet the user-specified requirements of ±2 m/s wind speed accuracy (or ±10%, whichever is greater) and ±20° wind direction accuracy over most of the expected ocean surface conditions. However, the results of the alias removal skill shown in Table A-1 are applicable only to a three-antenna, dual-polarized design. Since a future scatterometer may not be able to incorporate two instruments to provide full dual-polarized capability on both sides of the spacecraft, additional simulation studies have been conducted for other antenna and polarization configurations. The following paragraphs discuss the results of this study.

Scatterometer Alias Removal Skill. The alias removal skill of a wind scatterometer varies as a function of the number of antennas and polarizations used to measure the normalized radar cross section (σ^0) at each surface location. These σ^0 measurements are used to derive multi-valued wind vector solutions (aliases), each of which has a different wind direction and a slightly different wind speed. Only one of these solutions is closest to the true direction. The wind vector algorithm, which derives these solutions from the measured σ^0 values, ranks the aliases according to likelihood of their being the

Table A-1. Operational Performance for a NOSS Scatterometer Design

		SPEED			DIRECTION		% TIME SOLUTION IS CORRECT				POINTS EXCEEDING SPECS	
CASE	NO. OF POINTS	MEAN VALUE	MEAN ERROR	RMS ERROR	MEAN ERROR	RMS ERROR	1st	2nd	3rd	4th	SPEED	DIRECTION
I	1030	15.2 m/s	-.1 m/s	.76 m/s	0.18^0	6.9^0	88%	8%	3%	.4%	.6%	1.2%
II	1245	7.9 m/s	.02 m/s	.47 m/s	-1.4^0	8.3^0	84%	12%	3%	1%	.2%	4%
III	1386	8.3 m/s	.03 m/s	.57 m/s	-1.3^0	10.8^0	83%	14%	2%	1.2%	.6%	4.8%
IV	1184	7.9 m/s	.03 m/s	.44 m/s	-0.8^0	6.8^0	83%	13%	3%	.9%	.1%	1%
V	1088	6.9 m/s	.02 m/s	.47 m/s	2.2^0	8.8^0	86%	11%	3%	.5%	.7%	3%
VI	1101	9.2 m/s	.01 m/s	.54 m/s	$.9^0$	7.5^0	84%	11%	5%	.5%	.2%	2%

most nearly correct solution. The additional simulation studies have shown that the first pick is closest to the true direction for about 50 to 90 percent of the time, depending on the antenna and polarization combinations used to make the σ^o measurements. The likelihood of either of the first or second aliases being closest is better than 90 percent for almost any combination of antennas and polarizations. Because the first and second aliases are generally about 180° from each other in direction, they form the wind streamline. Under certain wind directions relative to the antennas, the first and second aliases may not always form a streamline, but may be separated only by angles as small as 45 to 60 degrees. However, this situation occurs less than 5% of the time. Table A-2 lists the approximate skill of the instrument for various antenna and polarization configurations.

Table A-2. Instrument Alias Skill Performance

CASE	Number of Antennas per Spacecraft Side	Number of Polarizations Per Wind Meas.	% Instrument Skill	
			1st Alias	1st or 2nd Alias
1	3 (Dual Pol.)	3V + 3H	85 - 90	95 - 98
2	3 (Single Pol.)	2V + 1H	68 - 73	90 - 95
3	3 (Single Pol.)	3V	48 - 53	90 - 95
4	2 (Dual Pol.)	2V + 2H	58 - 65	88 - 92

A scatterometer instrument can be designed to sample any number of antenna beams. Increasing the number of beams sampled beyond six, however, lowers the dwell time on any one beam and reduces the measurement accuracy at low windspeeds. Case 1 in Table A-2 provides

the best overall performance for a 6-beam, one-sided swath. To provide both-side coverage requires either a second instrument (as proposed for NOSS) with its increased power consumption, or a sampling of 12 beams with one instrument and acceptance of degraded low wind speed accuracy. Cases 2 and 3 can cover both sides of the spacecraft using one instrument to sample 6 beams. Case 4 will require one instrument to sample 8 beams in order to cover both sides of the spacecraft. From the standpoint of skill performance and overall wind speed and direction accuracy, Case 2 appears to be the best choice for the future flight configuration. This case provides two-sided coverage with one instrument, without accuracy degradation at low wind speed.

Alias removal algorithms that can significantly increase the first alias skill are under development. The algorithms work with a field of wind vector data provided by the instrument, along with the alias ranking. They use continuity checks, smoothing techniques, and meteorological principles, and they correct the alias ranking specified by the instrument where necessary.

Simulation studies using Case 1 (the NOSS design) and alias removal algorithms have shown that first alias skill can be raised to better than 95 percent. It is felt that similar results can be obtained for Case 2. Further simulation studies are being conducted to verify this conclusion.

The simulation studies were performed for both digital and analog filter designs. Since swath coverage is reduced in the analog filter design due to lack of overlap between the cells from the forward and aft antennas (caused by the earth's rotation effects), additional filters were added (a total of 17 for the main swath) in order to maintain swath coverage comparable to the digital filter design. The results of the study show, however, that for the analog case data gaps still exist in parts of the swath due to a lack of cells from one of the beams within the 50-km bin. This effect is illustrated in Figure A-12, which is a plot of the first two alias wind vectors (from the filter design of Case 1 simulating a flight

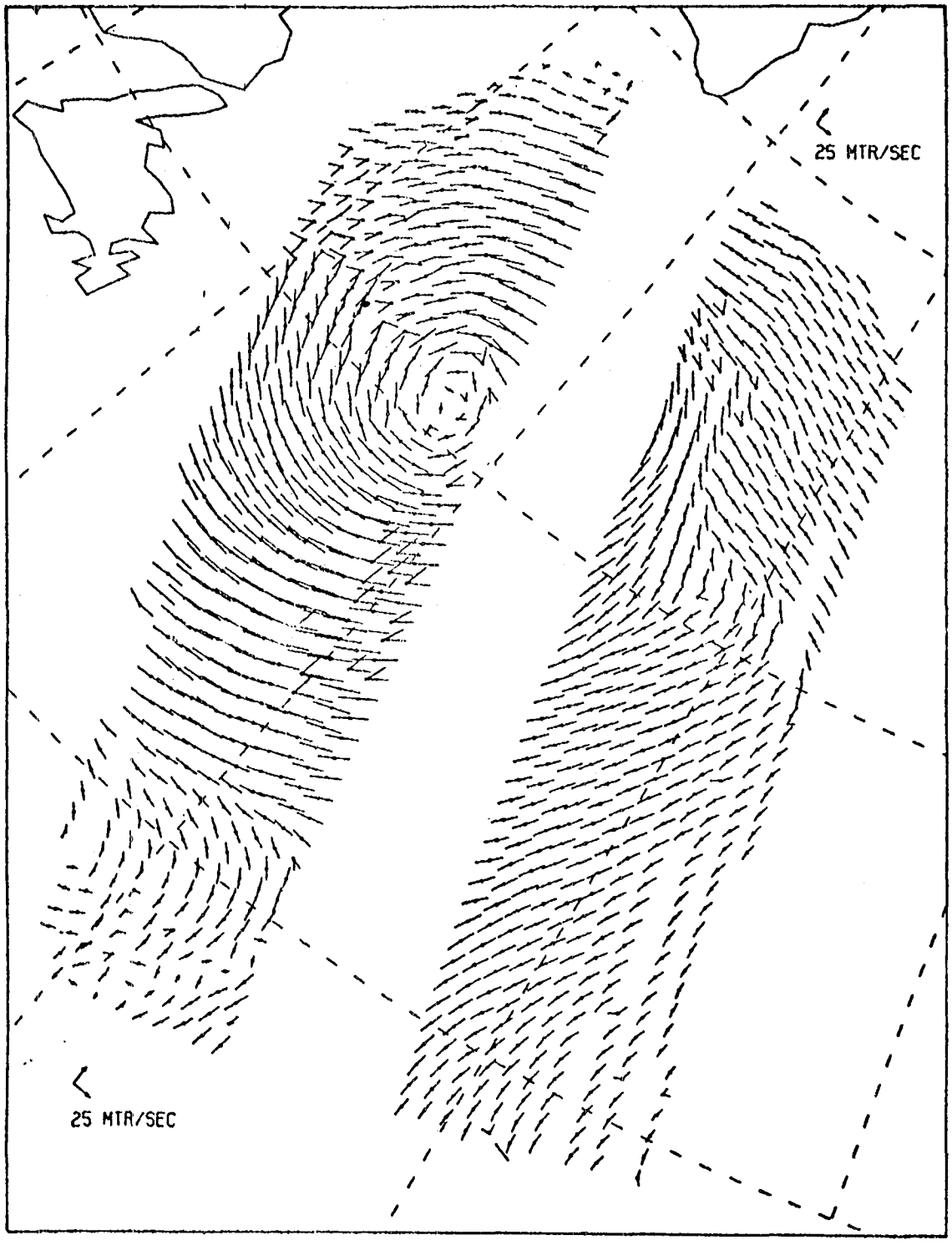

Figure A-12. Plot of the two most probable aliases from the simulation flight over the QE II wind field. Analog filter design (constant Doppler filters). 50-km wind solution resolution.

over the QE II wind field). Figure A-13 is a similar plot for the digital filter design, and Figure A-14 is a plot of the true wind vectors for each 50-km bin location.

The data gaps are quite obvious for the analog case (Fig. A-12). These same gaps do not occur in the digital case. A significant number of additional filters would need to be added to the analog design to fill in these gaps. This would increase power, weight and processing time requirements. A total of about 25 analog channels (50 crystal filters) probably would be needed to eliminate the gaps and provide a 600-km swath coverage similar to that of the digital filter design.

Figures A-12 and A-13 illustrate the streamlines that are generally formed by the first two aliases. However, as sometimes occurs, in some isolated areas the first two aliases do not form streamlines. The two alias plots show good comparison to the true wind vectors plotted in Figure A-14.

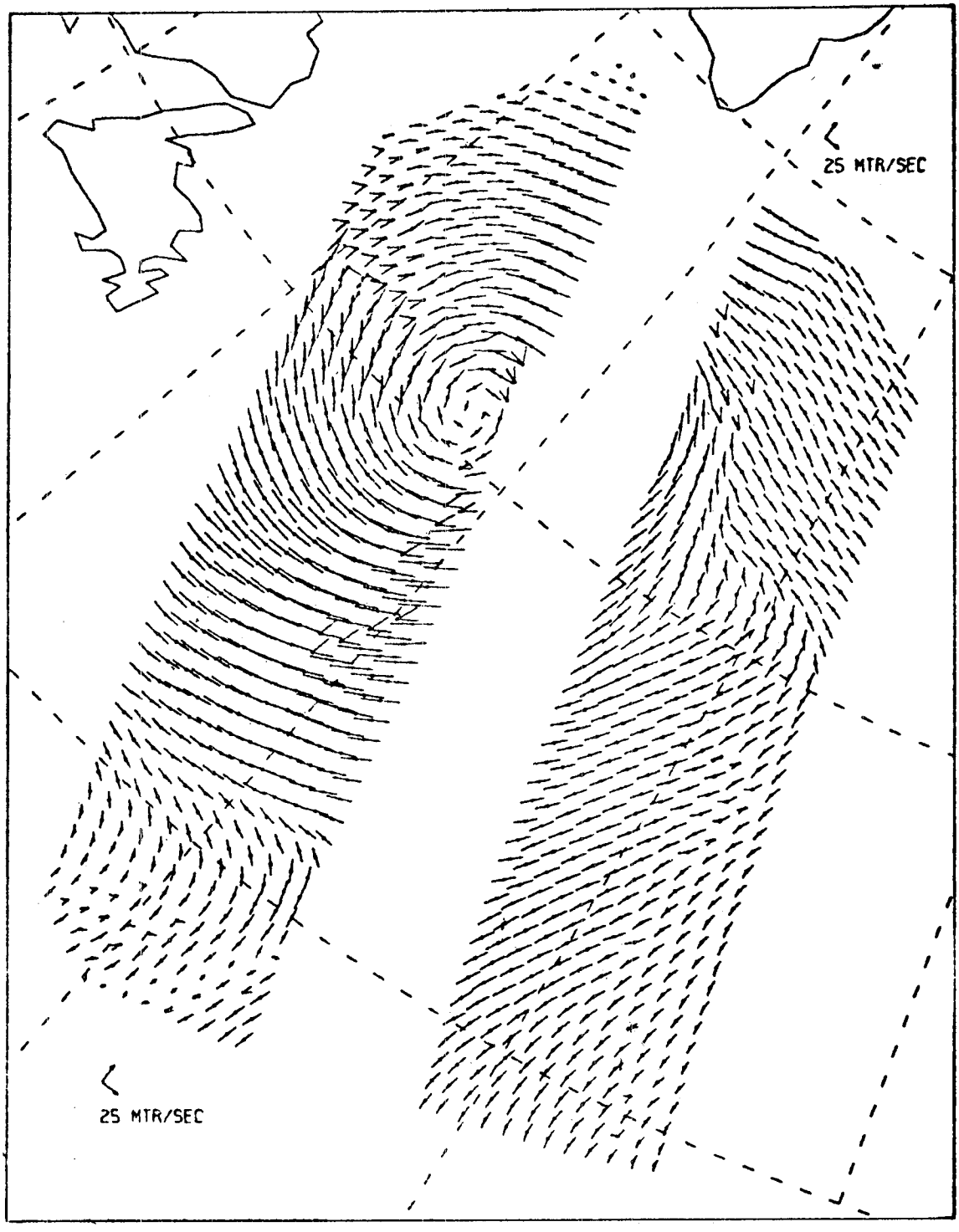

Figure A-13. Plot of the two most probable aliases from the simulation flight over the QE II wind field. Digital filter design (variable Doppler filters). 50-km wind solution resolution.

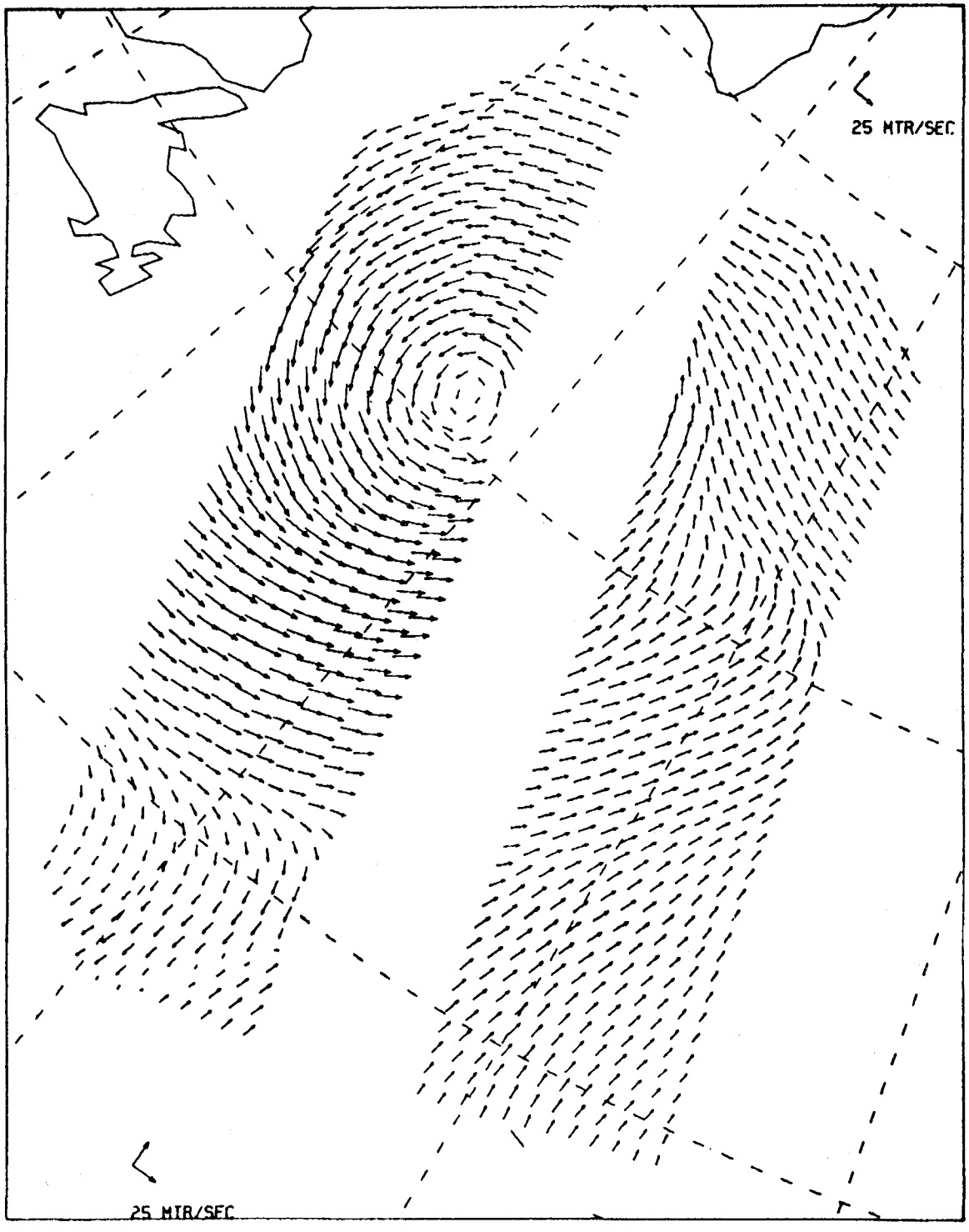

Figure A-14. Plot of the true surface wind vectors for the QE II wind field at the corresponding 50-km bin locations shown in Figures A-12 and A-13.

APPENDIX B

A DISCUSSION OF OCEAN MODELS[1]

Introduction

In the modern scientific world, mathematical models are widely used to increase our understanding of the environment. Oceanographers have used calculus, differential equations and fluid dynamics to explain phenomena in the ocean for centuries. The earliest computers were designed and used to calculate tides for a myriad of practical uses. As we have learned more about the ocean, the need to construct more complicated models has grown. The classical mathematician strives to use analytical techniques to obtain the solution to models. However, these mathematics are limited. The availability of computers has allowed us to consider more sophisticated and realistic models. For example, North Sea scientists have developed sophisticated tide and storm surge models, including realistic geometry and topography that can predict on an operational basis the coastal water level if the weather forecast is reasonable. Wave spectra and swell over the open sea also can be predicted accurately for commercial and military use, given accurate weather forecasts. These are only a few of the many ocean models in routine service today.

There are new and extremely important national requirements for additional ocean models. A few of the types of models that are being developed by the international modeling community are described below. The ocean models that calculate the state or circulation of an entire ocean or the world ocean are called General Circulation Models (GCM's). These models occupy the talent and resources of several modeling groups in the U.S. and other nations.

There are hundreds of other ocean modeling activities that we have not included. Many of the models not discussed, such as the

[1]This discussion was written for the National Academy of Sciences report entitled "A Resource Assessment for Ocean Circulation Modeling," 1982.

so-called mixed layer models or inertial motion calculations, can be done on existing computers.

Ocean modeling has developed slowly in comparison to meteorology due to the lack of data for verification. In the past decade, we have had important field experiments that obtained data for model comparison. Due to the lengthy list of national problems which require ocean modeling, it is generally agreed that the U.S. will continue to plan and execute field programs and encourage ocean modeling activities.

In many respects, modeling the ocean is scientifically straightforward. We know the pertinent equations from fluid dynamics and physics. If we have initial conditions and boundary conditions, it is reasonable to assume that a solution can be calculated. Unfortunately, as in meteorology, the inherent nonlinear and turbulent character of the ocean limits our capability to perform the calculation. We must compromise the complete problem and pose a solvable model. The usual limitation is economics. Even given the largest computers available, it is not possible to perform the calculations we would really like to do. However, there are a wealth of useful theoretical and practical models that can be constructed. In this report we are concentrating on the largest of these ocean models, which seem to be amenable to progress if sufficient investment is made in computer resources.

General circulation models can be divided into two categories, depending on whether the intended calculations will emphasize the adequate spatial resolution of the physical phenomena or a proper evolution of processes with very long time scales. (It is not possible to have both aspects simultaneously with currently available computing power.) The two types of models are complementary in many respects. Both have been progressively developed over a period of more than 10 years. In the early developmental stages, great care was taken to prove the correctness of the solution techniques (usually finite-difference methods), in the sense that the results of

analytical test problems and laboratory experiments could be reproduced. In this regard, the considerable experience of the meteorological and aerodynamical communities has been helpful in accelerating model development.

Eddy-resolving General Circulation Models (EGCM's)

It is well known from field observations (the MODE Group, 1978) that vigorous low-frequency circulations, with length scales close to the internal deformation radius (about 40 km), exist in the ocean. Theoretical considerations (Gill, *et al.*, 1974; Robinson and McWilliams, 1974) indicate that these motions are analogous to the synoptic disturbances in the atmosphere, which substantially redistribute heat and momentum, both horizontally and vertically, in very complex ways. Because of our limited understanding of these motions from theoretical and observational viewpoints, it is necessary to represent them explicitly in many numerical calculations.

Simulations of basin-wide ocean circulations with resolved eddies are useful for a variety of reasons. With regard to oceanic observations, models assist in the interpretation of existing observational data, and they can be used in the design of future observational programs. With regard to the dynamics of the eddies themselves, models provide complete simulated data sets which can be fully analyzed for dynamical information; they allow an assessment of abstract theoretical ideas within a more complete dynamical framework. As far as the effect of the eddies on the time-mean flow is concerned, the sensitivity of the oceanic circulation to changes in basic eddy parameters (some of which are poorly known from observation) can be determined; competing closure hypotheses for the parameterization of turbulent mixing can be tested. With regard to potential applications, the effect of strong currents and eddies on meridional heat transport (and hence on climate) can be assessed, and transports of biologically and chemically important substances (including pollutants) can be estimated.

Significant progress already has been made toward understanding the nature of the oceanic general circulation by means of eddy-resolving models. Models have played a dominant role in:

1. Identifying the possible sources of eddy energy (Holland and Lin, 1975a,b; Robinson *et al.*, 1977; Semtner and Mintz, 1977; Holland, 1978)
2. Reproducing a plausible distribution of eddy energy levels throughout a mid-latitude gyre (Schmitz and Holland, 1982)
3. Showing the nature of strong-current instabilities to be very sensitive to governing parameters (Haidvogel and Holland, 1978; Cox, 1979)
4. Demonstrating the ability of eddies to drive deep mean circulations (Holland and Rhines, 1980)
5. Pointing up the potentially dominant role of bottom friction as a dissipation mechanism (Holland, 1978)
6. Indicating the complexity and importance of eddy transports of heat and momentum (Semtner and Mintz, 1977; Harrison, 1978)
7. Exploring the possibility of potential vorticity mixing as a parameterization of eddy processes in some geographical areas (Rhines and Holland, 1979; McWilliams and Chow, 1981)
8. Showing fundamental differences between mid-latitude dynamics and Southern Ocean dynamics or equatorial dynamics (McWilliams *et al.*, 1978; Semtner and Holland, 1980).

An enormous amount of computer-intensive work remains to be done if the role of eddies in the general ocean circulation is to be well understood. Current stringent restrictions regarding domain size, grid resolution, generality of the physics, the length of time integrations, and the exploration of parameter space are all related to limited computer time. Such problems need to be overcome if continuing progress is to be made. The interaction of all reasonable physical processes must be considered if confidence is to be had in

the results. Considerations include the effects of bottom topography, coastal configuration, thermohaline forcing, time-dependent forcing, mixing along isopycnal surfaces, very strong non-linearity, and near-surface processes.

Oceanic General Circulation Models (OGCM's)

Oceanic general circulation models are used to depict the ocean currents and density structure in a time-averaged sense, without explicitly resolving the energetic mesoscale eddies. Typically, such models are configured to represent the circulation of an actual ocean basin rather than an idealized (e.g., rectangular) basin. Multiple circulation regimes may be involved. The emphasis is on prediction of the long-term equilibrium density field and the sensitivity of that equilibrium state either to parametric changes or to modifications in forcing. These models play a crucial role in understanding many aspects of the large-scale oceanic circulation and in answering important practical questions; for example:

1. The models are capable of representing in a unified manner the important physical processes occurring in various parts of the global ocean (e.g., water mass formation in high latitudes, the maintenance of the mid-latitude thermoclines and gyre circulations, and the representation of upwelling and mean zonal currents in the tropics).
2. As progress on the parameterization of mesoscale eddies takes place using EGCM's, the overall validity of OGCM's will increase.
3. Verification of improved representations of the oceanic circulation can be made against the known time mean fields of temperature and salinity, as well as against the transient distributions of radioactive trace substances.
4. Short-term climate variations, now thought to be associated with air-sea interactions in the tropics, can be studied in order to improve long-range weather forecasting.

5. Long-term climate changes, such as those related to increased CO_2 in the atmosphere, can be modeled.
6. Biological and chemical models can be integrated into the physical models for various scientific and engineering studies.

OGCM's already have made significant contributions to the understanding of the large-scale ocean circulation. These models have begun to show how the ocean transports and stores heat as a vital part of the climatic system (Bryan and Lewis, 1979; Bryan, *et al.*, 1975; Washington *et al.*, 1980). They have given insight into the formation of the thermocline and deep water masses as well as near-surface temperature anomalies (Bryan and Cox, 1967; Semtner, 1976; Haney, *et al.*, 1978). They have been applied to predict the distribution of geochemical and other tracer substances in the ocean (Holland, 1971; Sarmiento, 1981). In the future these models will be needed to give quantitative answers to a large number of questions, spanning a range from intrinsic ocean dynamics to important societal issues involving climate change, pollution control, and oceanic resource management.

The computational requirements of OGCM's are sizable, even though eddies are not explicitly resolved. For example, a simulation of Pacific Ocean circulation with adequate horizontal resolution (1° grid spacing) for sufficient time to allow formation of surface and intermediate waters (50 years) would require about 1000 hours on a class-six machine (computer with speed exceeding 50 million floating operations per second and high-speed memory of at least 1 million words).

OGCM's have always been strongly computer-limited in the past. In order to obtain sufficiently long time integrations, spatial grid sizes have been far too large to represent even time-mean currents adequately, or to allow inclusion of crude eddy parameterizations with anything close to the correct order of magnitude. Improved spatial resolution is absolutely necessary if we are going to have confidence in the practical measures suggested by model applications. An example of an important calculation that has tremendous potential significance is the prediction of the oceanic circulation and the associated

climate of the Cretaceous period, during which most of the known oil and gas deposits were laid down. A knowledge of the regions of upwelling near the surface with cool, relatively anoxic water at depth would identify production regions for organically rich sediments. The vastly different arrangement of the earth's continents during the Cretaceous is now becoming sufficiently well known to geologists that a prediction of the poorly known climate and ocean circulation during that period should be carried out. A resulting improvement in the strategy for locating new oil reserves could have billion-dollar consequences in the field of energy production.

Regional/Process Models

These models are useful for understanding the interaction of selected physical processes in limited spatial and temporal domains. They give insight into certain aspects of local dynamics without the need for global or basin-wide equilibrium. Most of the reasons put forth in the section on EGCM's as to their utility are equally valid for regional/process models. Examples of such models, which have already yielded substantial insights into ocean dynamics, are

1. Models of the local equilibrium of a mesoscale eddy field with bottom topography (Rhines, 1975, 1977; Bretherton and Haidvogel, 1976; Owens and Bretherton, 1978; Owens, 1979)
2. Numerical models of oceanic jet instabilities (Cox, 1980; McWilliams and Chow, 1981)
3. Open boundary forecast models (Robinson and Haidvogel, 1980)
4. Models of Gulf Stream rings and solitary waves (McWilliams and Flierl, 1979)
5. Models of the Indian Ocean seasonal cycle (Cox, 1976; Philander and Pacanowski, 1981)
6. Equatorial models with simplified vertical structure (Hurlburt *et al.*, 1976; O'Brien *et al.*, 1978; Cane, 1979; Gent and Semtner, 1980)

7. Oceanic mixed layer models (Mellor and Durbin, 1975; Kim, 1976; Kraus, 1977; Garwood, 1979)
8. Models of Gulf of Mexico (Hurlburt and Thompson, 1980,1982)
9. Southern Ocean models

Although regional/process models are somewhat less demanding than EGCM's and OGCM's in terms of computer time, throughout the oceanographic community many groups using such models feel computer-limited to a significant extent. An improved effort in process modeling would have beneficial effects, not only for our understanding of local processes but also for the improvment of the treatment of these processes in EGCM's and OGCM's.

It should be noted that process models are really the only means that we have for studying the full turbulent cascade of energy in the ocean, provided that very high resolution can be employed. Horizontal grid spacings down to several kilometers are needed for such studies. It is likely that in certain modeling applications, the correct representation of the important turbulence process in strong current regions will require imbedding of high-resolution, local models within larger-domain EGCM's or OGCM's. In this case, the computing requirement of the regional/process component of the model might exceed that of the model in which it was imbedded.

It must be stressed that process models have significantly improved the understanding of the local dynamical balances in many parts of the world ocean. They have also assisted in the optimal design of various oceanographic field programs (CUEA, POLYMODE, EPOCS, PEQUOD, and SEQUAL). The models remain a primary link with the real ocean, in that they relate more closely to real time series of data, including new types of data obtained by satellites.

APPENDIX C

SPACECRAFT CONSIDERATIONS FOR SCATTEROMETRY

Possible Instrument Configurations

The purpose of the S-Cubed (S^3) Science Working Group is to focus the ocean science requirements for satellite surface stress information and to advise NASA of the satellite data needs. As such, the Working Group is not particularly concerned with the hardware, software, or space vehicle considerations which must be addressed in order to deliver the geophysical product, as long as that product can meet the science requirements.

Nevertheless, the Working Group is aware that NASA is conducting various engineering feasibility studies of possible instrument configurations. To the extent that any of the configurations can meet our minimum scientific needs, the Working Group endorses those efforts and urges NASA to support the development and flight of a spaceborne scatterometer system.

A study of the TIROS spacecraft system was undertaken to determine the feasibility of adding a scatterometer system to the projected NOAA J Satellite. Preliminary results indicate that minimum requirements might be met by adding a sufficient number of solar panels to meet the increased power requirements and, otherwise, by remaining within the available margins of weight, space, and data handling capacity of the satellite. None of the operational meteorological sensors would be affected, although significant repackaging would be required. The resulting satellite would carry the following meteorological package:

1. Advanced Very High Resolution Radiometer (AVHRR-2)
2. High Resolution Infra-red Sounder (HRIS-2)
3. Microwave Sounding System (MSS)
4. Data Collection System (ARGOS DCS)
5. Search and Rescue Transponder (S.A.R.)
6. Solar Backscatter Ultra-Violet Spectral Radiometer (SBUV-2)

The added instrumentation for the S^3 experiment would be a scatterometer similar in design to the SASS scatterometer flown on SEASAT. The major change would be the addition of an extra antenna on each side (three antennas on each side versus two on the original SEASAT SASS) in order to minimize the vector directional ambiguity problem. With the additional solar panel area necessary to power the scatterometer, there would probably be enough power available to digitally process the scatterometer's radar Doppler return, although this option was not specifically studied. The use of fixed crystal filters to gate the antenna Doppler return into discrete resolution cells was the processing method used on SEASAT. Since the Earth-rotation Doppler varies with latitude, and the filter frequencies are fixed, the corresponding resolution cells from the forward- and after-looking antennas do not overlay one another. (There is also the smaller additional effect of the Earth's having moved between the time of the first and second antenna looks at the same latitude.) These effects shrink the nominal swath coverage at low latitudes, as illustrated in Table C-1.

More important is the introduction of the complicated ground data processing problem of selecting the correct Doppler resolution cells from the different antennas for overlaying and inverting the wind stress signal. It is estimated that almost half of the SEASAT scatterometer ground data processing was involved in cell selection. By gating the Doppler filter frequencies in the spacecraft (programmable, digital filtering), the cells can be made coincident, thus keeping a constant swath width and simplifying the data processing.

For identifying the atmospheric liquid water content, an ESMR (Electrical Scanning Microwave Radiometer), similar to that flown previously in the NIMBUS Research Satellite Program, could be added with little difficulty. The ESMR has a single channel, at 19.35 GHZ, that is sensitive to liquid water and covers a swath of 1545 km at a resolution of 20 km.

Table C-1. TIROS Scatterometer Swath Size (km)*

	Fixed Filter			Programmable Filter		
	Left	Center (Uncovered)	Right	Left	Center (Uncovered)	Right
Lat						
0:	515	443	515	598	376	598
30:	531	438	544	598	376	598
60:	607	407	619	598	376	598

*Orthogonal to ground track

Overall instrument parameters for the scatterometer are given in Table C-2. The meteorological and oceanographic instruments are designed to operate continuously for two years. After that, reduced duty cycles may be necessary due to the normal degradation of the solar panel's power efficiency. Oceanographic data will be generated at a rate of less than 1000 BPS and will be formatted into available NOAA data stream. The spacecraft orbit parameters are given in Table C-3.

With scatterometer incidence angles of 20 to 60 degrees on each side, these orbit parameters will result in a swath coverage of 500 to 600 km on either side of nadir, with an uncovered swath directly beneath the satellite having a width of something greater than 400 km. These coverages are shown in Table C-1. Note that the swath coverage varies with latitude due to Earth's rotation and variable Doppler effects. For fixed Doppler frequency filters, the simplest way to obtain a constant swath width is to add more cells at the outer edge of the swath to be used only at equatorial latitudes. Also shown in Table C-1 is the effect of using programmable digital Doppler filtering rather than the fixed filter SEASAT-type design. The configuration of a two-sided, fixed Doppler scatterometer in NOAA J orbit results in a mean time for repeat coverage of about a day

Table C-2. TIROS Scatterometer Instrument Characteristics

Frequency - 13.995 GHZ
Resolution - 50 km
Incidence Angles - 20-60 degrees
Power - 160 W (typical); 183 W (maximum)
Data rate - 720 BPS
Fixed Doppler Processing
100% Duty Cycle

Table C-3. Nominal NOAA J Orbit Parameters

Parameter	Value
Altitude	833 km
Inclination	98.739 Deg
Nodal Period	101.584 Min
Nodal Regression	25.396 Deg/Revolution
Nodal Precession	.9856 Deg/Day
Orbits/Day	14.175 Orbits/Day
Sun Angle Range	0-68 Deg

and a half at an arbitrary point on the equator, decreasing to less than a day north of 40°N (Table C-4). However, because of the way in which a satellite sweeps the earth, leaving gaps in its coverages, the time taken to cover all points at a given latitude is much longer. The coverage pattern for a single day is shown in Figure C-1. The uncovered diamonds shrink with succeeding orbits until they are essentially eliminated after 3 days. The character of the time required for maximum coverage is discontinuous with latitude. This requirement is shown in Figure C-2 for a fixed filter scatterometer and in Figure C-3 for a programmable filter version.

Table C-4. Scatterometer Maximum and Mean Revisit Times

Scatterometer	Max Time	Mean Time at Equator
TIROS (Fixed Filter)	4.48 Days @ 5 deg lat	1.53 days
TIROS (Fixed Filter, with 25 km tolerance)	3.56 days @ 30-31 deg lat	1.41 days
TIROS (Programmable)	3.49 days @ 21-23 deg lat	1.71 days
Space Platform	7.42 days @ 2 deg lat	1.54 days

Fixed Filter, Two-sided SCAT

14 orbits

h = 833 km θ_i = 20°, 60°(nominal)

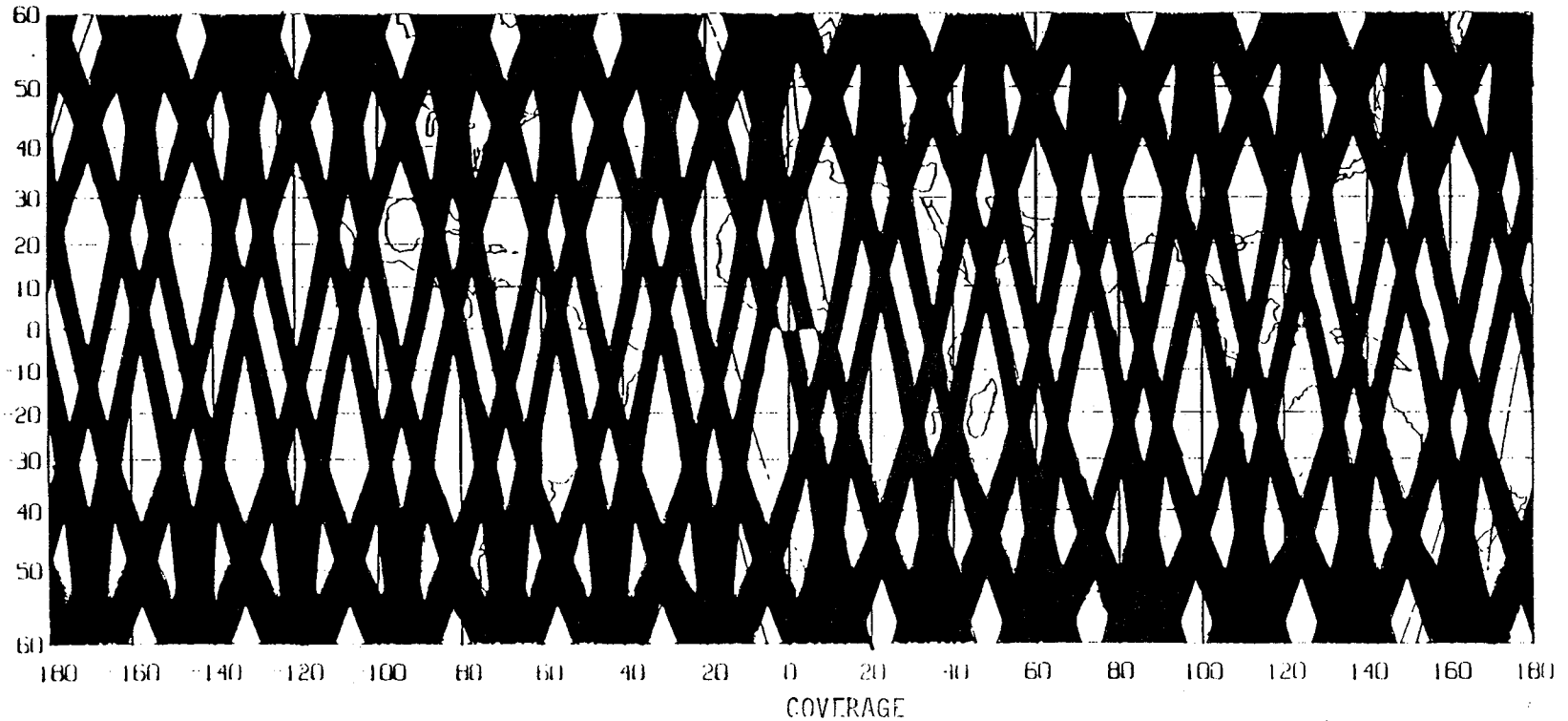

Figure C-1. Swath coverage pattern for a single day.

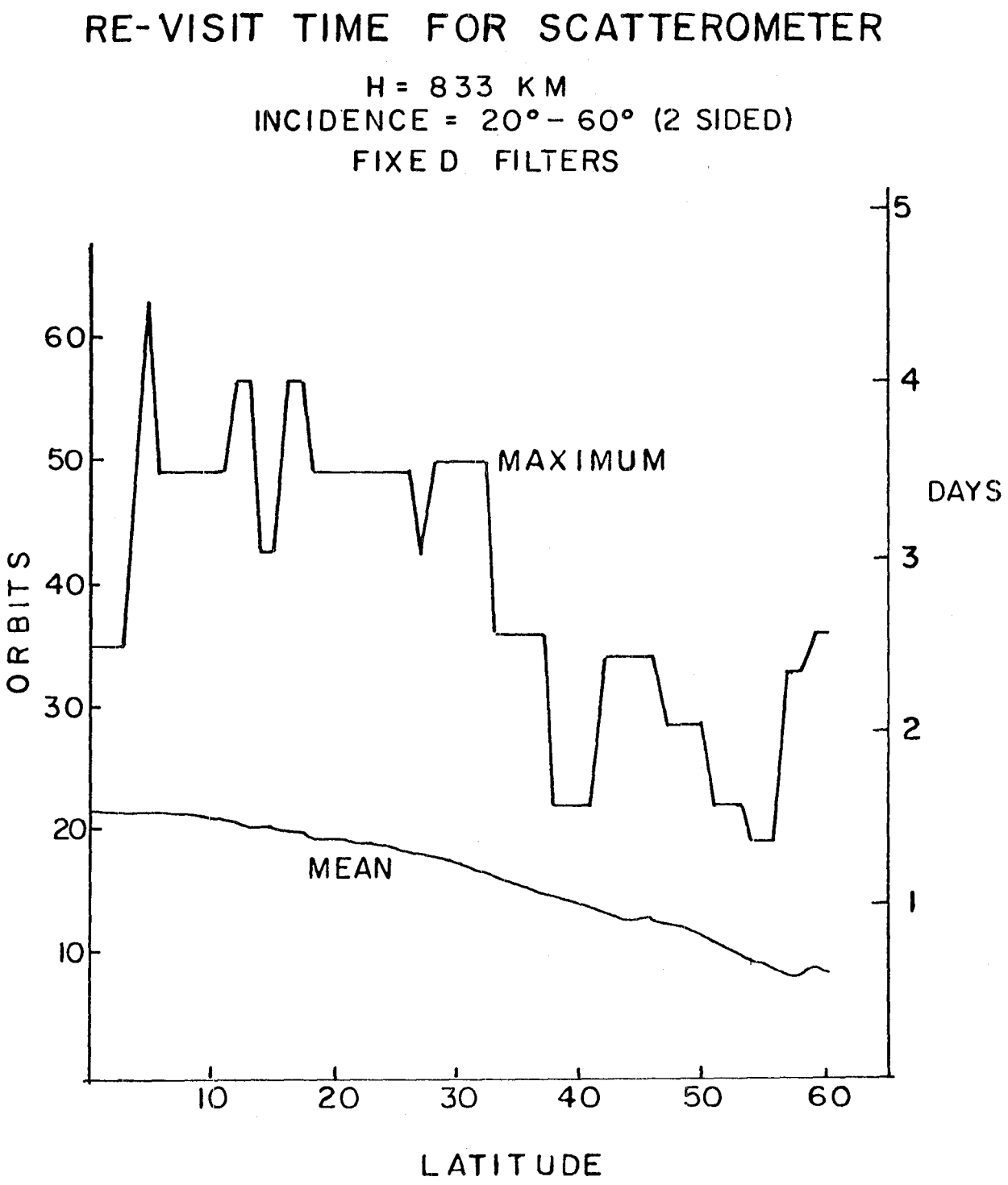

Figure C-2. Time requirement for maximum coverage (fixed filter scatterometer).

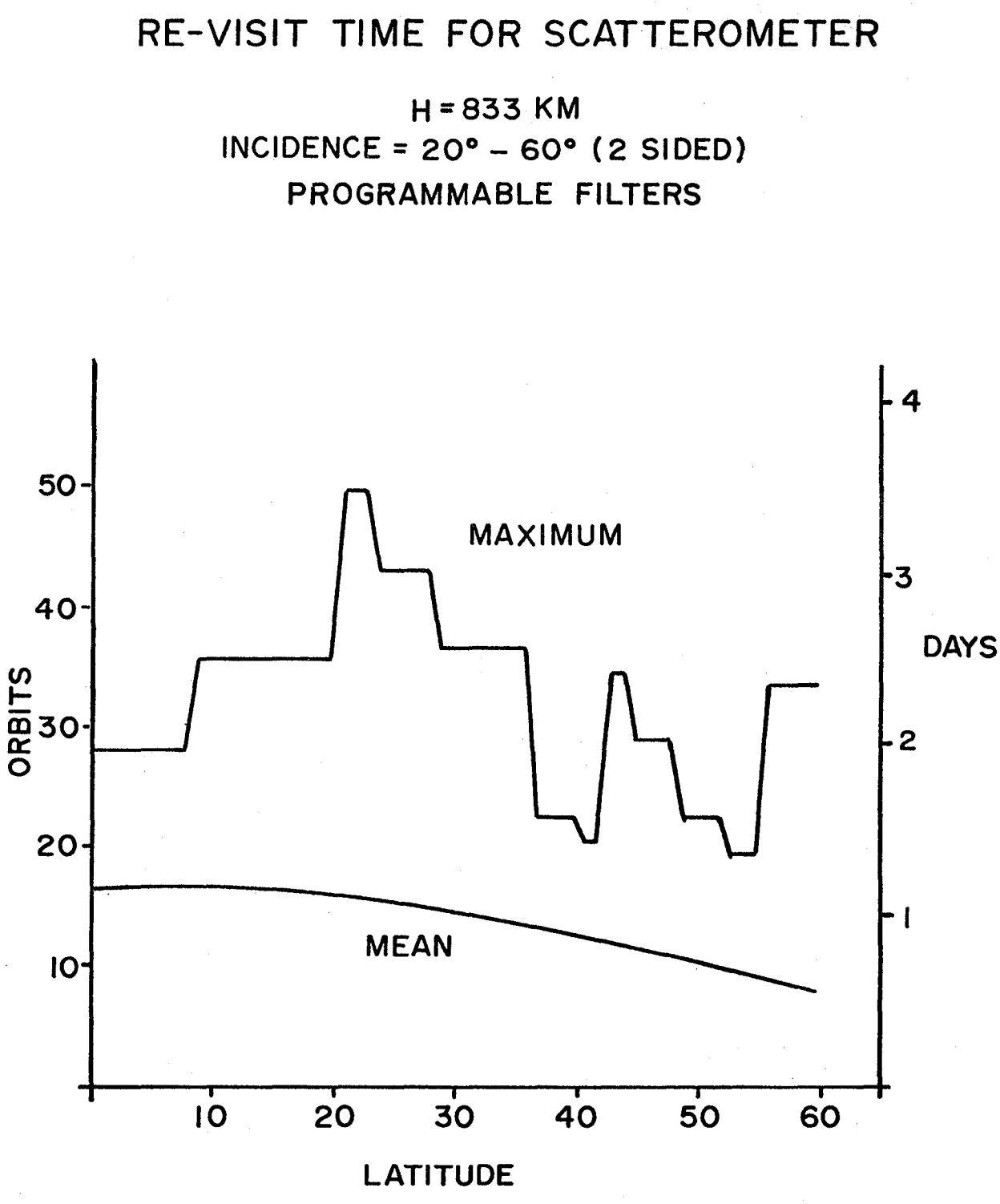

Figure C-3. Time requirement for maximum coverage (programmable filter scatterometer).

APPENDIX D

GLOSSARY OF TERMS

algorithm	Step-by-step procedure for solving a mathematical problem
AOML	Atlantic Oceanic and Meteorological Laboratories
backscatter	A measure of radio frequency energy reflected back from the ocean surface
Beaufort estimates	A wind scale system of estimating and reporting wind speeds
beta effect	The change in ocean dynamics due to the variation of the Coriolis force with latitude
bomb	Oceanic extratropical cyclone that deepens explosively
Bragg scattered	Resonantly backscattered
bulk formulae	An empirical law to determine air-sea fluxes, e.g., $\tau_o = \rho c_o v^2$
C_{10}	Drag coefficient at 10 m
capillary wave	An ocean wave of sufficiently short wavelength that the restoring force is surface tension
Coriolis force	Apparent force that, as a result of the Earth's rotation, deflects moving objects to the right in the northern hemisphere and to the left in the southern hemisphere
CUEA	Coastal Upwelling Ecosystems Analysis
DFT	Discrete Fourier Transform
DMSP	Defense Military Satellite Program
DOC	Department of Commerce
DOD	Department of Defense
EGCM	Eddy-resolving General Circulation Model

El Niño	Sudden appearance of warm water at the eastern boundary of an equatorial ocean basin
EPOCS	Equatorial Pacific Ocean Climate Studies
ESMR	Electrical Scanning Microwave Radiometer
Equatorial Undercurrent	Strong east-to-west setting current
FFT	Fast Fourier Transform
FNOC	Fleet Numerical Oceanographic Center
footprint	An impression or mark made by a foot
frozen field advection	Horizontal transport due to a time-independent velocity field
GCM	General Circulation Model
General Circulation Model	Numerical model used to understand 3-dimensional oceanic circulations in bounded domains
GEOS	Geodynamic Earth Observations System
geostrophic wind	wind measurement inferred from pressure data
GLAS	Goddard Laboratory for Atmospheric Sciences
GMT	Greenwich Mean Time
GOES	Geostationary Environmental Satellite
IMST	Institute Mechanique de la Statistique de la Turbulence
In situ wind	Actual wind determination versus a remote determination
internal Kelvin wave	Patch of deep, warm equatorial water moving rapidly west to the east
IR imagery	Infrared radiation imagery
isotropic	Field of view of a particular measurement cell on the ocean surface
ITCZ	Intertropical Convergence Zone

JASIN	Joint Air-Sea Interaction Experiment
microwave radiometer	An instrument that measures the electromagnetic energy in the microwave region; microwave radiation has wavelengths of 0.01-100 cm
nadir	The point of the celestial sphere that is directly opposite the zenith and vertically downward from the observer
NAS	National Academy of Sciences
NASA	National Aeronautics and Space Administration
nature run	A controlled calculation of a meteorological model
NCC	National Climate Center
NCRS	Normalized cross-section, σ^0
NESS	National Environmental Satellite Service
neutral stability wind	The boundary layer wind in an adiabatic atmosphere
NMC	National Meteorological Center
NOAA	National Oceanic and Atmospheric Administration
NORDA	Naval Ocean Research and Development Activity
NOSS	National Oceanic Satellite System
NOSS SCATT	NOSS scatterometer
N-ROSS	Navy Remote Ocean Sensing System
NWP	National Weather Prediction
OGCM	Oceanic General Circulation Model
OWS	Ocean Weather Ship
PBL	Planetary Boundary Layer
PEQUOD	Pacific Equatorial Ocean Dynamics
QE II	Queen Elizabeth II

radiometric imager	A satellite instrument for digitizing electromagnetic energy
regional/process models	Models of physical processes in limited spatial and temporal domains
Reynolds flux	The representation of the transfer of momentum due to turbulent fluctuations
S^3	Satellite Surface Stress (S-Cubed)
SAR	Search and Rescue
SASS	SEASAT Scatterometer
sea clutter	Radar reflection from ocean waves
SEASAT	Sea Satellite
SEQUAL	Seasonal Equatorial Atlantic Experiment
σ^o	normalized cross-section
SOS	Sum of Squares
SSMI	Special Sensor Microwave Imager
SST	Sea surface temperature
swath width	Cross-track of ocean surface
synoptic scale phenomena	The scale of migratory high and low pressure systems of the lower troposphere with wavelengths of 1,000 to 2,500 km
synthetic aperture radar	imaging radar
thermocline	Region separating the ocean's upper warm layer from the bottom
TIROS	Television and Infrared Observation Satellite
TOGA	Tropical Ocean - Global Atmosphere
TOPEX	Topography Experiment
U_{10}	Wind at 10 m
UIF	User Interface Facility: provides data directory and regional products to user

upper ocean mixed layer	Warm surface layer in the tropical oceans
von Kármán's constant	An empirical component in a logarithmic velocity profile
wind stress	Ocean surface winds
wind stress curl	A vector operation on the wind stress field which physically represents the rotation of the wind

REFERENCES

Adamec, D., and J. J. O'Brien, 1978: The seasonal upwelling in the Gulf of Guinea due to remote forcing, J. Phys. Oceanogr., 10, 1929-1951.

Amorocho, J., and J. J. DeVries, 1980: A new evaluation of the wind stress coefficient over water surfaces, J. Geophys. Res., 85, 433-442.

Amorocho, J., and J. J. DeVries, 1981: Reply, J. Geophys. Res., 86, 4308.

Atlas, R., M. Halem, and M. Ghil, 1982: The effect of model resolution and satellite sounding data on GLAS model forecasts, Mon. Wea. Rev. (to appear).

Barnett, T. P., 1977: An attempt to verify some theories of El Niño. J. Phys. Oceanogr., 7, 633-647.

Barnett, T. P., 1978: Role of oceans in the global climate system, IN Changing Climate, J. Gribbins, Ed., Cambridge University Press, Cambridge, England, 157-177.

Boring, J. D., E. R. Flynt, M. W. Long, and V. R. Widerquist, 1957: Sea return study. Final Rept. Contract NObsr-49063, Engineering Experiment Station, Georgia Inst. of Technology.

Bracalente, E. M., D. H. Boggs, W. L. Grantham, and J. L. Sweet, 1980: The SASS scattering coefficient (σ^0) algorithm, IEEE J. Ocean Eng., OE-5, 145-153.

Bradley, G. A., 1971: Remote sensing of ocean winds using a radar scatterometer. Ph.D. dissertation, Univ. of Kansas, Lawrence, Kansas.

Bretherton, F. P., and D. B. Haidvogel, 1976: Two-dimensional turbulence above topography, J. Fluid Mech., 78, 129-154.

Brown, R. A., 1982: On a satellite scatterometer as an anemometer, J. Geophys. Res. (submitted).

Brown, R. A., and W. T. Liu, 1982: An operational large scale marine planetary boundary layer model, J. Appl. Meteorol. (in press).

Bryan, K., and M. D. Cox, 1967: A numerical investigation of the oceanic general circulation, Tellus, 19, 54-80.

Bryan, K., and L. J. Lewis, 1979. A water mass model of the world ocean, J. Geophys. Res., 84, 2503-2517.

Bryan, K., S. Manabe, and R. C. Pacanowski, 1975: A global ocean atmosphere climate model, Part II, the oceanic circulation, J. Phys. Oceanogr., 5, 30-46.

Busalacchi, A. J., and J. J. O'Brien, 1980: The seasonal variability in a model of the tropical Pacific, J. Phys. Oceanogr., 10, 1929-1951.

Busalacchi, A. J., and J. J. O'Brien, 1981: Interannual variability of the Equatorial Pacific in the 1960's, J. Geophys. Res., 86, 10,901-10,907.

Busalacchi, A. J., J. J. O'Brien, and K. Takeuchi, 1982: Interannual variability of the Equatorial Pacific, J. Geophys. Res. (submitted).

Businger, J. A., J. C. Wyngaard, T. Izumi, and E. F. Bradley, 1971: Flux profile relationships in the atmospheric surface layer, J. Atmos. Sci., 28, 181-189.

Cane, M. A., 1979: The response of an equatorial ocean to simple wind stress patterns, II, numerical results, J. Marine Res., 37, 253-299.

Cane, M. A., 1980: On the dynamics of equatorial currents, with application to the Indian Ocean, Deep-Sea Res., 27, 525-544.

Cane, M., and V. J. Cardone, 1981: The potential impact of scatterometry on oceanography: A wave forecasting case, Oceanography from Space, J. F. R. Gower, Ed., Plenum Press, New York, 587-595.

Cane, M. A., V. J. Cardone, M. Halem, and I. Halberstram, 1981: On the sensitivity of numerical weather prediction to remotely sensed marine surface wind data: A simulation study, J. Geophys. Res., 86, 8093-8106.

Cardone, V. J., J. D. Young, W. J. Pierson, R. K. Moore, J. A. Greenwood, C. Greenwood, A. K. Fung, R. Salfi, W. L. Chang, M. Afarani, and M. Koman, 1976: The measurement of the winds near the ocean surface with a radiometer-scatterometer on Skylab, NASA Johnson Space Center, Houston, TX. Final Rept. on EPN550 Contract No. NAS-9-13642.

Chang, S. W., and R. A. Anthes, 1978: Numerical simulations of the ocean's nonlinear, baroclinic response to translating hurricanes, J. Phys. Oceanogr., 8, 468-480.

Cheney, R. E., J. G. Marsh, B. Beckley, T. M. Martin, J. J. McCarthy, and H. J. Rhee, 1981: Global mesoscale variability from repeat tracks of SEASAT altimeter data. Paper presented at Fall Meeting of the A.G.U., Dec. 7-11, 1981, San Francisco.

Clancy, R. M., and P. J. Martin, 1981: Synoptic forecasting of the oceanic mixed layer using the Navy's operational environmental data base: Present capabilities and future applications, Bull. Am. Meteorol. Soc., 62, 770-784.

Coantic, M., and A. Favre, 1973: Activities in, and preliminary results of, air-sea interactions research at IMST. Paper Pres. at the Second IUTAM-IUGG Symp. on Turbulent Diffusion in Environmental Pollution, 8-14 April, 1973, Charlottesville, Virginia.

Cox, M. D., 1976: Equatorially trapped waves and the generation of the Somali Current, Deep-Sea Res., 23, 1139-1152.

Cox, M. D., 1979: A numerical study of Somali Current eddies, J. Phys. Oceanogr., 9, 311-326.

Cox, M. D., 1980: Generation and propagation of 30-day waves in a numerical model of the Pacific, J. Phys. Oceanogr., 10, 1168-1186.

Cox, M. D., 1981: A numerical study of surface cooling processes during summer in the Arabian Sea. IN Monsoon Dynamics, J. Lighthill and R. Pearce, Eds., Cambridge University Press, 529-540.

Daley, J. C., 1973: Wind dependence of radar sea return, J. Geophys. Res., 78, 7823-7833.

Davidson, K. L., G. E. Schacher, C. W. Fairall, and J. D. Jarrell, 1981: Observational results pertaining to scatterometer interpretation. IN Oceanography from Space, J. F. R. Gower, Ed., Plenum Press, New York, 597-606.

Davis, R. E., R. de Szoeke, and P. Niiler, 1981: Variability in the upper ocean during MILE. Part II, Modeling the mixed layer response. Deep-Sea Res., 28A, 1453-1475.

Evanson, A. J., and G. Veronis, 1975: Continuous representation of wind stress curl over the world ocean, J. Mar. Res., Suppl. to Vol. 33, 131-144.

Ewing, G. C., 1965: Oceanography from Space. Conf. Proc., Ref. 65-10, Woods Hole Oceanogr. Inst., Woods Hole, MA.

Fofonoff, N. P., 1981: The Gulf Stream System. IN Evolution of Physical Oceanography, B. A. Warren and C. Wunsch, Eds., The MIT Press, Cambridge, MA, 112-139.

Gallegos-Garcia, A., W. J. Emery, R. O. Reid, and L. Magaard, 1981: Frequency-wavenumber spectra of sea surface temperature and wind-stress curl in the Eastern North Pacific, J. Phys. Oceanogr., 11, 1059-1077.

Garratt, J. R., 1977: Review of drag coefficients, Mon. Wea. Rev., 105, 915-929.

Garwood, R. W., Jr., 1979: Air-sea interaction and dynamics of the surface mixed layer, Rev. Geophys. Space Phys., 17, 1507-1524.

General Electric Co., 1980: Final Study Report: NOSS Scatterometer Digital Data Processor. Rept. No. 80SDS4246, NASA LARC Contract Purchase Order L518B and 8163B.

Gent, P. R., and A. J. Semtner, 1980: Energy trapping at the equator in a numerical ocean model, J. Phys. Oceanogr., 10, 823-842.

Gill, A. E., J. S. A. Green, and A. J. Simmons, 1974: Energy partition in the large-scale ocean circulation and the production of mid-ocean eddies, Deep-Sea Res., 21, 499-528.

Goldenberg, S. B., and J. J. O'Brien, 1981: Time and space variability of tropical Pacific wind stress, Mon. Wea. Rev., 109, 1190-1207.

Grant, C. R., and B. S. Yaplee, 1957: Backscattering from water and land at centimeter and millimeter wave lengths, Proc. IRE, 45, 976-982.

Grantham, W. L., E. M. Bracalente, C. L. Britt, Sr., F. J. Wentz, W. L. Jones, and L. C. Schroeder, 1982: Performance evaluation of an operational spaceborne scatterometer, IEEE/Geoscience and Remote Sensing, GE-20, 3, July (in press).

Grantham, W. L., E. M. Bracalente, W. L. Jones, and J. W. Johnson, 1977: The Seasat-A satellite scatterometer, IEEE J. Oceanic Eng., OE-2, 200-206.

Greenspan, H. P., 1963: A note concerning topography and inertial currents, J. Mar. Res., 21, 147-154.

Guinard, N. W., and J. C. Daley, 1970: An experimental study of a sea clutter model, Proc. IEEE, 58, 543-550.

Gyakum, J. R., 1980: On the evolution of the QE II storm. Preprints, Eighth Weather Forecasting and Analysis Conference. AMS, Boston, 23-28.

Haidvogel, D. B., and W. R. Holland, 1978. The stability of ocean currents in eddy-resolving general circulation models, J. Phys. Oceanogr., 8, 393-413.

Halem, M., E. Kalnay, W. E. Baker, and R. Atlas, 1982: An assessment of the FGGE satellite observing system during SOP-1, Bull. Amer. Meteor. Soc. (to appear).

Haney, R. L., 1980: A numerical case study of the development of large-scale thermal anomalies in the Central North Pacific Ocean, J. Phys. Oceanogr., 10, 541-556.

Haney, R. L., W. S. Shiver, and K. H. Hunt, 1978: A dynamical-numerical study of the formation and evolution of large-scale ocean anomalies, J. Phys. Oceanogr., 8, 952-969.

Harrison, D. E., 1978: On the diffusion parameterization of mesoscale eddy effects from a numerical ocean experiment, J. Phys. Oceanogr., 8, 913-918.

Harrison, D. E., 1981: Eddy lateral vorticity transport and the equilibrium of the North Atlantic subtropical gyre, J. Phys. Oceanogr., 11, 1154-1159.

Hastenrath, S., and P. Lamb, 1979: Climatic Atlas of the Indian Ocean. Part I. Surface Circulation and Climate. Part 2. The Oceanic Heat Budget, Univ. of Wisconsin Press, Madison, WI, 104 pp.

Hoffman, R. N., 1982: SASS wind ambiguity removal by direct minimization, Mon. Wea. Rev. (to appear).

Holland, W. R., 1971: Ocean tracer distributions, Tellus, 23, 371-392.

Holland, W. R., 1978: The role of mesoscale eddies in the general circulation of the ocean-numerical experiments using a wind-driven quasigeostrophic model, J. Phys. Oceanogr., 8, 363-392.

Holland, W. R., and L. B. Lin, 1975a: On the generation of mesoscale eddies and their contribution to the oceanic general circulation, I, A preliminary numerical experiment, J. Phys. Oceanogr., 5, 642-657.

Holland, W. R., and L. B. Lin, 1975b: On the generation of mesoscale eddies and their contribution to the oceanic general circulation, II, A parameter study, J. Phys. Oceanogr., 5, 658-669.

Holland, W. R., and P. B. Rhines, 1980: An example of eddy-induced ocean circulation, J. Phys. Oceanogr., 10, 1010-1031.

Hoskins, B. J., and D. J. Karoly, 1981: The steady linear response of a spherical atmosphere to thermal and orogenic forcing, J. Atmos. Sci., 38, 1179-1196.

Hurlburt, H. E., J. C. Kindle, and J. J. O'Brien, 1976: A numerical simulation of the onset of El Niño, J. Phys. Oceanogr., 6, 621-631.

Hurlburt, H. E., and J. D. Thompson, 1980: A numerical study of Loop Current intrusions and eddy shedding, J. Phys. Oceanogr., 10, 1611-1651.

Hurlburt, H. E., and J. D. Thompson, 1982: The dynamics of the Loop Current and shed eddies in a numerical model of the Gulf of Mexico, Hydrodynamics of Semi-enclosed Seas, J. C. J. Nihoul, Ed., Elsevier Scientific Pub. Co., Amsterdam, 243-297.

Johnson, J. W., L. A. Williams, E. M. Bracalente, F. B. Beck, and W. L. Grantham, 1980: SEASAT-A satellite scatterometer instrument evaluation, IEEE J. Oceanic Eng., OE-5, 2, 138-144.

Johnson, R. G., and C. Daley, 1980: Seasat-A optimum ship routing/offshore case study, JPL/NASA ASVT Experiment 16, Ocean Routes Inc.

Jones, W. L., and L. C. Schroeder, 1978: Radar backscatter from the ocean: Dependence on surface friction velocity, Boundary Layer Meteorol., 13, 133-149.

Jones, W. L., L. C. Schroeder, D. Boggs, E. M. Bracalente, R. A. Brown, G. Dome, W. J. Pierson, and F. J. Wentz, 1982: The SEASAT-A satellite scatterometer: The geophysical evaluation of remotely sensed wind vectors over the ocean, J. Geophys. Res., 87, 3297-3317.

Jones, W. L., L. C. Schroeder, and J. L. Mitchell, 1977: Aircraft measurements of the microwave scattering signature of the ocean, IEEE Trans. Antennas Propagat., AP-25, 52-61.

Jones, W. L., F. J. Wentz, and L. C. Schroeder, 1978: Algorithm for inferring wind stress from SEASAT-A, J. Spacecraft and Rockets, 15, 368-374.

Julian, P. R., and A. K. Cline, 1974: The direct estimation of spatial wavenumber spectra of atmospheric variables, J. Atmos. Sci., 31, 1526-1539.

Kao, S. K., 1970: Wavenumber-frequency spectra of temperature in free atmosphere. J. Atmos. Sci., 17, 1000-1007.

Käse, R. H., and D. J. Olbers, 1980: Wind-driven inertial waves observed during Phase III of GATE, Suppl. I, Deep-Sea Res., 27, 191-216.

Katsaros, K. B., and K. E. Richmond, 1981: Simultaneous measurements of high frequency wave height and wind stress in Lake Washington. Paper Pres. at IUCRM Colloq. on Waves and Turbulence, 18-22 May, 1981, AOML/SAIL, Miami, Florida.

Kaula, W., 1970: The terrestrial environment: Solid earth and ocean physics. NASA Contractor Rept. CR-1579, NASA, Washington, D.C.

Kim, J.-W., 1976: A generalized bulk model of the oceanic mixed layer, J. Phys. Oceanogr., 6, 686-695.

Kindle, J. C., 1979: Equatorial Pacific Ocean variability - Seasonal and El Niño time scales. Ph.D. dissertation, Florida State University, Tallahassee, FL.

Kirwan, A. D., Jr., G. McNally, S. Pazan, and R. Wert, 1979: Analysis of surface current response to wind, J. Phys. Oceanogr., 9, 401-412.

Koblinsky, C. J., T. Keffer, and P. P. Niiler, 1979: A compilation of observations from moored current meters and associated oceanographic observations. Data Report 75, Oregon State Univ., Corvallis, Oregon, 119 pp.

Kraus, E. B., Ed., 1977. Modelling and Prediction of the Upper layers of the Ocean, Pergamon Press, New York, 325 pp.

Krishen, K., 1971: Correlation of radar backscattering cross sections with ocean wave height and wind velocity, J. Geophys. Res., 76, 6528-6539.

Large, W. G., and S. Pond, 1981: Open ocean momentum flux measurements in moderate to strong winds, J. Phys. Oceanogr., 11, 324-336.

Leetmaa, A., 1972: The response of the Somali Current to the southwest monsoon of 1970, Deep-Sea Res., 19, 319-325.

Leetmaa, A., 1973: The response of the Somali Current at 2°S to the southwest monsoon of 1971, Deep-Sea Res., 20, 397-400.

Leetmaa, A., and A. F. Bunker, 1978: Updated charts of the mean annual wind stress, convergences in the Ekman layers and Sverdrup transports in the North Atlantic, J. Mar. Res., 36, 311-322.

Leetmaa, A., J. P. McCreary, Jr., and D. W. Moore, 1981: Equatorial currents: Observations and theory. IN Evolution of Physical Oceanography, B. A. Warren and C. Wunsch, Eds., MIT Press, Cambridge, MA, 184-197.

Legeckis, R., 1978: A survey of worldwide sea surface temperature fronts detected by environmental satellites, J. Geophys. Res., 83, 4501-4522.

Lin, L. B., and H. E. Hurlburt, 1981: Maximum simplifications of nonlinear Somali Current dynamics. IN Monsoon Dynamics, J. Lighthill and R. Pearce, Eds., Cambridge University Press, 541-556.

Liu, W. T., and W. G. Large, 1982: Determination of surface stress by SEASAT-SASS: A case study with JASIN data, J. Phys. Oceanogr. (in press).

McCreary, J. P., 1976: Eastern tropical ocean response to changing wind systems: With application to El Niño, J. Phys. Oceanogr., 6, 632-645.

McNally, G. J., 1981: Satellite-tracked drift buoy observations of the near-surface flow in the Eastern Midlatitude North Pacific, J. Geophys. Res., 86, 8022-8030.

McWilliams, J. C., and J. H. S. Chow, 1981: Equilibrium geostrophic turbulence: I. A reference solution in a β-plane channel, J. Phys. Oceanogr., 11 (in press).

McWilliams, J. C., and G. R. Flierl, 1979: On the evolution of isolated nonlinear vortices, J. Phys. Oceanogr., 9, 1155-1182.

McWilliams, J. C., W. R. Holland, and J. H. Chow, 1978: A description of numerical Antarctic Circumpolar Currents, Dyn. Atmos. Oceans, 2, 213-291.

Mellor, G. L., and P. A. Durbin, 1975: The structure and dynamics of the ocean surface mixed layer, J. Phys. Oceanogr., 5, 718-728.

Miles, J. W., 1960: On the generation of surface waves by turbulent shear flows, J. Fluid Mech., 7, 469.

Mitsuyasu, H., and T. Honda, 1975: The high frequency spectrum of wind-generated waves. IN Reports of Research, Institute for Applied Mechanics, Kyushu University, Japan, Vol. XXII, No. 71, 327-355.

MODE Group, The, 1978: The Mid-Ocean Dynamics Experiment, Deep-Sea Res., 25, 859-910.

Montgomery, D. R., 1981: Commercial applications of satellite oceanography, Oceanus, 24, 3, 56-65.

Moore, D. W., and S. G. H. Philander, 1977: Modeling of the tropical oceanic circulation. IN The Sea, Vol. VI, E. D. Goldberg, Ed., Wiley Interscience, New York, 319-361.

Moore, R. K., I. J. Birrer, E. M. Bracalente, G. Dome, and F. Wentz, 1982: Evaluation of atmospheric attenuation from SMMR brightness temperatures for the SEASAT scatterometer, J. Geophys. Res., (in press).

Moore, R. K., and A. D. Fung, 1979: Radar determination of winds at sea, Proc. IEEE, 67, 1504-1521.

Moore, R. K., and W. J. Pierson, Jr., 1966: Measuring sea state and estimating surface winds from a polar orbiting satellite, Proc. Inter. Symp. Electromagnetic Sensing of the Earth from Satellites, Miami Beach, Florida, R1-R28.

Moore, R. K., and W. J. Pierson, Jr., 1971: World-wide oceanic wind and wave predictions using a satellite radar radiometer, J. Hydronaut., 5, 52-60.

Moore, R. K., and J. D. Young, 1977: Active microwave measurement from space of sea-surface winds, IEEE J. Oceanic Eng., OE-2, 309-317.

Müller, P., and C. Frankignoul, 1981: Direct atmospheric forcing of geostrophic eddies, J. Phys. Oceanogr., 11, 287-308.

Munk, W. H., 1950: On the wind-driven ocean circulation, J. Meteor., 7, 79-93.

Munk, W., 1981: Internal waves and small-scale processes. IN: Evolution of Physical Oceanography. B. A. Warren and C. Wunsch, Eds., MIT Press, Cambridge, MA, 264-291.

Namias, J., 1978: Multiple causes of the North American abnormal Winter, 1976-77, Mon. Wea. Rev., 106, 279-295.

National Research Council, 1970: Remote sensing with specific reference to oceanography. National Academy of Sciences, Washington, D.C.

Newton, R. W., and J. W. Rouse, Jr., 1972: Experimental measurements of 2.25 cm backscatter from sea surfaces, IEEE Trans. Geosci. Electron., GE-10, 2-7.

O'Brien, J. J., D. Adamec, and D. W. Moore, 1978: A simple model of upwelling in the Gulf of Guinea, Geophys. Res. Lett., 5, 641-644.

O'Brien, J. J., and R. O. Reid, 1967: The non-linear response of a two-layer, baroclinic ocean to a stationary, axially symmetric hurricane: Part I. Upwelling induced by momentum transfer, J. Atmos. Sci., 24, 197-207.

Ocean Routes, 1980: SEASAT-A Optimum Ship Routing/Offshore Case Study. JPL/NASA ASVT Experiment 16, 69 pp.

Owens, W. B., 1979: Simulated dynamic balances for mid-ocean mesoscale eddies, J. Phys. Oceanogr., 9, 337-359.

Owens, W. B., and F. P. Bretherton, 1978: A numerical study of mid-ocean mesoscale eddies, Deep-Sea Res., 25, 1-14.

Pedlosky, J., 1965: A necessary condition for the existence of an inertial boundary layer in a baroclinic ocean, J. Mar. Res., 23, 69-72.

Peteherych, S., W. A. Appleby, P. Woiceshyn, J. Spagnol, and L. Chu, 1981: Application of SEASAT scatterometer wind measurements for operational weather forecasting. Unpublished manuscript.

Philander, S. G. H., 1979: Equatorial waves in the presence of the Equatorial Undercurrent, J. Phys. Oceanogr., 9, 254-262.

Philander, S. G. H., and R. C. Pacanowski, 1981: The response of equatorial oceans to periodic forcing, J. Geophys. Res., 86, 1903-1916.

Pierson, W. J., 1981: The variability of winds over the ocean. IN Spaceborne Synthetic Aperature Radar for Oceanography, R. C. Beal, P. G. DeLeonibus, and I. Katz, Eds., Johns Hopkins Univ. Press, Baltimore, MD, 56-74.

Plant, W. J., and J. W. Wright, 1977: Growth and equilibrium of short gravity waves in a wind wave tank, J. Fluid Mech., 82, 767-793.

Pollard, R. T., 1977: Observations and models of the structure of the upper ocean. IN Modeling and Prediction of the Upper Layers of the Ocean, E. B. Kraus, Ed., Pergamon Press, 102-117.

Preller, R. H., and H. E. Hurlburt, 1982: A reduced gravity numerical model of circulation in the Alboran Sea. IN Hydrodynamics of Semi-enclosed Seas, J. C. J. Nihoul, Ed., Elsevier Scientific Pub. Co., Amsterdam, 75-89.

Price, J. F., 1981: Upper ocean response to a hurricane, J. Phys. Oceanogr., 11, 153-175.

Price, J. F., 1982: Internal wave wake of a moving hurricane (submitted for publication).

Ramage, C. S., C. W. Adams, A. M. Hori, B. J. Kilonsky, and J. C. Sadler, 1980: Meteorological Atlas of the 1972-73 El Niño. Dept. of Meteorology, Univ. of Hawaii, Honolulu, HI, 101 pp.

Rhines, P. B., 1975: Waves and turbulence on a β-plane, J. Fluid Mech., 69, 417-443.

Rhines, P. B., 1977: The dynamics of unsteady currents. IN The Sea, Vol. VI, E. D. Goldberg, Ed., John Wiley and Sons, Inc., New York, 189-318.

Rhines, P. B., and William R. Holland, 1979: A theoretical discussion of eddy-driven mean flows, Dyn. of Atmos. and Oceans, 3, 289-325.

Robinson, A. R., and D. B. Haidvogel, 1980: Dynamical forecast experiments with a barotropic open ocean model, J. Phys. Oceanogr., 10, 1909-1928.

Robinson, A. R., D. E. Harrison, Y. Mintz, and A. J. Semtner, 1977: Eddies and the general circulation of an idealized oceanic gyre: a wind and thermally driven primitive equation numerical experiment, J. Phys. Oceanogr., 7, 182-207.

Robinson, A. R., and J. C. McWilliams, 1974: The baroclinic instability of the open ocean, J. Phys. Oceanogr., 4, 281-294.

Ross, D., and W. L. Jones, 1978: On the relationship of radar backscatter to wind speed and fetch, Bound. Layer Meteorol., 13, 133-149.

Sanders, R., and J. R. Gyakum, 1980: Synoptic-dynamic climatology of the bomb, Mon. Wea. Rev., 108, 1589-1606.

Sarmiento, J. L., 1981: A simulation of bomb tritium entry into the Atlantic Ocean. Part II, the tritium model and results (in preparation).

Schmitz, W. J., Jr., 1978: Observations of the vertical distribution of low frequency kinetic energy in the Western North Atlantic, J. Mar. Res., 36, 295-310.

Schmitz, W. J., and W. R. Holland, 1982: A preliminary comparison of selected numerical eddy-resolving general circulation experiments with observations, J. Mar. Res., 40, 75-117.

Schroeder, L. C., D. H. Boggs, G. Dome, I. M. Halberstam, W. L. Jones, W. J. Pierson, and F. J. Wentz, 1982a: The relationship between wind vector and normalized radar cross section used to derive SEASAT-A satellite scatterometer winds, J. Geophys. Res., 87, 3318-3336.

Schroeder, L. C., W. L. Grantham, J. L. Mitchell, and J. L. Sweet, 1982b: SASS measurements of the KU-band radar signature of the ocean, IEEE J. Oceanic Eng., OE-7, 1, 3-14.

Semtner, A. J., Jr., 1976: Numerical simulation of the Arctic Ocean circulation, J. Phys. Oceanogr., 6, 409-425.

Semtner, A. J., Jr., and W. R. Holland, 1980: Numerical simulation of the equatorial ocean circulation, Part I, A basic case in turbulent equilibrium, J. Phys. Oceanogr., 10, 667-693.

Semtner, A. J., Jr., and Y. Mintz, 1977: Numerical simulation of the Gulf Stream and mid-ocean eddies, J. Phys. Oceanogr., 7, 208-230.

Smith, S. D., 1980: Wind stress and heat flux over the ocean in gale force winds, J. Phys. Oceanogr., 10, 709-726.

Smith, S. D., 1981: Comment on "A new evaluation of the wind stress coefficient over water surfaces," J. Geophys. Res., 86, 1307.

Stommel, H., 1948: The westward intensification of wind driven ocean currents. Trans. Amer. Geophys. Union, 29, 202-206.

Veronis, G., 1973: Model of world ocean circulation. I. Wind driven, two layer, J. Mar. Res., 31, 228-288.

Veronis, G., 1981: Dynamics of large-scale ocean circulation. IN Evolution of Physical Oceanography, B. A. Warren and C. Wunsch, Eds., MIT Press, Cambridge, MA, 140-183.

Wallace, J. M., and C. P. Chang, 1969: Spectrum analysis of large-scale disturbance in the tropical lower troposphere, J. Atmos. Sci., 26, 1010-1025.

Washington, W., A. J. Semtner, Jr., G. A. Meehl, D. Knight, and T. A. Mayer, 1980: A general circulation experiment on seasonal cycles with a coupled atmosphere, ocean and sea-ice model, J. Phys. Oceanogr., 10, 1887-1908.

Webster, P. J., 1981: Mechanisms determining the atmospheric response to sea surface temperature anomalies, J. Atmos. Sci., 38, 554-571.

Wentz, F. J., 1978: Documentation for Program WINVEC: Computations of statistics on the sea-surface friction velocity and wind direction. RSS Tech. Rept. 78-001, Remote Sensing Systems, Sausalito, CA.

Wentz, F. J., 1981: The effect of atmospheric attenuation on microwave scatterometer measurements. RSS Tech. Rept. 091781, Remote Sensing Systems, Sausalito, CA.

White, W., R. Bernstein, G. McNally, S. Pazan, and R. Dickson, 1980: The thermocline response to transient atmospheric forcing in the interior mid-latitude North Pacific, 1976-1978, J. Phys. Oceanogr., 10, 372-384.

Willebrand, J., 1978: Temporal and spatial scales of the wind field over the North Pacific and North Atlantic, J. Phys. Oceanogr., 8, 1080-1094.

Willebrand, J., S. G. H. Philander, and R. C. Pacanowski, 1980: The oceanic response to large scale atmospheric disturbances, J. Phys. Oceanogr., 10, 411-429.

Willson, M. A. G., 1975: A wavenumber-frequency analysis of large-scale tropospheric motions in the extratropical northern hemisphere, J. Atmos. Sci., 32, 478-488.

Wiltse, C. J., S. P. Schlesinger, and C. M. Johnson, 1957: Backscattering characteristics of the sea in the region from 10 to 50 kMc, Proc. IRE, 45, 220-227.

Wright, J. W., 1966: Backscattering from capillary waves with application to sea clutter, IEEE Trans. Antennas Propagat., AP-14, 749-754.

Wurtele, M. G., P. M. Woiceshyn, S. Peteherych, M. Borowski, and W. S. Appleby, 1982: Wind direction alias removal studies of SEASAT scatterometer derived wind fields. J. Geophys. Res. (to be published).

Wyrtki, K., 1975: El Niño - The dynamic response of the equatorial Pacific Ocean to atmospheric forcing, J. Phys. Oceanogr., 5, 572-584.

Wyrtki, K., and G. Meyers, 1976: The trade wind field over the Pacific Ocean, J. Appl. Meteorol., 15, 698-704.

Yu, T. W., and R. D. McPherson, 1979: Surface pressure analysis using scatterometer-derived wind data from the SEASAT-A satellite. Fourth Conference on Numerical Weather Prediction, Oct. 29-Nov. 1, 1979, Silver Spring, MD, 351-355.

Yu, T. W., and R. D. McPherson, 1981: Global data assimilation experiments with scatterometer winds from SEASAT-A. Fifth Conference on Numerical Weather Prediction, Nov. 2-6, 1981, Monterey, CA, 9-13.

End of Document